

**Studies of Various Pentamethylcyclopentadienyl Nitrosyl Complexes of
Molybdenum and Tungsten**

by

Aaron Stanley Holmes

B.Sc., The University of British Columbia, 2015

A THESIS SUBMITTED IN PARTIAL FULFILLMENT OF
THE REQUIREMENTS FOR THE DEGREE OF

MASTER OF SCIENCE

in

THE FACULTY OF GRADUATE AND POSTDOCTORAL STUDIES
(Chemistry)

THE UNIVERSITY OF BRITISH COLUMBIA
(Vancouver)

July 2017

© Aaron Stanley Holmes, 2017

Abstract

$\text{Cp}^*\text{W}(\text{NO})(\text{H})(\eta^3\text{-CH}_2\text{CHCHMe})$ (**2.1**) [$\text{Cp}^* = \eta^5\text{-C}_5\text{Me}_5$] effects the formation of unsymmetrical ketones from hydrocarbons and CO via C–H activation, C–H functionalization, and C–C coupling. $\text{Cp}^*\text{W}(\text{NO})(\text{CO})_2$ is also formed during the reactions, and can be conveniently converted back into complex **2.1**, thereby completing a full synthetic cycle for the conversion of hydrocarbons into ketones.

cis- $\text{Cp}^*\text{W}(\text{NO})(\text{H})(\kappa^2\text{-PPh}_2(\text{C}_6\text{H}_4))$ (**3.1**) has been previously shown to effect the thermal C–H activation of benzene. In an effort to extend this investigation, novel $\text{Cp}^*\text{W}(\text{NO})(\text{R})(\text{H})(\text{L})$ [$\text{R} = \text{alkyl}$, $\text{L} = \text{phosphine}$ or phosphite] complexes have been synthesized and characterized, and their ability to effect C–H activation has been investigated. Upon heating, complex **3.1** in various neat hydrocarbon solutions forms *trans*- $\text{Cp}^*\text{W}(\text{NO})(\text{H})(\kappa^2\text{-PPh}_2(\text{C}_6\text{H}_4))$ (**3.2**), an isomerization product, and $\text{Cp}^*\text{W}(\text{NO})(\text{PPh}_3)_2$, a disproportionation product, both of which are inactive species. In an attempt to avoid the problems of isomerization and disproportionation, the novel complexes *trans*- $\text{Cp}^*\text{W}(\text{NO})(\text{CH}_2\text{CMe}_3)(\text{H})(\text{P}(\text{OPh})_3)$ (**3.3**) and *trans*- $\text{Cp}^*\text{W}(\text{NO})(\text{H})_2(\text{P}(\text{OPh})_3)$ (**3.4**) have been synthesized. Unfortunately, complex **3.3** does not effect the thermal C–H activation of hydrocarbon substrates in neat solutions. Instead, the elimination of neopentane, release of free $\text{P}(\text{OPh})_3$, and subsequent decomposition of the organometallic fragment occur, even at room temperature.

The use of bidentate bisphosphine ligands in order to circumvent the problems experienced in the previous section has been investigated. The complex $\text{Cp}^*\text{Mo}(\text{NO})(\kappa^2\text{-dmpe})$ (**4.1**) [$\text{dmpe} = 1,2\text{-bis}(\text{dimethylphosphino})\text{ethane}$] does not effect the thermal C–H activation of hydrocarbons, but it does display some interesting reactivity towards electrophiles. Reaction of

4.1 with elemental sulfur results in the formation of either $(\mu\text{-S})[\text{Cp}^*\text{Mo}(\text{NO})(\kappa^1\text{-dmpeS})]_2$ (**4.3**) or $\text{Cp}^*\text{Mo}(\text{NO})(\eta^2\text{-S}_2)(\kappa^1\text{-dmpeS})$ (**4.4**) depending on the ratio of reactants used. Complex **4.3** is, to the best of my knowledge, the only example of an organometallic bimetallic complex that contains a $\text{M}=\text{S}=\text{M}$ linkage, with no other bridging linkages between the two metal centres. Reaction of **4.1** with benzyl bromide results in $(\mu\text{-dmpe})[\text{Cp}^*\text{Mo}(\text{NO})\text{Br}_2]_2$ (**4.5**) and bibenzyl. This product suggests radical processes wherein bibenzyl is formed via homolytic coupling. In addition, reaction of **4.1** with bromoalkanes results in $[\text{Mo}(\text{NO})(\text{Br})_2(\kappa^2\text{-dmpe})]_2$ (**4.6**), alkane, olefin, and Cp^*H . This transformation most likely also involves radical processes and is a rare example of the liberation of Cp^*H from a transition-metal organometallic complex.

Lay Summary

This thesis describes investigations into synthesizing molybdenum- and tungsten-containing complexes that can activate, or break, C–H bonds in hydrocarbons, such as methane and ethane, in order to convert them into more valuable chemicals. This thesis describes the successful conversion of hydrocarbons into ketones mediated by a tungsten complex in such a way that the tungsten can be recycled and reused, thereby reducing chemical waste. Numerous other molybdenum- and tungsten-containing complexes have been synthesized, but have so far been unsuccessful in activating C–H bonds of hydrocarbons. Nevertheless, these complexes perform other interesting and attractive transformations, including examples of reactivity rarely seen in chemistry. Although these complexes do not perform the desired C–H activation chemistry, this research has established some new fundamental principles in the field of organometallic chemistry, and more investigations are needed to fully develop them.

Preface

Some of the research presented in this thesis was performed in collaboration with other members of the Legzdins group. Except where noted, all the research including the syntheses, reactions, characterization of compounds, and data analyses were carried out by the author (Aaron S. Holmes). The experimental design was developed by the author in collaboration with other members of the Legzdins group. All of the work presented in this thesis was performed under the supervision and guidance of Prof. Peter Legzdins.

All mass spectrometric data was collected by Mr. Marshall Lapawa and Mr. Marco Yeung, and elemental analyses were performed by Mr. Derek Smith, all of the UBC microanalytical facility. All GC analyses were performed by Dr. Yun Ling of the UBC microanalytical facility. X-ray crystallographic data collection, solution, and refinement for all solid-state molecular structures were performed by Dr. Brian O. Patrick of the UBC X-ray crystallography facility.

The work presented in Chapter 2, sections 2.2.1 and 2.4.2, has been reported in an article in the journal of *Inorganic Chemistry* published by the American Chemical Society as: Baillie, R. A.; Holmes, A. S.; Lefèvre, G. P.; Patrick, B. O.; Shree, M. V.; Wakeham, R. J.; Legzdins, P.; Rosenfeld D. C. *Inorg. Chem.* **2015**, *54*, 5915–5929. Reproduced with permission from *Inorganic Chemistry*. Copyright (2015) American Chemical Society. Portions of the text and some of the Figures and Schemes used were written or drawn by the author. The work presented in Chapter 2, excluding 2.2.1 and 2.4.2, has been reported in an article in the journal *Organometallics* published by the American Chemical Society as: Baillie, R. A.; Lefèvre, G. P.; Wakeham, R. J.; Holmes, A. S.; Legzdins, P. *Organometallics* **2015**, *34*, 4085–2092.

Reproduced with permission from Organometallics. Copyright (2015) American Chemical Society. Portions of the text and some of the Figures and Schemes used were written or drawn by the author.

The work presented in Chapter 3 has been reported in an article in the journal *Inorganic Chemistry* published by the American Chemical Society as: Fabulyak, D.; Handford, R. C.; Holmes, A. S.; Levesque, T. M.; Wakeham, R. J.; Patrick, B. O.; Legzdins, P.; Rosenfeld, D. C. *Inorg. Chem.* **2017**, *56*, 573–582. Reproduced with permission from *Inorganic Chemistry*. Copyright (2017) American Chemical Society. Portions of the text and some of the Figures and Schemes used were written or drawn by the author.

Table of Contents

Abstract.....	ii
Lay Summary	iv
Preface.....	v
Table of Contents	vii
List of Tables	xi
List of Figures.....	xii
List of Schemes	xiv
List of Abbreviations	xvi
Acknowledgements	xxii
Dedication	xxii
Chapter 1: Introduction	1
1.1 Nitrosyl Ligands in Organometallics	2
1.2 Work in the Legzdins Group with Cp*M(NO) Complexes	3
1.3 Scope of This Thesis.....	8
Chapter 2: Synthesis and Reactivity of Cp*W(NO)(H)(η^3-CH₂CHCHMe).....	11
2.1 Introduction.....	12
2.2 Results and Discussion	16
2.2.1 Synthesis of Cp*W(NO)(H)(η^3 -CH ₂ CHCHMe) (2.1).....	16
2.2.2 Reaction of 2.1 with Benzene and CO.....	18
2.2.3 Reaction of 2.1 with Mesitylene and CO.....	21
2.3 Summary.....	25

2.4	Experimental Section	26
2.4.1	General Methods	26
2.4.2	Preparation of Cp*W(NO)(H)(η^3 -CH ₂ CHCHMe) (2.1)	27
2.4.3	Reaction of 2.1 with Benzene and CO	31
2.4.4	Reaction of 2.1 with Mesitylene and CO	32
Chapter 3: Synthesis and Reactivity of Cp*W(NO)(R)(H)(L) Complexes		35
3.1	Introduction	36
3.2	Results and Discussion	38
3.2.1	Synthesis of <i>cis</i> -Cp*W(NO)(H)(κ^2 -PPh ₂ (C ₆ H ₄)) (3.1)	38
3.2.2	Attempted Synthesis of Cp*W(NO)(CH ₂ CMe ₃)(H)(PPh ₃)	40
3.2.3	Thermolysis of 3.1 in Hydrocarbons	42
3.2.3.1	Thermolysis reactions at 80 °C	42
3.2.3.2	Thermolysis reactions at 50 °C	43
3.2.4	Thermal Isomerization of 3.1 into <i>trans</i> -Cp*W(NO)(H)(κ^2 -PPh ₂ (C ₆ H ₄)) (3.2)	43
3.2.5	Synthesis of <i>trans</i> -Cp*W(NO)(CH ₂ CMe ₃)(H)(P(OPh) ₃) (3.3)	46
3.2.6	Synthesis of <i>trans</i> -Cp*W(NO)(H) ₂ (P(OPh) ₃) (3.4)	51
3.2.7	Related Cp*W(NO)(R)(H)(L) Systems within the Research Group	52
3.3	Summary	53
3.4	Experimental Section	54
3.4.1	General Methods	54
3.4.2	Synthesis of <i>cis</i> -Cp*W(NO)(κ^2 -PPh ₂ (C ₆ H ₄))(H) (3.1)	55
3.4.3	Isomerization of <i>cis</i> -Cp*W(NO)(κ^2 -PPh ₂ (C ₆ H ₄))(H)	56
3.4.4	Synthesis of <i>trans</i> -Cp*W(NO)(CH ₂ CMe ₃)(H)(P(OPh) ₃) (3.3)	57

3.4.5	Synthesis of <i>trans</i> -Cp*W(NO)(H) ₂ (P(OPh) ₃) (3.4)	59
3.4.6	X-ray Crystallography	60
Chapter 4: Synthesis and Reactivity of Cp*Mo(NO)(κ²-dmpe) Systems		63
4.1	Introduction.....	64
4.2	Results and Discussion	65
4.2.1	Synthesis of Cp*Mo(NO)(κ ² -dmpe) (4.1)	65
4.2.2	Reactions of 4.1 with Hydrocarbons.....	72
4.2.3	Reactions of 4.1 with Chalcogens.....	73
4.2.3.1	Synthesis of (μ-S)[Cp*Mo(NO)(κ ¹ -dmpeS)] ₂ (4.3).....	73
4.2.3.2	Synthesis of Cp*Mo(NO)(η ² -S ₂)(κ ¹ -dmpeS) (4.4)	82
4.2.3.3	Reaction of 4.1 with Oxygen	86
4.2.4	Reactions of 4.1 with Organic Halides	87
4.2.4.1	Reaction of 4.1 with Benzyl Bromide.....	87
4.2.4.2	Reaction of 4.1 with 1-Bromopropane.....	92
4.2.4.3	Reaction of 4.1 with 1-Bromooctane	97
4.2.4.4	Reaction of 4.1 with Bromobenzene.....	101
4.2.4.5	Reactions of 4.1 with Other Organic Halides	101
4.3	Summary.....	101
4.4	Experimental Section	103
4.4.1	General Methods.....	103
4.4.2	Synthesis of Cp*Mo(NO)(κ ² -dmpe) (4.1)	105
4.4.3	Synthesis of [Cp*Mo(NO)(Cl)(κ ² -dmpe)]Cl (4.2)	106
4.4.4	Synthesis of (μ-S)[Cp*Mo(NO)(κ ¹ -dmpeS)] ₂ (4.3).....	107

4.4.5	Synthesis of Cp*Mo(NO)(η^2 -S ₂)(κ^1 -dmpeS) (4.4)	109
4.4.6	Reaction of 4.1 with Oxygen	110
4.4.7	Reaction of 4.1 with Benzyl Bromide.....	111
4.4.8	Reaction of 4.1 with 1-Bromopropane.....	112
4.4.9	Reaction of 4.1 with 1-Bromooctane	114
4.4.10	Reaction of 4.1 with Bromobenzene	115
4.4.11	X-ray Crystallography	115
Chapter 5: Conclusion and Future Works		121
5.1	Summary and Conclusions	122
5.2	Future Directions	125
5.2.1	Optimization of the Conversion of Hydrocarbons and CO into Unsymmetrical Ketones as well as an Investigation of an Expanded Scope of Substrates.....	125
5.2.2	Investigation of Cp*M(NO)(R)(H)(L) Utilizing Bound Cyclopentadienyl-Phosphine Ligands	126
5.2.3	Mechanistic Investigations into the Reaction of 4.1 with Organic Halides as well as an Investigation of an Expanded Scope of Substrates	127
References		129
Appendices.....		139
Appendix A Supplementary Materials for Chapter 2		139
Appendix B Supplementary Materials for Chapter 3		143
Appendix C Supplementary Materials for Chapter 4		150

List of Tables

Table 3.1. X-ray crystallographic data for complex 3.3	62
Table 4.1. X-ray crystallographic data for complexes 4.1 , 4.2 , and 4.3	119
Table 4.2. X-ray crystallographic data for complexes 4.4 , 4.5 , and 4.6	120

List of Figures

Figure 2.1. Four solution molecular structures of the isomers of 2.1	18
Figure 2.2. (a) Isomers of complex 2.1 with the methyl substituent on the η^3 -allyl ligand proximal to the nitrosyl ligand, thus forming ketone 2.2a . (b) Isomers of complex 2.1 with the methyl substituent on the η^3 -allyl ligand proximal to the hydride ligand, thus forming ketone 2.2b	21
Figure 2.3. (a) Isomers of complex 2.1 with the methyl substituent on the η^3 -allyl ligand proximal to the nitrosyl ligand, thus forming ketone 2.3a upon reaction with mesitylene. (b) Isomers of complex 2.1 with the methyl substituent on the η^3 -allyl ligand proximal to the hydride ligand, thus forming ketone 2.3b upon reaction with mesitylene.....	23
Figure 3.1. (a) Expansions of ^1H and $^1\text{H}\{^{31}\text{P}\}$ NMR spectra (400 MHz, C_6D_6) from δ 3.79 to 4.20 ppm showing the hydride resonance of complex 3.1 . (b) Expansions of the ^1H and $^1\text{H}\{^{31}\text{P}\}$ NMR spectra (400 MHz, C_6D_6) from δ 2.10 to 2.50 ppm showing the hydride resonance of complex 3.2	45
Figure 3.2. Solid-state molecular structure of 3.3	49
Figure 3.3. View of the solid-state molecular structure of 3.3 along the W–Cp* axis displaying the vacant coordination slot between the phosphite and nitrosyl ligands where the hydride ligand resides	50
Figure 4.1. Solid-state molecular structure of 4.1	69
Figure 4.2. Solid-state molecular structure of 4.2	71
Figure 4.3. A portion of complex 4.3 displaying the κ^1 -dmpeS ligand and indicating the trend observed in the ^1H and ^{13}C APT NMR spectra in C_6D_6	75

Figure 4.4. Solid-state molecular structure of 4.3	79
Figure 4.5. View of the solid-state molecular structure of 4.3 along the C_2 axis of symmetry that relates the two crystallographically equivalent halves of the bimetallic molecule.....	80
Figure 4.6. Solid-state molecular structure of 4.4	85
Figure 4.7. Expansion of the $^{31}\text{P}\{^1\text{H}\}$ NMR spectrum (162 MHz, C_6D_6) from 19.8 to 40.8 ppm of the complex resulting from the exposure of 4.1 to O_2	87
Figure 4.8. The major disordered fragment of the solid-state molecular structure of 4.5	91
Figure 4.9. The major component of the solid-state molecular structure of 4.6	96
Figure 4.10. View of the major component of the solid-state molecular structure of complex 4.6 along the $\text{Br}(2)\text{--Br}(2)'$ axis showing the inversion centre symmetry that relates the two halves of the bimetallic molecule	97
Figure 4.11. Expansion of the ^1H NMR spectrum (400 MHz, C_6D_6) from δ 2.14 to 6.44 ppm showing the resonances attributable to the two methine protons of <i>trans</i> -2-octene and the single non-methyl proton of pentamethylcyclopentadiene and their relative integrations.....	99
Figure 5.1. Examples found in the literature of complexes possessing a bidentate cyclopentadienyl-phosphine ligand	127

List of Schemes

Scheme 1.1. Preparation of Cp'M(NO)- and Cp'M(NO) ₂ -containing complexes	4
Scheme 1.2. General synthesis of Cp*W(NO)(H)(η ³ -allyl) complexes	4
Scheme 1.3. General synthesis of Cp*W(NO)(R)(H)(L) complexes	5
Scheme 1.4. Synthesis of Cp*Mo(NO)(κ ² -dmpe)	5
Scheme 1.5. Some characteristic chemistry of CpW(NO)(CH ₂ SiMe ₃) ₂	6
Scheme 1.6. Some thermal chemistry of Cp*W(NO)(=CHCMe ₃) that is generated by thermolysis of Cp*W(NO)(CH ₂ CMe ₃) ₂	7
Scheme 1.7. Thermolyses of Cp*W(NO)(CH ₂ CMe ₃) ₂ and Cp*W(NO)(H)(η ³ -allyl) in <i>n</i> -alkanes	8
Scheme 2.1. Early examples of C–H activations reported by (a) Bergman and (b) Graham.....	13
Scheme 2.2. Selective terminal C–H activations of hydrocarbons by Cp*W(NO)(CH ₂ CMe ₃)(η ³ -allyl) complexes	14
Scheme 2.3. Syntheses of unsymmetrical ketones.....	15
Scheme 2.4. Synthesis of Cp*W(NO)(H)(η ³ -CH ₂ CHCHMe) (2.1)	17
Scheme 2.5. One-pot reaction of complex 2.1 with benzene and CO	19
Scheme 2.6. Proposed mechanism of the one-pot conversion mediated by complex 2.1	20
Scheme 2.7. One-pot reaction of 2.1 with mesitylene and CO.....	22
Scheme 2.8. Formation of unsymmetrical ketones	24
Scheme 3.1. Activation of C ₆ H ₆ by <i>trans</i> -Cp*W(NO)(CH ₂ SiMe ₃)(H)(PMe ₃)	36
Scheme 3.2. C–H activation of C ₆ H ₆ by <i>cis</i> -Cp*W(NO)(H)(κ ² -PPh ₂ (C ₆ H ₄)).....	37
Scheme 3.3. Synthesis and proposed mechanism for 3.1	39
Scheme 3.4. Attempted synthetic route for Cp*W(NO)(CH ₂ CMe ₃)(H)(PPh ₃).....	41

Scheme 3.5. Possible isomerization of 3.1 into 3.2 upon heating	44
Scheme 3.6. Synthesis of complex 3.3	47
Scheme 3.7. Synthesis of complex 3.4	51
Scheme 4.1. Lewis-Acid Induced Intramolecular C–H Activation	64
Scheme 4.2. Two-step synthesis of 4.1	66
Scheme 4.3. Reaction of 4.1 with a stoichiometric amount of elemental sulfur	74
Scheme 4.4 Reaction of 4.1 with an excess of elemental sulfur	82
Scheme 4.5. Reaction of 4.1 with benzyl bromide	88
Scheme 4.6. Reaction of complex 4.1 with two equivalents of benzyl bromide	89
Scheme 4.7. Reaction of 4.1 with 1-bromopropane	92
Scheme 4.8. Identified products of the reaction of 4.1 with 5 equiv 1-bromopropane	94
Scheme 4.9. Reaction of 4.1 with 1-bromooctane	100
Scheme 4.10. General reaction of complex 4.1 with 1-bromopropane	100

List of Abbreviations

1D	1-dimensional
Å	angstrom, 10^{-10} m
anal.	analysis
APT	attached proton test
atm	atmosphere
β	beta, the position twice removed from the point of reference
bpy	2,2'-bipyridine
br	broad (spectral)
^{13}C	carbon-13
$^{13}\text{C}\{^1\text{H}\}$	proton-decoupled carbon-13
ca.	circa (approximately)
calcd	calculated
cm^{-1}	wavenumber
CO	carbon monoxide
coe	cyclooctene
COSY	correlation spectroscopy
Cp	cyclopentadienyl, $\eta^5\text{-C}_5\text{H}_5$
$\text{Cp}^{i\text{-Pr}}$	isopropylcyclopentadienyl, $\eta^5\text{-C}_5\text{H}_4i\text{-Pr}$
Cp^*	pentamethylcyclopentadienyl, $\eta^5\text{-C}_5\text{Me}_5$
D	deuterium, ^2H

d	doublet (spectral); day
dd	doublet of doublets (spectral)
ddd	doublet of doublets of doublets (spectral)
°	degree (of angle or temperature)
deg	degree (angle)
°C	degrees Celcius
Δ	heat
δ	delta, chemical shift in ppm
dtcb	<i>trans</i> -2-[3-(4- <i>tert</i> -butylphenyl)-2-methyl-2-propenylidene]malononitrile
DFT	density field theory
dmpe	1,2-bis(dimethylphosphino)ethane
dmpeS	(2-(dimethylphosphino)ethyl)dimethylphosphine sulfide
dppe	1,2-bis(diphenylphosphino)ethane
EA	elemental analysis
Eds.	editors
e.g.	for example
EI	electron impact
equiv	equivalents
ESI	electrospray ionization
ESR	electron spin resonance
Et	ethyl, C ₂ H ₅
EtOAc	ethyl acetate

eV	electron volt
η	eta, used to denote hapticity
FT-IR	Fourier transform infrared
g	gram
GC	gas chromatography
GCMS	gas chromatography-mass spectrometry
^1H	proton, hydrogen
$^1\text{H}\{^{31}\text{P}\}$	phosphorus-decoupled proton
h	hour
HMBC	heteronuclear multiple-bond correlation
HRMS	high-resolution mass spectrometry
HREI	high-resolution electron impact
HSQC	heteronuclear single-quantum correlation
Hz	hertz
<i>i</i> -Pr	isopropyl, C_3H_7
IR	infrared
irrad.	irradiated
<i>J</i>	coupling constant
$^nJ_{\text{AB}}$	<i>n</i> -bond coupling constant between atoms A and B
κ	kappa, used to denote denticity
LA	Lewis acid
LDI	laser desorption ionization

LREI	low-resolution electron impact
<i>m</i>	meta
m	multiplet (spectral)
M	molarity, mol/L
M ⁺	molecular ion
MALDI	matrix assisted laser desorption ionization
Me	methyl, CH ₃
Mes	mesityl, CH ₂ (3,5-(CH ₃) ₂ C ₆ H ₃)
mg	milligram
MHz	megahertz
min	minute
mL	millilitre
mmol	millimole
mol	mole
⁹² Mo	molybdenum-92
⁹⁸ Mo	molybdenum-98
mp	melting point
MS	mass spectrometry
μ	mu, denotes a bridging ligand
<i>m/z</i>	mass-to-charge ratio
<i>n</i>	normal
NMR	nuclear magnetic resonance

NO	nitrosyl
NOE	nuclear Overhauser effect
NOESY	nuclear Overhauser effect spectroscopy
ν	nu, stretching frequency
<i>o</i>	ortho
<i>p</i>	para
^{31}P	phosphorus-31
$^{31}\text{P}\{^1\text{H}\}$	proton-decoupled phosphorus-31
pent	pentet (spectral)
π	pi
Ph	phenyl, C_6H_5
ppm	parts per million
psig	pounds per square inch gauge
q	quartet (spectral)
r.t.	room temperature
σ	sigma
1D NOE	1D selective nuclear Overhauser effect
s	singlet (spectral); strong (spectral)
sext	sextet (spectral)
t	triplet (spectral)
<i>t</i> -Bu	<i>tert</i> -butyl, C_4H_9
THF	tetrahydrofuran

TOF	time of flight
UV	ultraviolet
vw	very weak (spectral)
w	weak (spectral)
^{182}W	tungsten-182
^{183}W	tungsten-183
^{184}W	tungsten-184
^{186}W	tungsten-186
xs	excess
Xantphos	4,5-bis(diphenylphosphino)-9,9-dimethylxanthene
•	used to denote a radical

Acknowledgements

My greatest thanks has to go to my supervisor, Prof. Peter Legzdins. Without him, I would not be where I am at this moment, and I am ever thankful for having met him during my undergraduate studies. To be frank, I was a lazy and unmotivated undergraduate student who was okay with just doing okay. But that changed that when I met with Prof. Legzdins and expressed an interest in doing undergraduate research under his supervision. Peter told me that I needed to show that I was capable and invested, and he also told me some hard, but honest, truths. And so, thank you Peter, for knocking some sense in to me. I needed it, and it got me to where I am right now, and I kind of like where I am in life at the moment.

I also have to say thank you to my parents, Pattarida and John— better known as mum and dad. Without your love, help, and support through my entire university career, this would not have been possible.

I would like to say thank you to all the wonderful people I've met and worked alongside in the lab. You all taught me so much and made this whole process so much fun. I am glad I met all of you, and you have all helped me grow and mature in your own way. I hope we all stay in contact for many years to come.

I would also like to thank my close friends who have made this all so enjoyable and helped keep me sane when the chemistry was driving me insane.

And last but not least, I would like to thank The DOW Chemical Company for providing the funding that made this work possible.

To my friends and family who made this all so much fun.

Chapter 1: Introduction

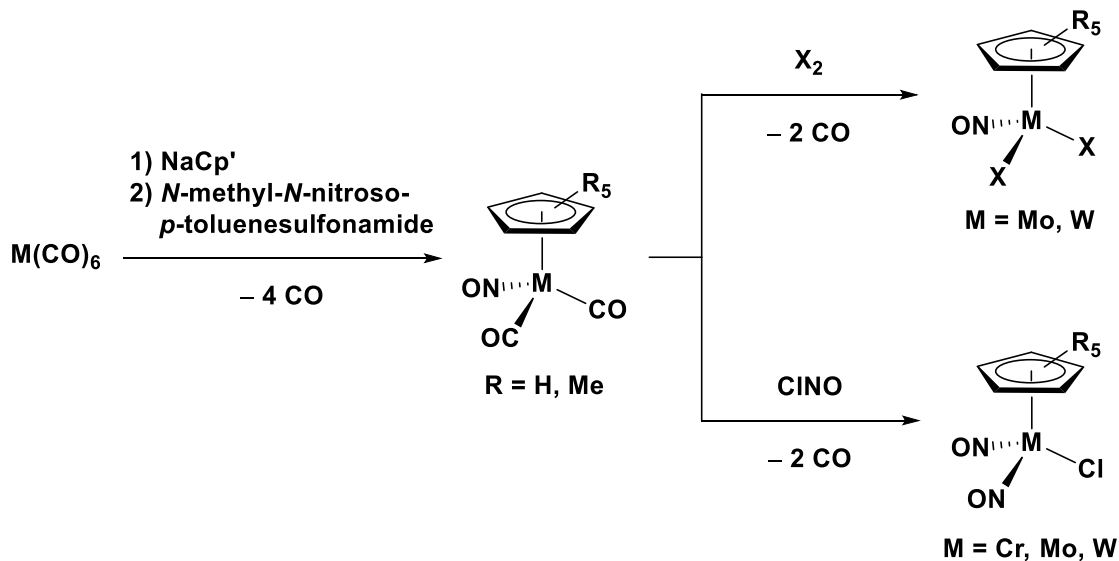
1.1 Nitrosyl Ligands in Organometallics

The use of nitric oxide [NO] as a ligand in transition-metal [M] chemistry to form complexes containing M–NO linkages imparts unique chemistry both to the metal centre and the nitrosyl ligand itself.¹ The chemistry of metal-nitrosyl complexes continues to attract the attention of scientists for a variety of reasons.^{1–3} For instance, the important role that nitric oxide plays in the environment since it has been implicated in the depletion of the ozone layer as well as in the formation of photochemical smog and acid rain.⁴ Another example of the significance of nitric oxide is its involvement in biological systems, such as its role as a signalling molecule in blood-pressure regulation and neural communication,⁵ or its use as a bioimaging agent wherein nitric oxide can be detected via imaging techniques such as ESR and fluorometry.⁶ In both of the aforementioned roles, metal ions are known to mediate some of the processes, and so establishment of the characteristic reactivity of bound nitric oxide is still a focus of worldwide research.⁷ A third feature of metal-nitrosyl chemistry, and foremost with respect to this thesis, is the characteristic chemistry of the metal-nitrosyl complexes themselves.⁸ Nitric oxide is a strong π -acceptor ligand that stabilizes metals in relatively low oxidation states, and this results in complexes wherein the metal centres display chemical properties that are often markedly different from those exhibited by their isoelectronic and isostructural carbonyl complexes that contain M–CO bonds, even though CO is also a relatively strong π -acceptor ligand. The unique chemistry of metal-nitrosyl complexes has been illustrated within the work of the Legzdins group through our research of the diverse physical and chemical properties of cyclopentadienyl nitrosyl group 6 metal complexes.

1.2 Work in the Legzdins Group with Cp'M(NO) Complexes

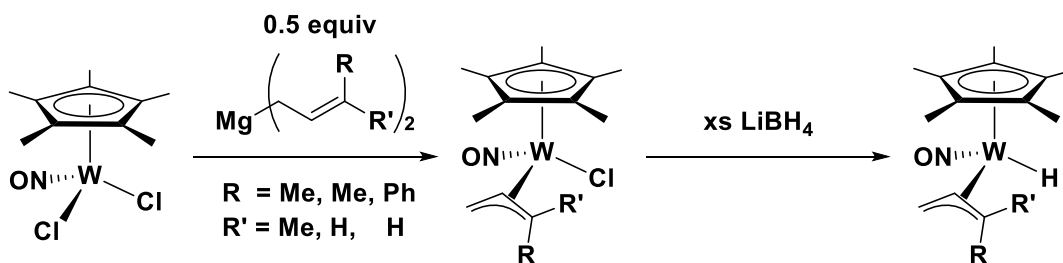
The vast majority of complexes that have been studied within the Legzdins group contain the 14e Cp'M(NO) [Cp' = η^5 -C₅H₅ (Cp) or η^5 -C₅Me₅ (Cp*); M = Cr, Mo, or W] core fragment that serves as a molecular scaffold on which various organometallic and inorganic complexes are constructed. These complexes originate from the precursor Cp'M(NO)(CO)₂ compounds which are readily synthesized from sequential reactions of commercially available M(CO)₆ with NaCp' and *N*-methyl-*N*-nitroso-*p*-toluene sulfonamide in THF (Scheme 1.1).⁹ Reaction of Cp'M(NO)(CO)₂ compounds with ClNO in CH₂Cl₂ affords Cp'M(NO)₂Cl precursor complexes¹⁰⁻¹² which can undergo metathesis reactions with a range of reagents in order to form other Cp'M(NO)₂R derivatives.¹³⁻¹⁵ A subsequent reaction of Cp'Mo(NO)(CO)₂ or Cp'W(NO)(CO)₂ with a source of X₂ [X = halogen], wherein the most commonly used reagent is PCl₅, results in the corresponding dihalide complexes which are used as convenient precursors for a host of Cp'M(NO)R₂ complexes.^{16,17} These molybdenum and tungsten Cp'M(NO)X₂ complexes possess a dimeric halide-bridged structure in the solid state; however, the physical and chemical properties of the compounds in donor solvents are consistent with their existing as solvated monomers.¹⁸ Consequently, they are exclusively represented by their monomeric formulae throughout this thesis.

Scheme 1.1. Preparation of Cp'M(NO)- and Cp'M(NO)₂-containing complexes



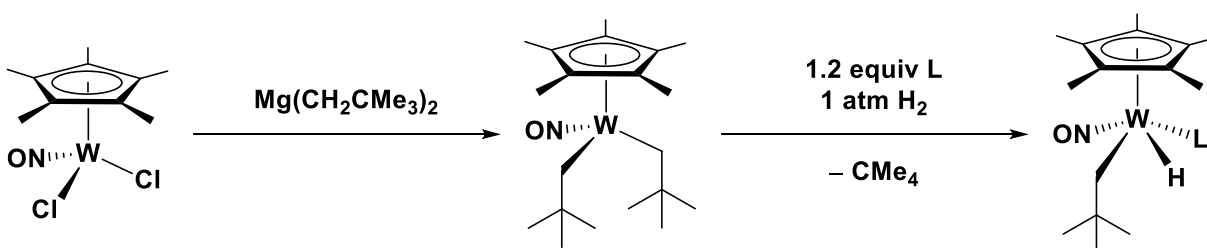
From the Cp'M(NO)Cl₂ precursor complexes, a wide range of organometallic compounds possessing the Cp'M(NO) fragment with different ancillary ligands can be synthesized. In essence, all the complexes discussed in this thesis can be traced back to these precursor complexes. For example, the synthesis of Cp*W(NO)(H)(η³-allyl) complexes is carried out by reacting the Cp*W(NO)Cl₂ precursor with a stoichiometric amount of an appropriate allyl-binary reagent followed by the addition of lithium borohydride (Scheme 1.2).

Scheme 1.2. General synthesis of Cp*W(NO)(H)(η³-allyl) complexes



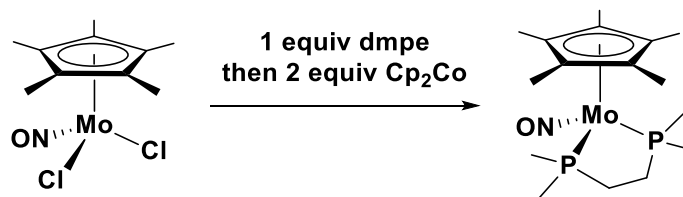
Various $\text{Cp}^*\text{W}(\text{NO})(\text{R})(\text{H})(\text{L})$ [R = alkyl, L = Lewis base] complexes can also be synthesized from $\text{Cp}^*\text{W}(\text{NO})\text{Cl}_2$. Reaction of $\text{Cp}^*\text{W}(\text{NO})\text{Cl}_2$ with $\text{Mg}(\text{CH}_2\text{CMe}_3)_2$ in solution results in the formation of $\text{Cp}^*\text{W}(\text{NO})(\text{CH}_2\text{CMe}_3)_2$, which is then used to synthesize the various $\text{Cp}^*\text{W}(\text{NO})(\text{R})(\text{H})(\text{L})$ complexes. Summarized in Scheme 1.3 is the general synthesis of these complexes, starting from the $\text{Cp}^*\text{W}(\text{NO})\text{Cl}_2$ precursor, wherein the final step is a reaction of $\text{Cp}^*\text{W}(\text{NO})(\text{CH}_2\text{CMe}_3)_2$ in solution with a Lewis base under a hydrogen atmosphere.

Scheme 1.3. General synthesis of $\text{Cp}^*\text{W}(\text{NO})(\text{R})(\text{H})(\text{L})$ complexes



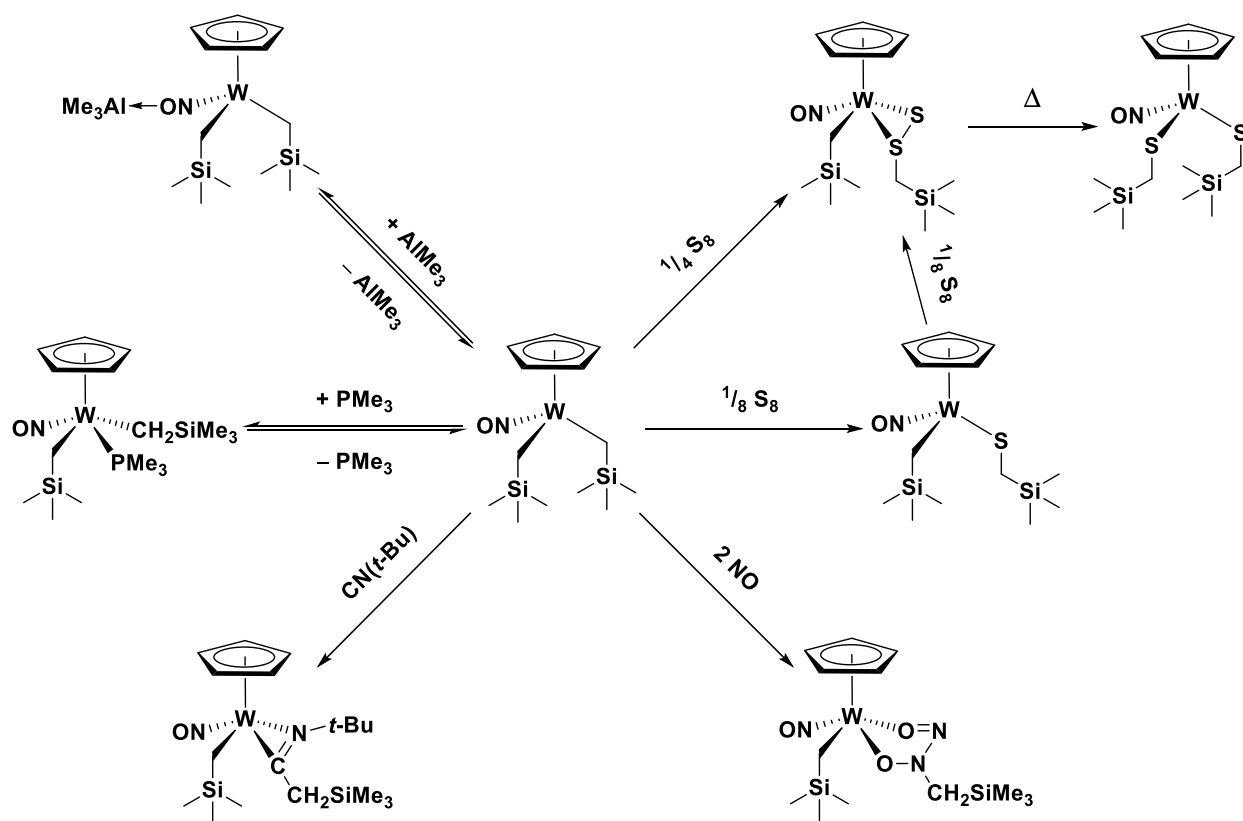
Complexes possessing a bidentate bisphosphine ligand also can be conveniently synthesized from reactions of the $\text{Cp}^*\text{M}(\text{NO})\text{Cl}_2$ precursors with the bisphosphine proligand followed by a subsequent reduction of the metal centres. For example, summarized in Scheme 1.4 is the reaction of $\text{Cp}^*\text{Mo}(\text{NO})\text{Cl}_2$ with dmpe [dmpe = 1,2-bis(dimethylphosphino)ethane] and cobaltocene which results in the complex $\text{Cp}^*\text{Mo}(\text{NO})(\kappa^2\text{-dmpe})$.

Scheme 1.4. Synthesis of $\text{Cp}^*\text{Mo}(\text{NO})(\kappa^2\text{-dmpe})$



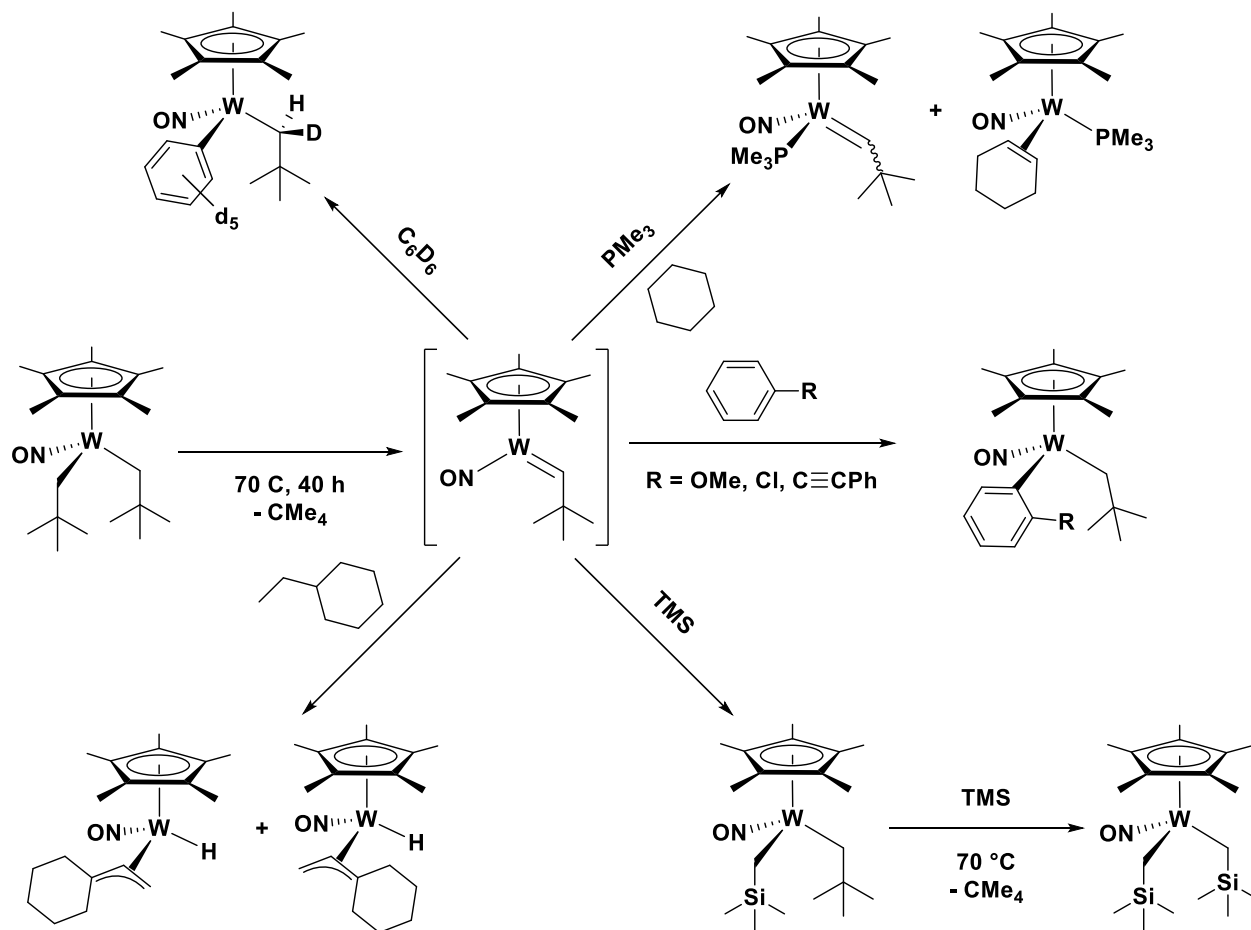
Previous work in the Legzdins group has established that these Cp'M(NO)-containing complexes display a large range of interesting chemistry.¹⁹ For instance, the Lewis acidity of 16e CpW(NO)(CH₂SiMe₃)₂ is clearly illustrated by the various transformations summarized in Scheme 1.5.

Scheme 1.5. Some characteristic chemistry of CpW(NO)(CH₂SiMe₃)₂



In addition, thermolyses of Cp'M(NO)(alkyl)₂ complexes in some hydrocarbon solvents result in the elimination of alkane and formation of transient 16e Cp'M(NO)(alkylidene) species that effect a variety of C–H activation reactions, as illustrated for Cp*W(NO)(CH₂CMe₃)₂ in Scheme 1.6.

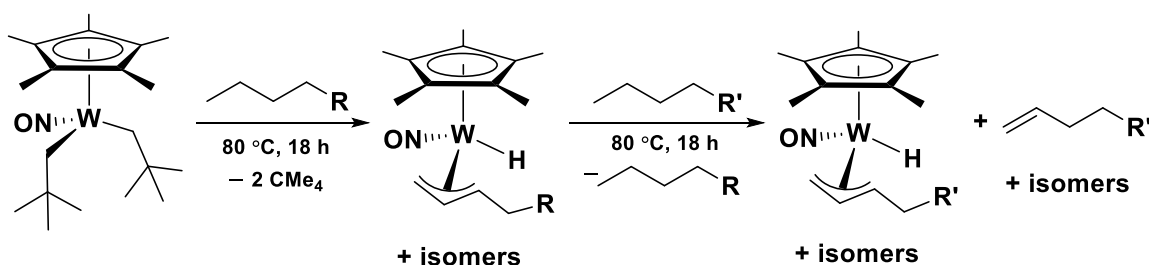
Scheme 1.6. Some thermal chemistry of $\text{Cp}^*\text{W}(\text{NO})(=\text{CHCMe}_3)$ that is generated by thermolysis of $\text{Cp}^*\text{W}(\text{NO})(\text{CH}_2\text{CMe}_3)_2$



Consistent with the thermal chemistry summarized in Scheme 1.6, the thermolysis of $\text{Cp}^*\text{W}(\text{NO})(\text{CH}_2\text{CMe}_3)_2$ in neat solutions of linear alkanes results in three successive C–H activations of the hydrocarbon substrates and results in the formation of $\text{Cp}^*\text{W}(\text{NO})(\text{H})(\eta^3\text{-allyl})$ complexes wherein the $\eta^3\text{-allyl}$ ligand is derived from the hydrocarbon substrate (Scheme 1.7).²⁰ These allyl hydrido compounds exist in solution as multiple isomers that differ by the orientation of their allyl ligands. Interestingly, further thermolysis of these allyl complexes in a solution of a

different *n*-alkane substrate results in allyl ligand exchange and the formation of a new Cp*W(NO)(H)(η^3 -allyl) complex wherein the allyl ligand is derived from the new alkane substrate. Additionally, alkenes derived from the original allyl ligand are formed from thermolysis and thus, overall, the Cp*W(NO)(CH₂CMe₃)₂ complex is mediating the dehydrogenation of *n*-alkanes into alkenes.

Scheme 1.7. Thermolyses of Cp*W(NO)(CH₂CMe₃)₂ and Cp*W(NO)(H)(η^3 -allyl) in *n*-alkanes



The work described in this thesis extends these previous investigations to encompass new chemistry exhibited by Cp*W(NO)(H)(η^3 -allyl), Cp*W(NO)(R)(H)(L), and Cp*Mo(NO)(κ^2 -dmpe) complexes as outlined in the next section.

1.3 Scope of This Thesis

A few overarching questions arise from the investigations into Cp*M(NO)-containing complexes. The first question addressed in this thesis is whether the C–H activating ability seen in some Cp*W(NO)- or Cp*Mo(NO)-containing complexes, such as the thermal chemistry of the Cp*W(NO)(CH₂CMe₃)₂ compound, can be extended to other novel systems that contain this 14e

fragment but with different ancillary ligands. Furthermore, will these new systems be able to mediate not only the C–H activation, but also the C–H functionalization of hydrocarbon substrates into larger more complex molecules? Additionally, can this be done via complete synthetic or catalytic cycles wherein the organometallic products can be readily converted back to the reactive species? If these novel complexes cannot effect the C–H activation of hydrocarbons, what type of characteristic chemistry do these complexes exhibit? Specifically, what chemistry do these complexes show towards electrophiles?

Chapter 2 presents the synthesis and chemistry of the $\text{Cp}^*\text{W}(\text{NO})(\text{H})(\eta^3\text{-CH}_2\text{CHCHMe})$ complex, wherein investigations into C–H activations of hydrocarbon substrates performed by the complex are discussed. Similar complexes have been shown to effect the C–H activation of hydrocarbon substrates, and thus the C–H activating ability of $\text{Cp}^*\text{W}(\text{NO})(\text{H})(\eta^3\text{-CH}_2\text{CHCHMe})$ is of high interest. The subsequent functionalization of the hydrocarbyl ligands into more complex chemical entities is also described, and a full synthetic cycle wherein hydrocarbon substrates are converted into more complex chemicals is presented.

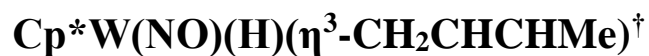
Chapter 3 discusses the syntheses and properties of $\text{Cp}^*\text{W}(\text{NO})(\text{R})(\text{H})(\text{L})$ complexes, wherein L is a phosphine or phosphite ligand and R is an alkyl ligand. Complexes of this type have, in the past, been shown to mediate the $\text{C}(sp^2)\text{-H}$ activation of benzene. Thus, various novel complexes have been synthesized in order to study their characteristic chemistry towards hydrocarbons and C–H activation in an attempt to further this field. Each complex has been successfully isolated and characterized, and an interesting spectroscopic trend is observed that provides insight into the stereochemistry of all the compounds discussed. This study aims to answer the question as to whether C–H activation chemistry can be reproduced in similar RHL systems utilizing different Lewis bases, and if so, to expand the scope of activated hydrocarbon

substrates to include *n*-alkanes. Finally, this study provides insight into how the different Lewis bases can affect the physical and chemical properties of these types of complexes.

Chapter 4 discusses the investigations involving the Cp*Mo(NO)(κ^2 -dmpe) complex. This complex is a direct transition from Chapter 3 wherein the RHL complexes are plagued by problems that arise from the lability of the L ligands. Instead of monodentate Lewis base ligands, this study aims to circumvent some of those problems by using bidentate Lewis base ligands. Additionally, will the lability of phosphine and phosphite ligands, shown in the investigations of RHL systems, result in hemilabile ligands wherein a partial dissociation into a 16e Cp*Mo(NO)(κ^1 -dmpe) transition state complex is possible? Investigations into what characteristic chemistry the complex can perform with electrophiles is also discussed, and some interesting chemical reactions mediated by the complex, including some examples of rare chemical transformations in organometallic chemistry, are highlighted.

Chapter 5 presents the overall summary and conclusion of the research discussed in this thesis along with suggestions for potential future directions.

Chapter 2: Synthesis and Reactivity of

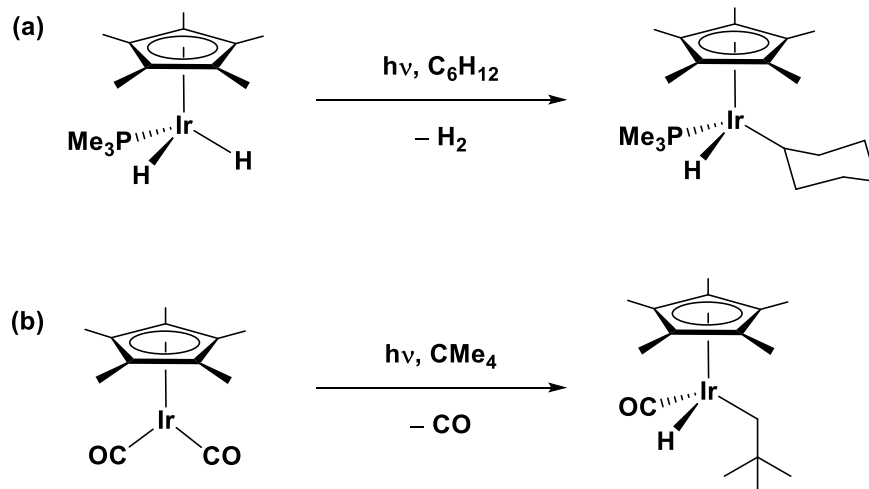


[†]Versions of this chapter has been published. Baillie, R. A.; Holmes, A. S.; Lefèvre, G. P.; Patrick, B. O.; Shree, M. V.; Wakeham, R. J.; Legzdins, P.; Rosenfeld, D. C. *Inorg. Chem.* **2015**, *54*, 5915–5929, and Baillie, R. A.; Lefèvre, G. P.; Wakeham, R. J.; Holmes, A. S.; Legzdins, P. *Organometallics* **2015**, *34*, 4085–4092. Reproduced with permission from Inorganic Chemistry and Organometallics. Copyright (2015) American Chemical Society.

2.1 Introduction

The selective functionalization of C–H bonds continues to attract interest from synthetic, biological, and theoretical chemists since recent advances in this field have begun to realize some of the early promise of this chemistry for the straightforward conversion of relatively simple substrates into more complex chemical entities.^{21–24} The functionalization of alkanes was first reported in the 1960s and 1970s wherein C–H bonds of saturated hydrocarbons were converted into C–Cl and C–O linkages,²⁵ but only later in the early 1980s was the intermolecular C–H activation of saturated alkanes reported by both the Bergman and Graham research groups utilizing iridium complexes (Scheme 2.1).^{26,27} In both of these reactions, the photolysis of the complexes with UV light results in the formation of reactive intermediate complexes that effect the C–H activation of hydrocarbon substrates resulting in η^1 -hydrocarbyl complexes. Although both of these early examples utilize Group 9 metal centres, this discovery opened up the field of C–H activation chemistry mediated by transition-metal centres,²⁵ and since then numerous advances have been made in this field and have expanded this chemistry to other metals in the *d*-block series.²⁸

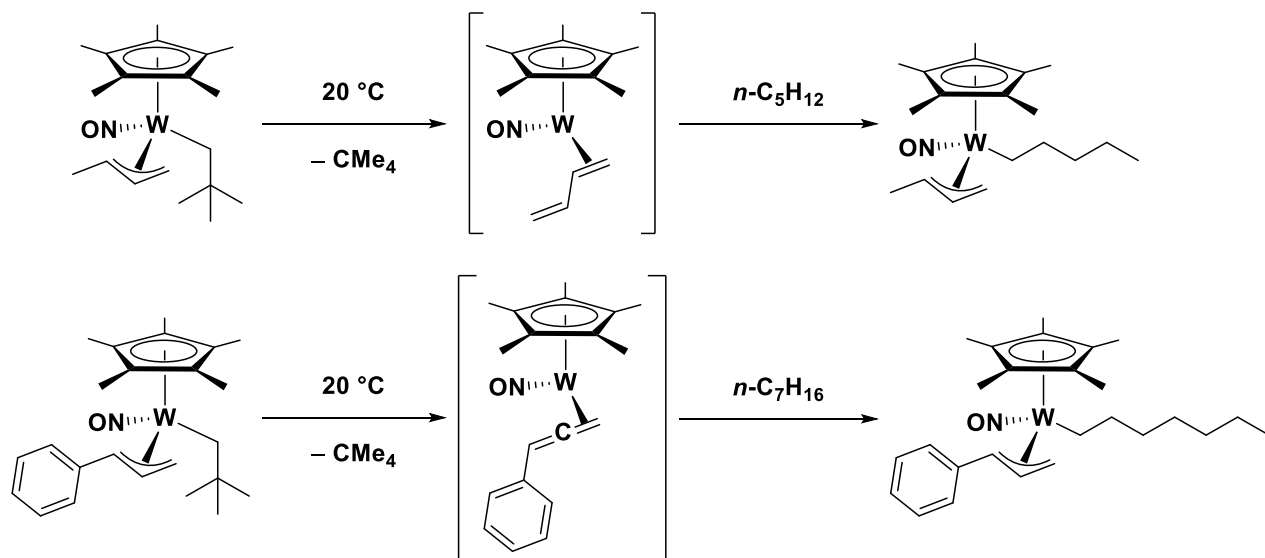
Scheme 2.1. Early examples of C–H activations reported by (a) Bergman and (b) Graham



An example of our recent contributions within the research group towards this field have involved the development of several 18e $\text{Cp}^*\text{W}(\text{NO})(\text{CH}_2\text{CMe}_3)(\eta^3\text{-allyl})$ [$\text{Cp}^* = \eta^5\text{-C}_5\text{Me}_5$] compounds for the selective single activations of terminal $\text{C}(sp^3)\text{-H}$ bonds of hydrocarbon substrates to produce isolable η^1 -hydrocarbyl complexes,²⁹ such as the activation of hydrocarbons by $\text{Cp}^*\text{W}(\text{NO})(\text{CH}_2\text{CMe}_3)(\eta^3\text{-CH}_2\text{CHCHMe})$ and $\text{Cp}^*\text{W}(\text{NO})(\text{CH}_2\text{CMe}_3)(\eta^3\text{-CH}_2\text{CHCHPh})$ to form the products depicted in Scheme 2.2.^{30,31} The newly formed hydrocarbyl ligands in these compounds may then be functionalized and released by a variety of reagents.²⁹

Scheme 2.2. Selective terminal C–H activations of hydrocarbons by

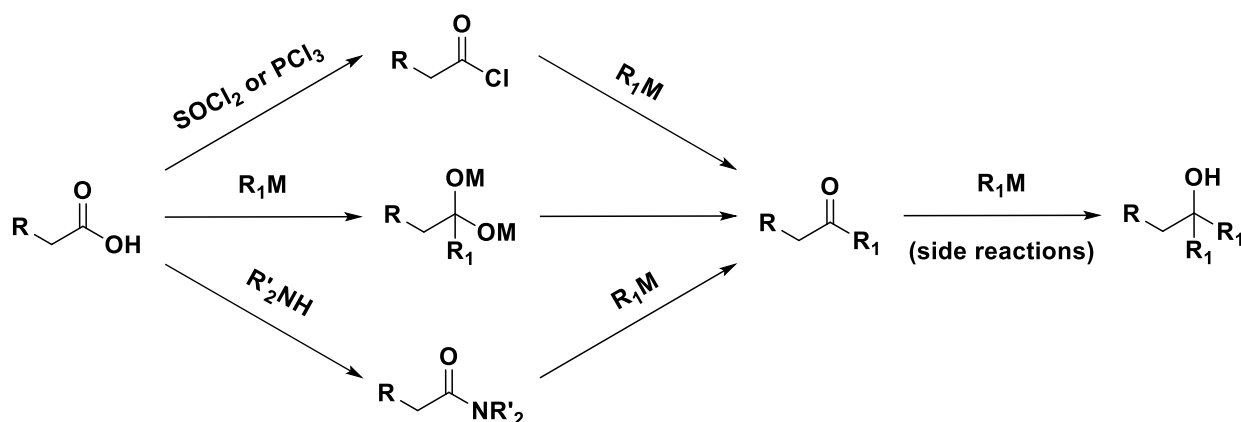
$\text{Cp}^*\text{W}(\text{NO})(\text{CH}_2\text{CMe}_3)(\eta^3\text{-allyl})$ complexes



This chapter describes investigations into a related $18\text{e } \text{Cp}^*\text{W}(\text{NO})(\text{H})(\eta^3\text{-allyl})$ complex and the unprecedented chemistry effected by the complex. This 18e complex can effect the activation of hydrocarbon $\text{C}(\text{sp}^3)\text{-H}$ and $\text{C}(\text{sp}^2)\text{-H}$ bonds under a high pressure of CO that ultimately results in the liberation of unsymmetrical ketones via the formation of new C–C bonds. The new methodology for preparing such ketones complements existing synthetic methods. In addition, this new method of forming unsymmetrical ketones from unfunctionalized hydrocarbons and CO is not only atom-economical, but is also part of a complete synthetic cycle wherein the final organometallic product, namely $\text{Cp}^*\text{W}(\text{NO})(\text{CO})_2$, can be conveniently converted back into the hydrido allyl reactant via $\text{Cp}^*\text{W}(\text{NO})\text{Cl}_2$, which is cleanly obtained by treatment of the dicarbonyl nitrosyl complex with PCl_5 .³²

The synthesis of unsymmetrical ketones has received considerable attention due to their use as reagents in many organic transformations.^{33–35} Commonly employed methods for the syntheses of these ketones involve transition-metal mediated reactions (e.g. carbonylative Stille reactions), but these usually employ costly metals such as palladium or use toxic reagents such as alkyl tin compounds.^{36–38} Additionally, reactive substrates such as carboxylic acid derivatives have also been utilized for this purpose,³⁹ as has cross-coupling between pre-existing ketones.⁴⁰ For instance, a typical synthesis for unsymmetrical ketones begins with the derivatization of carboxylic acid to an acid chloride or an amide functional group before treatment with an organometallic reagent, or with the direct treatment of the carboxylic acid with the organometallic reagent, or with the direct treatment of the carboxylic acid with the organometallic reagent (Scheme 2.3). However, these methods can pose significant complications due to the reactivity of the substrates and unwanted side reactions of the products.^{33–35} Thus, a new synthetic method wherein these ketones can be produced cleanly without the use of expensive transition-metal complexes or highly reactive compounds is desirable.

Scheme 2.3. Syntheses of unsymmetrical ketones

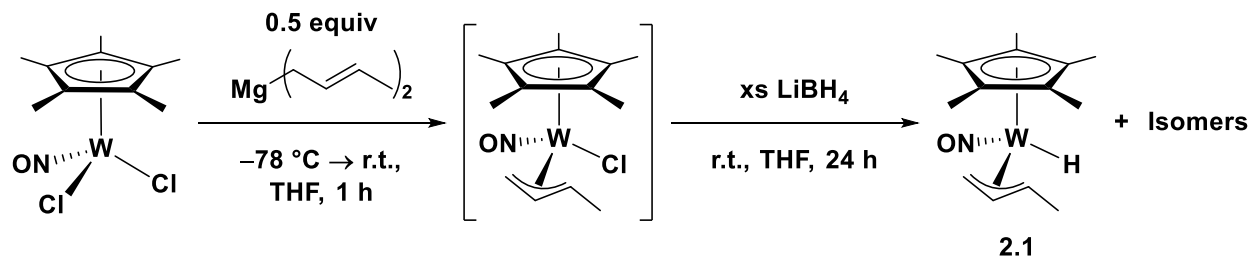


2.2 Results and Discussion

2.2.1 Synthesis of Cp*W(NO)(H)(η^3 -CH₂CHCHMe) (**2.1**)

Complex Cp*W(NO)(H)(η^3 -CH₂CHCHMe) (**2.1**) is synthesized from a two-step single-pot metathesis reaction of Cp*W(NO)Cl₂, Mg(CH₂CH=CHMe)₂, and LiBH₄ in THF (Scheme 2.4). The addition of a stoichiometric amount of Mg(CH₂CH=CHMe)₂ to Cp*W(NO)Cl₂ is carried out at -78 °C in THF, and after the addition the reaction mixture is allowed to warm to ambient temperatures while being stirred for at least 1 h to produce the intermediate complex, Cp*W(NO)(η^3 -CH₂CHCHMe)Cl. This 18e intermediate complex can be isolated, but such isolation is not necessary for the synthesis (and can even diminish the overall yield) of complex **2.1**. An excess of LiBH₄ is then added slowly to the reaction mixture, and the mixture is stirred for 24 hours. LiBH₄ is used as the hydride reagent because it gives more consistent results and higher yields of the hydride complexes than other reagents investigated, such as LiAlH₄ and NaBH₄.⁴¹ The excess LiBH₄ is then quenched with water in Et₂O, and the formed salts are removed by liquid-liquid extractions. Purification of **2.1** is carried out by flash column chromatography on a neutral alumina support, wherein the complex elutes as a yellow band with a gradient of 0–20% EtOAc in hexanes. Recrystallization of **2.1** from hexanes at -30 °C results in an analytically pure, yellow solid in a 19% yield.

Scheme 2.4. Synthesis of Cp*W(NO)(H)(η^3 -CH₂CHCHMe) (2.1)



The identification and NMR characterization of the isomers of **2.1** (Figure A.1) as well as the characterization of the complex in the solid-state by single-crystal X-ray diffraction was carried out by Dr. Rhett A. Baillie.⁴² The synthesis outlined above was performed by the author. The spectroscopic data are consistent with complex **2.1** existing as four coordination isomers in solution that differ by the orientation of the η^3 -allyl ligand, which can have an endo or an exo orientation with the methyl substituent either proximal or distal to the nitrosyl ligand (Figure 2.1). Isomer **2.1a** is produced in the greatest amount compared to the other three isomers, and it possesses a η^3 -CH₂CHCHMe ligand in an endo orientation in which the methyl substituent is proximal to the hydride. The favoured formation of isomer **2.1a** is likely a steric effect. Complex **2.1** has a melting point of 75–78 °C, and its reversibility has been established by dissolving the melt residue in C₆D₆ and analyzing it by ¹H NMR spectroscopy which reveals that the ¹H NMR spectrum of the melt residue matches that of **2.1**. Complex **2.1** is air- and moisture-stable in the solid state for several weeks; however, in solution the complex is slightly less stable, and a small degree of decomposition is observed after several days both in air and under an inert atmosphere.

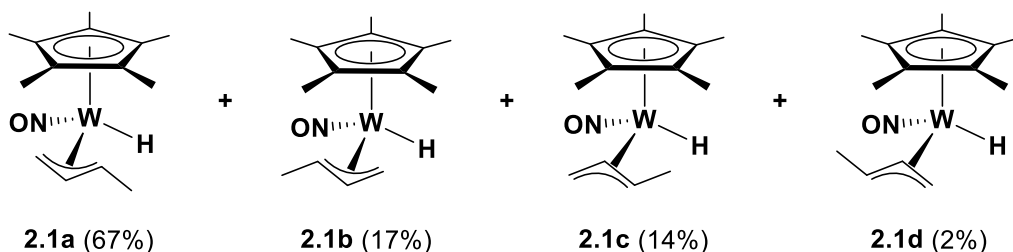
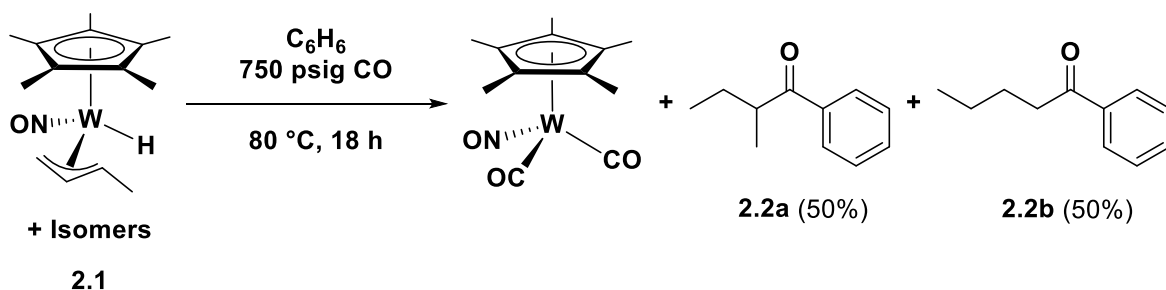


Figure 2.1. Four solution molecular structures of the isomers of **2.1** determined by ^1H Sel NOE NMR spectroscopy.⁴²

2.2.2 Reaction of **2.1** with Benzene and CO

The one-pot reaction of **2.1** with benzene under a high pressure of CO results in the formation of unsymmetrical ketones wherein the two alkyl portions of the ketone are derived from the η^3 -allyl ligand and benzene. Heating of a solution of **2.1** in benzene at 80 °C under 750 psig of CO results in formation of 2-methyl-1-phenylbutan-1-one (**2.2a**) and 1-phenylpentan-1-one (**2.2b**) after 18 hours (Scheme 2.5). Purification of the two ketone products is carried out via flash silica column chromatography, and the ketones coelute as a yellow band in a gradient of 0–1% EtOAc in hexanes. After the removal of volatiles, complexes **2.2a** and **2.2b** are isolated together in a 1:1 ratio in a yield of 53%. Additionally, $\text{Cp}^*\text{W}(\text{NO})(\text{CO})_2$, a precursor complex for these organometallic compounds (including **2.1**) is formed from the reaction and is also recovered via column chromatography.

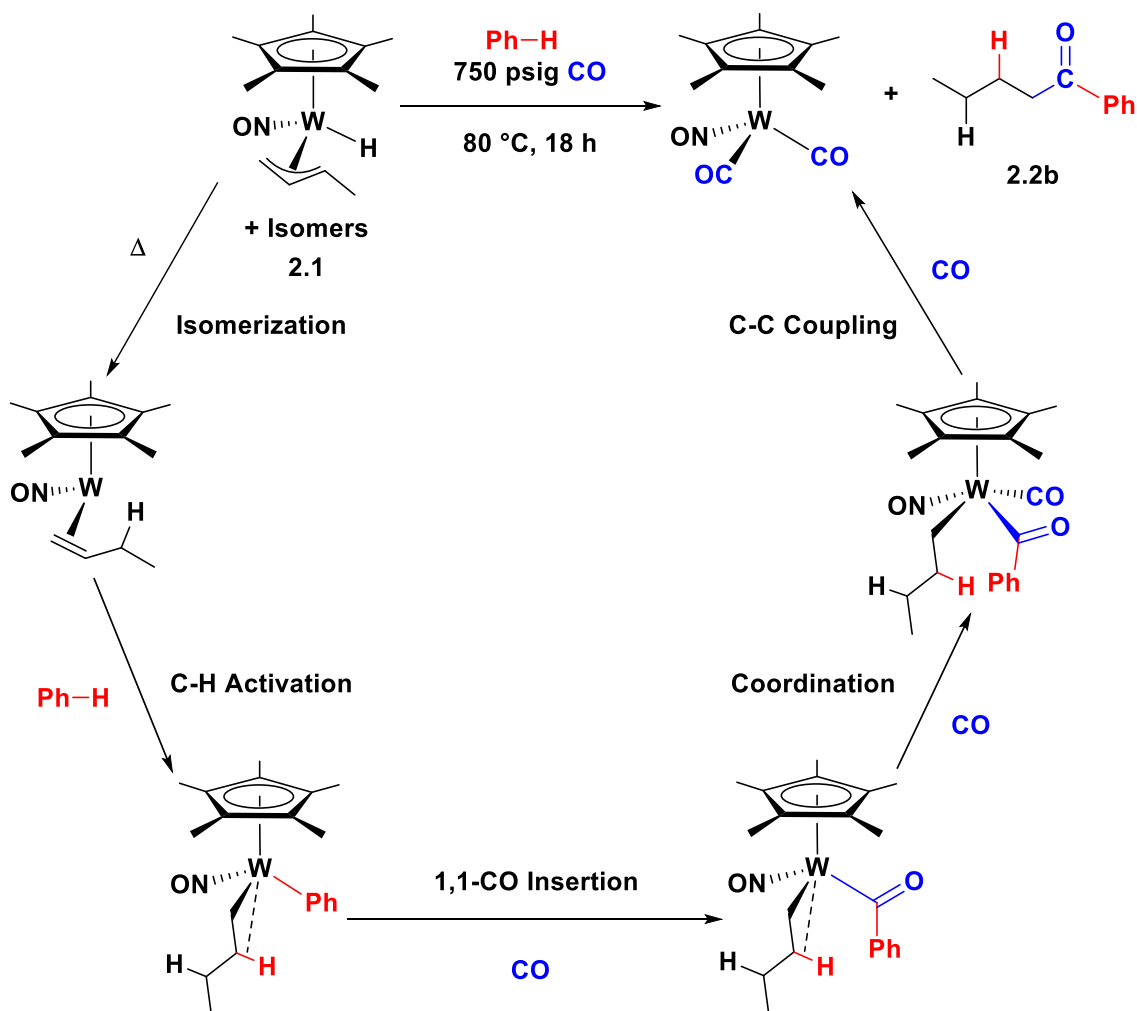
Scheme 2.5. One-pot reaction of complex **2.1** with benzene and CO



A plausible mechanism for this reaction highlighting all the relevant steps is shown in Scheme 2.6 in which the formation of ketone **2.2b** is depicted. This conversion involves the C–H activation of the hydrocarbon by a 16e η^2 -alkene intermediate, Cp*W(NO)(η^2 -CH₂=CHCHCHMe), which results in Cp*W(NO)(Ph)(alkyl), wherein the former allyl ligand has been hydrogenated by the hydride and the hydrogen atom from the C–H activation. These 16e η^2 -alkene intermediates of **2.1** have been shown to exist as multiple isomers in solution via trapping reactions involving the thermolysis of **2.1** in the presence of PMe₃.⁴¹ A subsequent 1,1-CO insertion into the W–Ph linkage followed by coupling of the newly formed acyl ligand to the alkyl ligand results in the formation of the unsymmetrical ketones **2.2a** and **2.2b**. The 16e Cp*W(NO)(alkyl)₂ and Cp*W(NO)(alkyl)(acyl) intermediate complexes invoked in the mechanism have β -agostic C–H interactions which aid in stabilizing the electron-deficient tungsten centres.^{43,44} The final organometallic product is the well-known dicarbonyl nitrosyl complex, Cp*W(NO)(CO)₂,³² which can be conveniently converted back into complex **2.1**, thus completing a synthetic cycle for the formation of unsymmetrical ketones. Additionally, this reaction can be performed with undried solvents and without rigorous exclusion of moisture and

air since both the organometallic reactant and product are stable in the presence of oxygen and water.

Scheme 2.6. Proposed mechanism of the one-pot conversion mediated by complex 2.1



The multiple isomers of complex **2.1** that exist in solution are consistent with the formation of two different ketones since **2.1** exists as four isomers in solution. $\text{Cp}^*\text{W}(\text{NO})(\eta^3\text{-allyl})$ -containing complexes also possess σ - π distorted η^3 -allyl ligands which is manifested in their having unequal C-C bond lengths. The shorter C-C linkage with the more sp^2 -character

carbon terminus is situated *trans* to the nitrosyl ligand in these complexes,⁴¹ and it is at this carbon that coupling with the hydride ligand occurs.⁴⁵ To summarize, the substituents on the allyl ligand influence its coordination to the metal centre, and the σ - π distortion of the η^3 -allyl ligand determines how it couples with the hydride ligand. These features are shown in Figure 2.2 wherein the formation of the two isomers, **2.2a** and **2.2b**, is outlined.

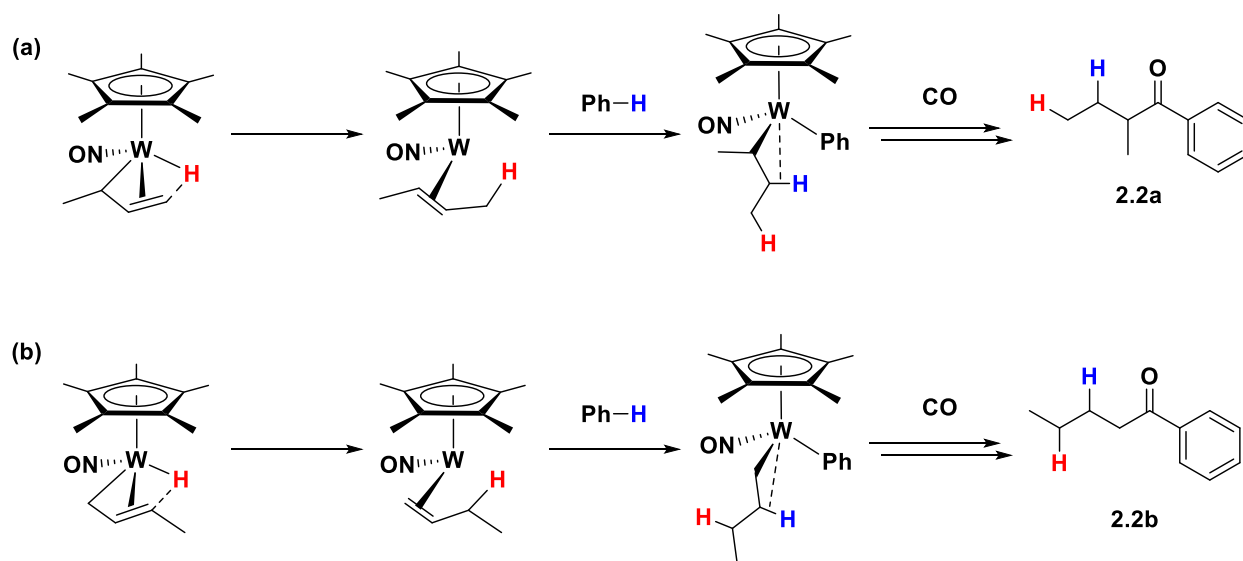


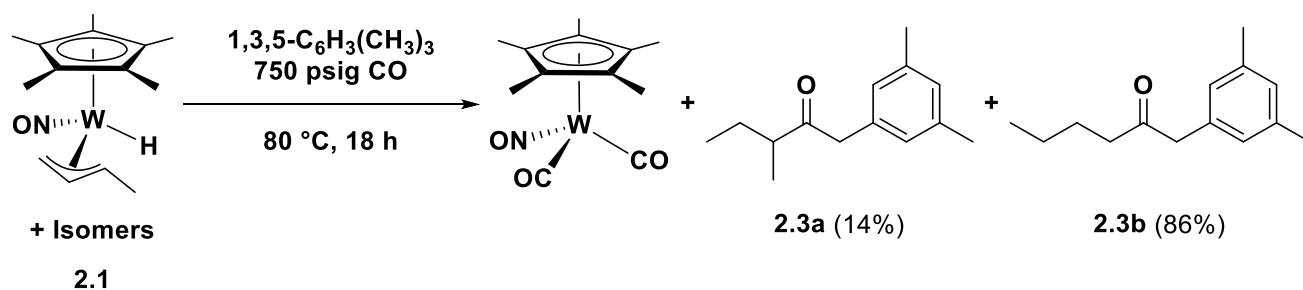
Figure 2.2. (a) Isomers of complex **2.1** with the methyl substituent on the η^3 -allyl ligand proximal to the nitrosyl ligand, thus forming ketone **2.2a**. (b) Isomers of complex **2.1** with the methyl substituent on the η^3 -allyl ligand proximal to the hydride ligand, thus forming ketone **2.2b**.

2.2.3 Reaction of 2.1 with Mesitylene and CO

Heating of **2.1** in mesitylene to 80 °C while under a high pressure of CO for 18 hours results in the formation of two novel ketones (Scheme 2.7). After the removal of volatiles,

purification of the crude product is performed via flash silica column chromatography, and the two ketones coelute in a gradient of 0–5% EtOAc in hexanes. 1-(3,5-dimethylphenyl)-3-methylpentan-2-one (**2.3a**) and 1-(3,5-dimethylphenyl)hexan-2-one (**2.3b**) are obtained in a ratio of 14:86, respectively, with a total yield of 50%. Additionally, Cp*W(NO)(CO)₂ is recovered in a 15% yield as the organometallic product of the reaction.

Scheme 2.7. One-pot reaction of 2.1 with mesitylene and CO



These organic products are analogous to those formed by **2.1** with CO and benzene, and the conversion probably follows the same proposed mechanism except that it involves the C(*sp*³)-H activation of mesitylene rather than the C(*sp*²)-H activation of benzene (Scheme 2.6). Additionally, the formation of the two different structural isomers **2.3a** and **2.3b** is also an effect of the different isomers of complex **2.1** that exist in solution (Figure 2.1). Studies of this reaction using a related complex, Cp*W(NO)(H)(η³-CH₂CHCMe₂), have been performed in tandem to the investigations using complex **2.1**.^{42,46} The results of DFT calculations for the conversion of Cp*W(NO)(H)(η³-CH₂CHCMe₂), mesitylene, and CO into ketones and Cp*W(NO)(CO)₂ corroborate the mechanistic proposals drawn in Scheme 2.6, indicating that complex **2.1** follows the same mechanistic pathway as well.⁴⁶

Of the two ketones, the linear isomer, **2.3b**, is produced in much greater amount than its branched isomer, **2.3a** (86% vs 14%, respectively). This is likely a steric effect due to the large bulk of a mesityl ligand when it is coordinated to the metal centre after the activation of mesitylene. Namely, the formation of the intermediate complex, $\text{Cp}^*\text{W}(\text{NO})(\text{alkyl})(\text{Mes})$ [$\text{Mes} = \text{CH}_2(3,5\text{-(CH}_3)_2\text{C}_6\text{H}_3)$], is heavily favoured when the methyl substituent on the allyl ligand is proximal to the hydride ligand and thus results in an intermediate complex with a linear alkyl ligand, and not favoured when the methyl substituent is proximal to the nitrosyl ligand and thus forms a branched alkyl ligand in the intermediate complex (Figure 2.3).

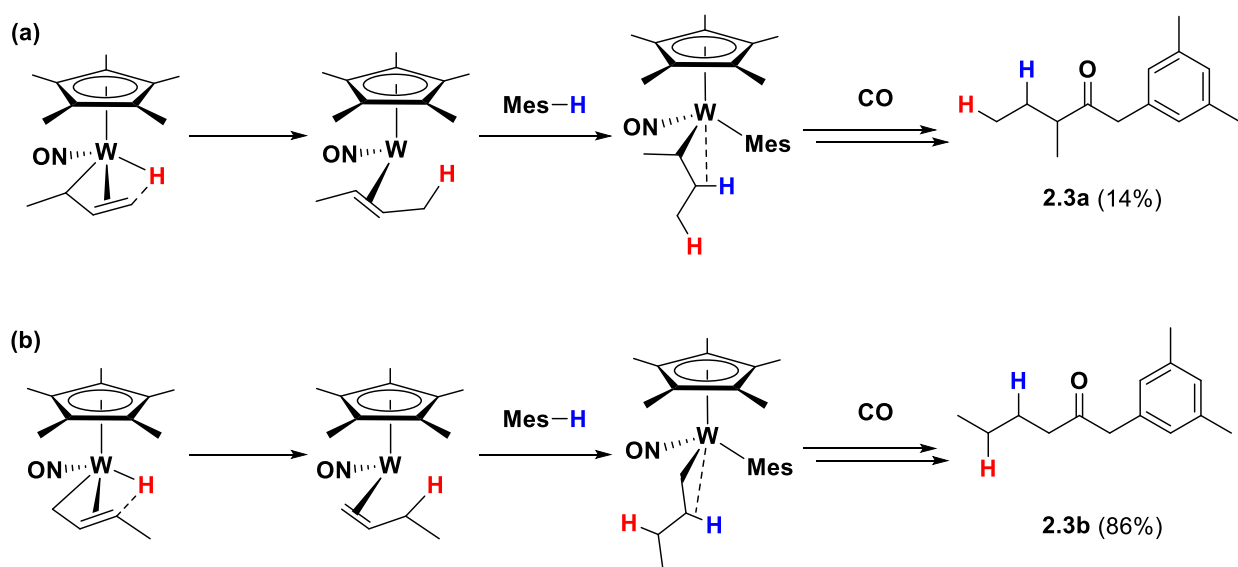
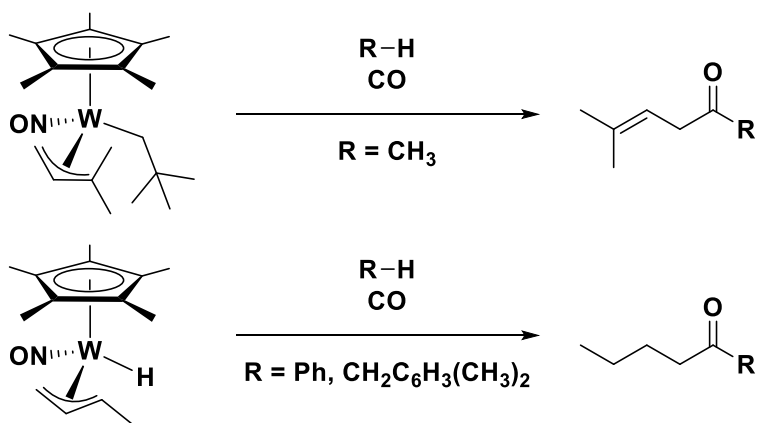


Figure 2.3. (a) Isomers of complex **2.1** with the methyl substituent on the η^3 -allyl ligand proximal to the nitrosyl ligand, thus forming ketone **2.3a** upon reaction with mesitylene. (b) Isomers of complex **2.1** with the methyl substituent on the η^3 -allyl ligand proximal to the hydride ligand, thus forming ketone **2.3b** upon reaction with mesitylene.

As described in the preceding two sections, complex **2.1** mediates the conversion of hydrocarbon substrates and CO into unsymmetrical ketones wherein the portion of the ketone derived from the allyl ligand is saturated. In a complementary manner, the complexes $\text{Cp}^*\text{W}(\text{NO})(\text{CH}_2\text{CMe}_3)(\eta^3\text{-CH}_2\text{CHCHPh})^{47}$ and $\text{Cp}^*\text{W}(\text{NO})(\text{CH}_2\text{CMe}_3)(\eta^3\text{-CH}_2\text{CHCMe}_2)^{48}$ mediate a similar conversion of hydrocarbon substrates and CO into unsymmetrical ketones wherein the portion of the ketone derived from the allyl ligand is unsaturated. Illustrated in Scheme 2.8 is the reaction of $\text{Cp}^*\text{W}(\text{CH}_2\text{CMe}_3)(\eta^3\text{-CH}_2\text{CHCMe}_2)$ with methane and CO to highlight the contrast between it and the reaction of **2.1** with hydrocarbons and CO, only the major organic products are shown. One of the key differences between these conversions and that seen with complex **2.1** is that the $\text{Cp}^*\text{W}(\text{NO})(\text{alkyl})(\eta^3\text{-allyl})$ complexes involve the formation of 16e η^2 -allene or -diene intermediate complexes which then effect the C–H activation of the hydrocarbon substrates and ultimately result in the formation of unsymmetrical ketones.

Scheme 2.8. Formation of unsymmetrical ketones



2.3 Summary

The complex $\text{Cp}^*\text{W}(\text{NO})(\text{H})(\eta^3\text{-CH}_2\text{CHCHMe})$ (**2.1**) can be readily synthesized from two sequential metatheses involving $\text{Cp}^*\text{W}(\text{NO})\text{Cl}_2$, $\text{Mg}(\text{CH}_2\text{CH}=\text{CHMe})_2$, and LiBH_4 in THF. This complex exists as four isomers in solution which differ by the coordination of their η^3 -allyl ligands to the metal centres, namely, whether the allyl ligands are in an endo or exo orientation and whether the methyl substituents are proximal or distal to the nitrosyl ligand. Heating of a mixture of isomers of complex **2.1** in benzene and under a high pressure of CO results in the formation of two ketones, 2-methyl-1-phenylbutan-1-one (**2.2a**) and 1-phenylpentan-1-one (**2.2b**), in a 1:1 ratio, as well as $\text{Cp}^*\text{W}(\text{NO})(\text{CO})_2$, a well known precursor complex. Reaction of a mixture of isomers of complex **2.1** in mesitylene while under a high pressure of CO and while being heated results in the formation of two novel ketones, 1-(3,5-dimethylphenyl)-3-methylpentan-2-one (**2.3a**) and 1-(3,5-dimethylphenyl)hexan-2-one (**2.3b**), as well as $\text{Cp}^*\text{W}(\text{NO})(\text{CO})_2$. These two ketones are isolated together in a ratio of 14:86, respectively, and this large difference is likely due to the large steric demand of the mesityl group on intermediates formed within the reaction. These reactions show the successful synthesis of unsymmetrical ketones resulting from the activation of $\text{C}(\text{sp}^3)\text{-H}$ and $\text{C}(\text{sp}^2)\text{-H}$ bonds of hydrocarbons without having to use late transition metals or highly reactive reagents. Additionally, these conversions may be performed in the presence of air or water as the initial and final organometallic complexes are both oxidatively and hydrolytically stable. DFT calculations performed on a related organometallic complex corroborate the proposed mechanism for these conversions of hydrocarbon and CO into ketones (Scheme 2.6). The final organometallic product of these

conversions is $\text{Cp}^*\text{W}(\text{NO})(\text{CO})_2$, and this can be readily converted back into complex **2.1**, thus completing a full synthetic cycle for the formation of unsymmetrical ketones.

2.4 Experimental Section

2.4.1 General Methods

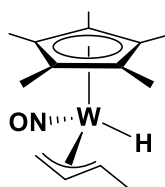
All reactions and subsequent manipulations involving organometallic reagents were performed under anhydrous and anaerobic conditions except where noted. High-vacuum and inert-atmosphere techniques were performed using double-manifold Schlenk lines or in Innovative Technologies LabMaster 100 and MS-130 BG dual-station gloveboxes equipped with freezers maintained at $-30\text{ }^\circ\text{C}$. Preparative scale reactions were performed with Schlenk or round bottom flasks; reactions were performed in thick-walled glass reaction flasks (larger scale) or J. Young NMR tubes (smaller scale), both of which were typically sealed with Kontes greaseless stopcocks. Tetrahydrofuran (THF) and diethyl ether (Et_2O) were dried over sodium/benzophenone ketyl and freshly distilled prior to use; *n*-pentane was dried over calcium hydride and freshly distilled prior to use; all other solvents were dried according to standard procedures. All binary magnesium reagents used were prepared from the corresponding Grignard reagents.⁴⁹ The complex $\text{Cp}^*\text{W}(\text{NO})\text{Cl}_2$ was prepared according to the published procedures.³² Pentamethylcyclopentadiene was obtained from the Boulder Scientific Company, and LiBH_4 (2.0 M in THF) was obtained from Sigma-Aldrich. All other chemicals and reagents were ordered from commercial suppliers and used as received. Unless otherwise specified, all IR samples were prepared as Nujol mulls sandwiched between NaCl plates, and their spectra were

recorded on a Thermo Nicolet model 4700 FT-IR spectrometer. Except where noted, all NMR spectra were recorded at room temperature on Bruker AV-400 (direct and indirect probes) and AV-600 instruments, and all chemical shifts are reported in parts per million and coupling constants in hertz. ^1H NMR spectra were referenced to the residual protio isotopomer present in C_6D_6 (7.16 ppm) or CDCl_3 (7.26 ppm). ^{13}C NMR spectra were referenced to C_6D_6 (128.39 ppm) or CDCl_3 (77.16 ppm). For the characterization of most complexes, two-dimensional NMR experiments, $\{^1\text{H}-^1\text{H}\}$ COSY, $\{^1\text{H}-^{13}\text{C}\}$ HSQC, and $\{^1\text{H}-^{13}\text{C}\}$ HMBC, were performed to correlate and assign ^1H , and ^{13}C NMR signals and establish atom connectivity; ^1H NOE NMR and $\{^1\text{H}-^{13}\text{C}\}$ NOESY were used for determination of solution structures. Low- and high-resolution mass spectra (EI, 70 eV) spectra were recorded by M. Lapawa of the UBC mass spectrometry facility using a Kratos MS-50 spectrometer, and elemental analyses were performed by D. Smith of the UBC microanalytical facility.

2.4.2 Preparation of $\text{Cp}^*\text{W}(\text{NO})(\text{H})(\eta^3\text{-CH}_2\text{CHCHMe)$ (2.1)

In a glovebox, a Schlenk flask was charged with $\text{Cp}^*\text{W}(\text{NO})\text{Cl}_2$ (2.448 g, 5.827 mmol) and a magnetic stir bar, and a second flask was charged with $\text{Mg}(\text{CH}_2\text{CH}=\text{CHMe})_2$ (0.543 g, 5.826 mmol, 93.2 g/mol titer) and a magnetic stir bar. On a double-manifold, THF (ca. 100 mL each) was cannulated into each flask. The flask containing the $\text{Cp}^*\text{W}(\text{NO})\text{Cl}_2$ was then placed in a dry ice/acetone bath ($-78\text{ }^\circ\text{C}$) while stirring of its contents continued, and once cold, the contents of the flask containing $\text{Mg}(\text{CH}_2\text{CH}=\text{CHMe})_2$ were cannulated slowly into the first flask. The reaction flask was removed from the dry ice/acetone bath, and its contents were stirred at room temperature for 1 h. Lithium borohydride in THF (2.0 M, 6.0 mL, 12 mmol) was

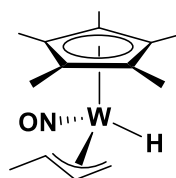
added to the Schlenk flask in a dropwise fashion. The resulting mixture developed a slightly reddish brown colour and was allowed to react at room temperature for 24 h. The volume of THF was reduced in vacuo, and water was added dropwise to the flask to neutralize the remaining LiBH₄. Liquid-liquid extractions using distilled water and Et₂O were carried out to remove salts from the mixture, and the organic layer was dried over anhydrous MgSO₄. The crude product was concentrated in vacuo and was purified by flash chromatography on neutral alumina. A yellow band was eluted with a gradient of 0–20% EtOAc in hexanes to obtain a bright yellow eluate. Solvent was removed from the eluate in vacuo to obtain Cp*W(NO)(H)(η³-CH₂CHCHMe) (**2.1**) as a dark yellow oil, and recrystallization from hexanes at –30 °C resulted in an analytically pure, yellow solid (0.455 g, 1.123 mmol, 19% yield). X-ray-quality crystals of **2.1a** were obtained via slow evaporation of an Et₂O solution of the complex at room temperature. In solution, four coordination isomers of **2.1** were identified by ¹H and ¹³C NMR spectroscopy. The solution structures of the individual isomers were elucidated by ¹H Sel NOE NMR spectroscopy. The NMR characterization of these isomers, the ¹H NOE NMR studies, and the characterization in the solid-state were performed by Dr. Rhett A. Baillie.⁴²



2.1a (67%)

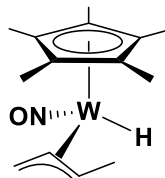
Characterization data for **2.1a**. IR (C₆D₆, cm⁻¹): 1571 (s, ν_{NO}). MS (LREI, *m/z*, probe temperature of 120 °C): 405 [M⁺, ¹⁸⁴W]. HRMS-EI *m/z*: [M⁺, ¹⁸⁶W] calcd for C₁₄H₂₃NO¹⁸⁶W,

407.13234; found, 407.13211. ^1H NMR (600 MHz, C_6D_6): δ -1.27 (s, $^1J_{\text{HW}} = 122.2$, 1H, *WH*), 0.16 (d, $^3J_{\text{HH}} = 10.3$, 1H, allyl *CH*₂), 1.74 (s, 15H, C_5Me_5), 1.83 (m, 1H, allyl *CHMe*), 2.26 (d, $^3J_{\text{HH}} = 5.8$, 3H, allyl *Me*), 2.75 (d, $^3J_{\text{HH}} = 7.3$, 1H, allyl *CH*₂), 4.61 (ddd, $^3J_{\text{HH}} = 13.1$, 10.3, 7.3, 1H, allyl *CH*). ^{13}C APT NMR (150 MHz, C_6D_6): δ 10.99 (C_5Me_5), 21.8 (allyl *Me*), 39.2 ($^1J_{\text{CW}} = 30.7$, allyl *CH*₂), 78.6 (allyl *CHMe*), 104.6 (allyl *CH*), 105.0 (C_5Me_5). Sel NOE (600 MHz, C_6D_6): δ irradiat. at -1.27, NOE at 2.26. mp 75–78 °C (reversible, confirmed by ^1H NMR). Anal. Calcd for $\text{C}_{14}\text{H}_{23}\text{NOW}$ (mixture of isomers): C, 41.50; H, 5.72; N, 3.46. Found: C, 41.22; H, 5.71; N, 3.26.



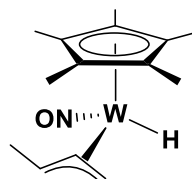
2.1b (17%)

Characterization data for **2.1b**. ^1H NMR (600 MHz, C_6D_6): δ -1.33 (s, $^1J_{\text{HW}} = 122.6$, 1H, *WH*), 0.59 (d, $^3J_{\text{HH}} = 13.5$, 1H, allyl *CH*₂), 0.97 (dq, $^3J_{\text{HH}} = 10.0$, 5.8, 1H, allyl *CHMe*), 1.72 (s, 15H C_5Me_5), 1.95 (d, $^3J_{\text{HH}} = 5.8$, 3H, allyl *Me*), 4.08 (d, $^3J_{\text{HH}} = 7.3$, 1H, allyl *CH*₂), 4.35 (ddd, $^3J_{\text{HH}} = 13.5$, 10.0, 7.3, 1H, allyl *CH*). ^{13}C APT NMR (150 MHz, C_6D_6): δ 11.01 (C_5Me_5), 18.6 (allyl *Me*), 51.9 (allyl *CH*₂), 58.8 ($^1J_{\text{CW}} = 23.2$, allyl *CHMe*), 104.8 (C_5Me_5), 104.9 (allyl *CH*). Sel NOE (600 MHz, C_6D_6): δ irradiat. at -1.33, NOE at 4.09.



2.1c (14%)

Characterization data for **2.1c**. ^1H NMR (600 MHz, C_6D_6): δ -1.24 (s, $^1J_{\text{HW}} = 124.3$, 1H, *WH*), 1.71 (s, 15H C_5Me_5), 2.06 (m, 1H, allyl *CH*₂), 2.14 (m, 3H, allyl *Me*), 2.28 (obscured, 1H, allyl *CH*₂), 2.82 (m, 1H, allyl *CH*), 3.65 (m, 1H, allyl *CHMe*). ^{13}C APT NMR (150 MHz, C_6D_6): δ 10.8 (C_5Me_5), 20.9 (allyl *Me*), 39.0 ($^1J_{\text{CW}} = 24.3$, allyl *CH*₂), 74.9 (allyl *CHMe*), 99.1 (allyl *CH*), 104.2 (C_5Me_5).

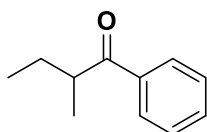


2.1d (2%)

Partial characterization data for **2.1d**. ^1H NMR (600 MHz, C_6D_6): δ -0.86 (s, $^1J_{\text{HW}} = 124.8$, 1H, *WH*), 1.69 (s, 15H C_5Me_5), 2.48 (m, 1H, allyl *CH*). ^{13}C APT NMR (150 MHz, C_6D_6): δ 10.9 (C_5Me_5), 94.1 (allyl *CH*), 104.3 (C_5Me_5).

2.4.3 Reaction of 2.1 with Benzene and CO

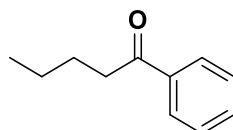
In a glovebox, a Parr 5500 reactor was charged with complex **2.1** as a mixture of isomers (0.159 g, 0.392 mmol) and benzene (ca. 30 mL), producing a dark yellow solution. The reactor was sealed, brought out of the glovebox, and then purged three times with CO. The reactor was then pressurized to 750 psig CO, and was heated at 80 °C for 18 h while its contents were stirred. The reactor was then brought to room temperature and vented. The final reaction mixture was transferred to a round-bottom flask and the solvent was removed in vacuo. The crude product was then purified via flash column chromatography on silica with a gradient of 0–1% EtOAc in hexanes to obtain the organic products 2-methyl-1-phenylbutan-1-one (**2.2a**) and 1-phenylpentan-1-one (**2.2b**) (0.034 g, 0.210 mmol, 53% yield) in a 1:1 ratio, as well as Cp*W(NO)(CO)₂ (<5% yield via NMR).



2.2a (50%)

Characterization data for 2-methyl-1-phenylbutan-1-one (**2.2a**). IR (cm⁻¹): 1690 (s, ν_{CO}). MS (LREI, *m/z*, probe temperature of 150 °C): 162 [M⁺]. ¹H NMR (400 MHz, CDCl₃): δ 0.91 (t, ³J_{HH} = 7.5, 3H, CH₃CH₂), 1.19 (d, ³J_{HH} = 6.9, 3H, CH₃CH), 1.45–1.56 (m, 1H, CH₂), 1.78–1.90 (m, 1H, CH₂), 3.40 (sext, ³J_{HH} = 6.7, 1H, CH₃CH), 7.44–7.48 (m, 2H, aryl *H*), 7.53–7.57 (m, 1H,

aryl *H*), 7.94–7.97 (m, 2H, aryl *H*). $^{13}\text{C}\{^1\text{H}\}$ NMR (100 MHz, CDCl_3): δ 11.9, 16.9, 26.6, 42.3, 128.4, 128.7, 132.9, 137.0, 204.6. These data match previously reported spectroscopic data.⁵⁰



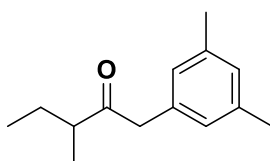
2.2b (50%)

Characterization data for 1-phenylpentan-1-one (**2.2b**). ^1H NMR (400 MHz, CDCl_3): δ 0.95 (t, $^3J_{\text{HH}} = 7.3$, 3H, CH_3), 1.41 (sext, $^3J_{\text{HH}} = 7.6$, 2H, CH_3CH_2), 1.72 (pent, $^3J_{\text{HH}} = 7.6$, 2H, $\text{CH}_3\text{CH}_2\text{CH}_2$), 2.97 (t, $^3J_{\text{HH}} = 7.4$, 2H, $\text{CH}_2\text{C}(\text{O})\text{Ph}$), 7.44–7.48 (m, 2H, aryl *H*), 7.53–7.57 (m, 1H, aryl *H*), 7.94–7.97 (m, 2H, aryl *H*). $^{13}\text{C}\{^1\text{H}\}$ NMR (100 MHz, CDCl_3): δ 14.1, 22.6, 26.8, 38.5, 128.2, 128.7, 133.0, 137.3, 200.8. These data match previously reported spectroscopic data.⁵¹

2.4.4 Reaction of 2.1 with Mesitylene and CO

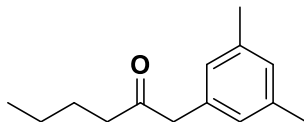
In a glovebox, a Parr 5500 reactor was charged with complex **2.1** as a mixture of isomers (0.290 g, 0.716 mmol) and mesitylene (ca. 15 mL), producing a dark yellow solution. The reactor was sealed and was then purged three times with CO. The reactor was finally pressurized to 750 psig CO, and the contents were stirred whilst heated at 80 °C for 18 h. The reactor was cooled to room temperature and then vented. The dark brown crude product was purified via

flash column chromatography on silica with a gradient of 0–5% EtOAc in hexanes wherein the two ketones coelute in the solvent. After the removal of volatiles, the two novel organic products, 1-(3,5-dimethylphenyl)-3-methylpentan-2-one (**2.3a**) and 1-(3,5-dimethylphenyl)hexan-2-one (**2.3b**), were obtained in a 14:86 ratio, respectively, as a yellow oil (0.074 g, 0.362 mmol, 50% yield). Cp*W(NO)(CO)₂ was also obtained from the column chromatography as a separate band (0.044 g, 0.109 mmol, 15% yield).



2.3a (14%)

Characterization data for 1-(3,5-dimethylphenyl)-3-methylpentan-2-one (**2.3a**). IR (cm⁻¹): 1716 (s, ν_{CO}). MS (LREI, *m/z*, probe temperature of 150 °C): 204 [M⁺]. HRMS-EI *m/z*: [M⁺] calcd for C₁₄H₂₀O: 204.15142; found: 204.15154. ¹H NMR (400 MHz, CDCl₃): δ 0.84 (t, ³J_{HH} = 7.5, 3H, CH₃CH₂), 1.06 (d, ³J_{HH} = 6.9, 3H, CH₃CH), 1.39 (pent, ³J_{HH} = 7.0, 2H, CH₃CH₂), 2.29 (s, 6H, ArMe₂), 2.58 (sext, ³J_{HH} = 6.8, 1H, CHC(O)), 3.64 (s, 2H, C(O)CH₂), 6.81 (s, 2H, *o*-aryl H), 6.89 (s, 1H, *p*-aryl H). ¹³C NMR (100 MHz, CDCl₃): δ 11.7, 16.2, 21.4, 26.1, 47.0, 48.6, 127.4, 128.6, 134.2, 138.2, 212.3.



2.3b (86%)

Characterization data for 1-(3,5-dimethylphenyl)hexan-2-one (**2.3b**): ^1H NMR (400 MHz, CDCl_3) δ 0.87 (t, $^3J_{\text{HH}} = 7.3$, 3H, CH_3CH_2), 1.26–1.29 (overlapped, CH_2), 1.53 (pent, $^3J_{\text{HH}} = 7.5$, 2H, CH_2), 2.29 (s, 6H, ArMe_2), 2.43 (t, $^3J_{\text{HH}} = 7.3$, 2H, $\text{CH}_2\text{C}(\text{O})$), 3.59 (s, 2H, $\text{C}(\text{O})\text{CH}_2$), 6.81 (s, 2H, *o*-aryl *H*), 6.89 (s, 1H, *p*-aryl *H*). ^{13}C NMR (100 MHz, CDCl_3): δ 13.9, 21.4, 22.4, 26.0, 41.8, 50.2, 127.3, 128.7, 134.4, 138.3, 209.1.

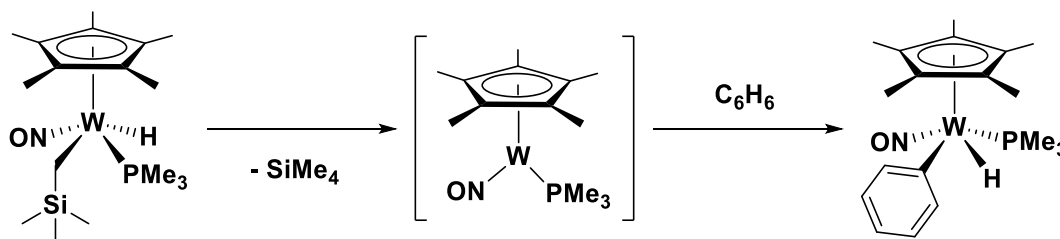
Chapter 3: Synthesis and Reactivity of Cp*W(NO)(R)(H)(L) Complexes[†]

[†] A version of this chapter has been published. Fabulyak, D.; Handford, R. C.; Holmes, A. S.; Levesque, T. M.; Wakeham, R. J.; Patrick, B. O.; Legzdins, P. L.; Rosenfeld, D. C. *Inorg. Chem.* **2017**, *56*, 573–582. Reproduced with permission from Inorganic Chemistry. Copyright (2017) American Chemical Society.

3.1 Introduction

Numerous examples of transition-metal coordination complexes with phosphine or phosphite ligands that display interesting characteristic chemistry exist in the literature.⁵² For instance, many of these complexes have been shown to catalyze asymmetric hydrogenation, hydroformylation, addition, and substitution reactions.^{53,54} The use of Lewis bases in transition-metal complexes is highly attractive as they allow for a considerable amount of electronic and steric tuning due to the vast amount of ligand design available. A family of complexes that has attracted our renewed interest consists of the hydrido complexes, *trans*-Cp*W(NO)(R)(H)(L) [Cp* = η^5 -C₅Me₅; R = alkyl, L = Lewis base].⁵⁵ The *trans* or *cis* nomenclature designates the relative position of the alkyl and hydrido ligands in the base of the four-legged piano-stool molecule. These complexes have attracted our renewed interest due to their C–H activating ability. These complexes are conveniently synthesized from reactions involving Cp*W(NO)(CH₂SiMe₃)₂, H₂, and Lewis base. A product of this reaction, *trans*-Cp*W(NO)(CH₂SiMe₃)(H)(PMe₃), is known to activate C₆H₆ to form *cis*-Cp*W(NO)(C₆H₅)(H)(PMe₃).⁵⁶ Kinetic, theoretical, and mechanistic studies of this activation process are consistent with the mechanism outlined in Scheme 3.1.

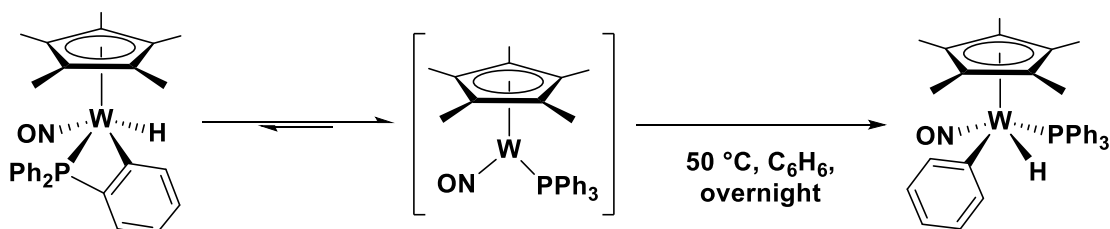
Scheme 3.1. Activation of C₆H₆ by *trans*-Cp*W(NO)(CH₂SiMe₃)(H)(PMe₃)



An initial *trans* to *cis* isomerization of the reactant followed by the subsequent reductive elimination of SiMe₄ generates the 16e reactive intermediate, Cp*W(NO)(PMe₃). This intermediate complex performs the intermolecular C–H activation of benzene resulting in the formation of *cis*-Cp*W(NO)(C₆H₅)(H)(PMe₃).

Similarly, the reaction of Cp*W(NO)(CH₂SiMe₃)₂, H₂, and PPh₃ results in *cis*-Cp*W(NO)(H)(κ²-PPh₂(C₆H₄)),⁵⁷ which probably forms via the elimination of SiMe₄ from Cp*(NO)(CH₂SiMe₃)(H)(PPh₃). A solid-state molecular structure obtained from single-crystal X-ray diffraction confirms that the alkyl and hydrido ligands are in a *cis* orientation.⁵⁸ This *ortho*-metalated complex is known to effect the intermolecular C–H activation of C₆H₆ via the 16e reaction intermediate, Cp*W(NO)(PPh₃) (Scheme 3.2).⁵⁹

Scheme 3.2. C–H activation of C₆H₆ by *cis*-Cp*W(NO)(H)(κ²-PPh₂(C₆H₄))



The chemistry summarized in Schemes 3.1 and 3.2 has been expanded to include the activation of other hydrocarbon substrates (*sp*² and *sp*³ hybridized C–H bonds) and their possible functionalization, as well as the synthesis of other novel complexes of this type utilizing other Lewis bases. One recent objective within the Legzdins research group has been the synthesis of complexes of the composition Cp*W(NO)(R)(H)(L) that will form 16e reactive intermediates upon thermolysis— through the elimination of the alkyl and hydrido ligands— that will then

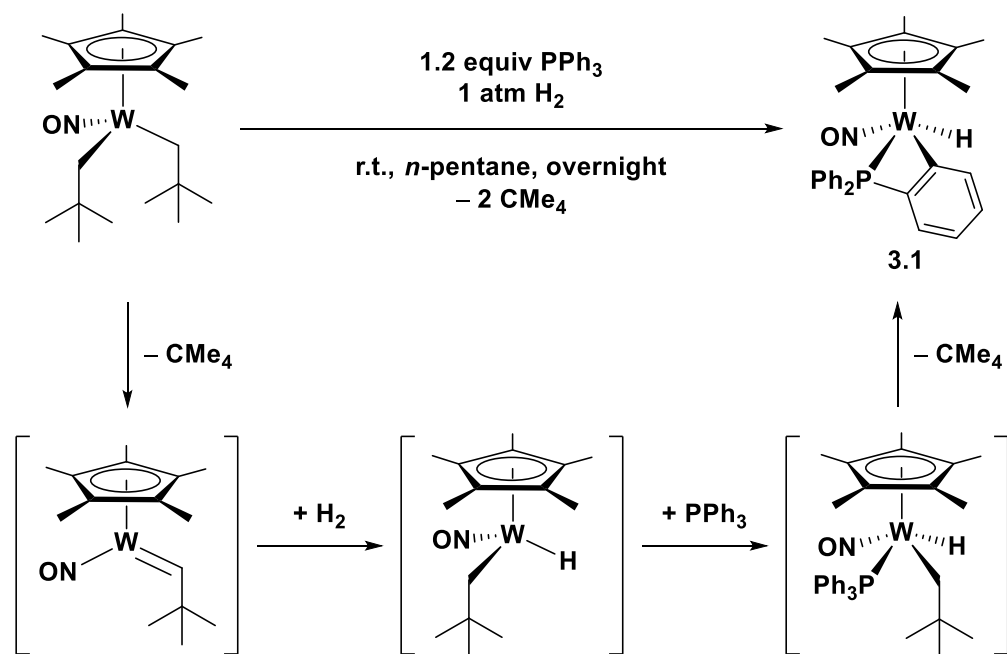
effect the C–H activation of various hydrocarbon substrates. My assignment within this project has been to synthesize complexes using PPh₃ and P(OPh)₃ proligands and to compare the results with the studies from other group members who have investigated other proligands. The findings of this investigation are described in this chapter.

3.2 Results and Discussion

3.2.1 Synthesis of *cis*-Cp*W(NO)(H)(κ²-PPh₂(C₆H₄)) (**3.1**)

Reaction of Cp*W(NO)(CH₂CMe₃)₂ and PPh₃ in *n*-pentane under 1 atm of hydrogen results in *cis*-Cp*W(NO)(H)(κ²-PPh₂(C₆H₄)) (**3.1**) as shown in Scheme 3.3.⁶⁰ The product is a green-yellow precipitate that deposits on the sides of the reaction flask. Complex **3.1** is purified via pentane washes, and after the removal of volatiles is obtained in a yield of 40% as a yellow solid.

Scheme 3.3. Synthesis and proposed mechanism for complex 3.1



As depicted, the initial step in the formation of **3.1** probably occurs with the formation of an alkyldiene complex following the elimination of neopentane.⁶¹ H₂ adds across the W=C linkage and results in [Cp*W(NO)(CH₂CMe₃)(H)], which then forms an adduct with PPh₃. The elimination of another equivalent of neopentane and the subsequent intramolecular oxidative addition of a C–H bond at the *ortho* position of a phenyl substituent of the PPh₃ ligand results in the *ortho*-metalated complex **3.1**. This reaction differs from the similar synthesis of *trans*-Cp*W(NO)(CH₂CMe₃)(H)(PMe₃), wherein the neopentyl and hydride ligands have not undergone reductive elimination.⁵⁶ Complex **3.1** has a ν_{NO} stretching frequency of 1545 cm⁻¹, indicating an overall increase in the electron density extant on the metal centre when compared to the initial reactant, and this is likely due to the σ -donation of the PPh₃ ligand (PPh₃ has a pK_a

of 2.73).⁶² The ¹H NMR spectrum of **3.1** in C₆D₆ exhibits a resonance attributable to the hydrido ligand at δ 4.00 ppm with a ¹J_{HW} of 101.1 Hz and a ²J_{HP} of 10.8 Hz (Figure B.1).

The synthesis of complex **3.1** has been previously reported by a different route wherein Cp*W(NO)(CH₂SiMe₃)₂ is used as the initial reactant, and the reaction is left to proceed for a shorter time.⁵⁷ The change in starting reactant and reaction time results in a negligible difference in the yield of the desired complex.

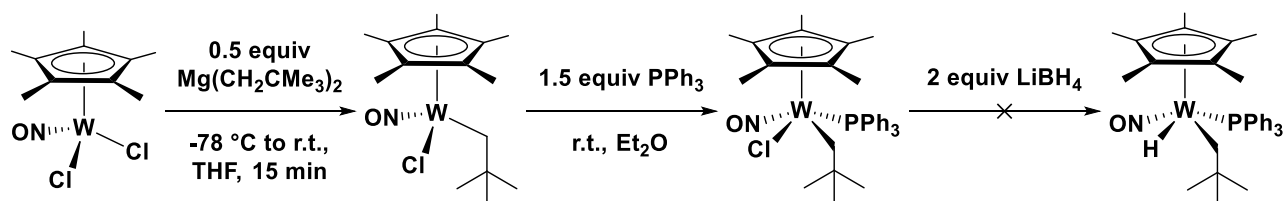
Examples of *ortho*-metalation of a phenyl substituent of a phosphorus ligand coordinated to a metal centre are known in the literature.^{63–65} A recent example with similarities to **3.1** is the iridium(III) complex, Ir(Cl)(H)(κ²-P(*t*-Bu)₂(C₆H₄)(P(*t*-Bu)₂Ph)), which forms after one hour from a reaction of (Ir(μ-Cl)(coe)₂)₂ [coe = *cis*-cyclooctene] with 1.5 equivalents of P(*t*-Bu)₂Ph in CH₂Cl₂ at ambient temperatures.⁶⁶ Initially, the reaction probably forms the complex Ir(Cl)(coe)(P(*t*-Bu)₂Ph)₂, which then quickly performs the oxidative addition of the *ortho* C–H bond of a phenyl substituent. This spontaneous *ortho*-metalation is reversible since reaction with CO or NO⁺—from [NO]BF₄—results in the reductive elimination of the alkyl and hydrido ligands, thus forming the complex *trans*-Ir(Cl)(CO)(P(*t*-Bu)₂Ph)₂ or *trans*-[Ir(Cl)(NO)(P(*t*-Bu)₂Ph)₂]BF₄, respectively. The *ortho*-metalation of **3.1** is also readily reversible, similar to the complex above, but the elimination can be induced by heating of the complex rather than by the addition of proligand.

3.2.2 Attempted Synthesis of Cp*W(NO)(CH₂CMe₃)(H)(PPh₃)

As outlined above, the reaction of Cp*W(NO)(CH₂CMe₃)₂ with PPh₃ in the presence of H₂ does not result in the formation of the desired Cp*W(NO)(R)(H)(L) complex, but instead

results exclusively in an *ortho*-metalated complex— **3.1**. The synthesis and isolation of $\text{Cp}^*\text{W}(\text{NO})(\text{CH}_2\text{CMe}_3)(\text{H})(\text{PPh}_3)$ has been attempted from sequential metatheses reactions involving $\text{Cp}^*\text{W}(\text{NO})(\text{Cl})_2$, $\text{Mg}(\text{CH}_2\text{CMe}_3)_2$, PPh_3 , and LiBH_4 . The aim of this synthesis has been to isolate the desired $\text{Cp}^*\text{W}(\text{NO})(\text{R})(\text{H})(\text{L})$ complex, which is unobtainable from the synthesis of **3.1**, and to use this complex as a precursor towards a 16e reactive intermediate needed to effect the C–H activation of hydrocarbons. The complete synthetic route attempted is shown in Scheme 3.4.

Scheme 3.4. Attempted synthetic route for $\text{Cp}^*\text{W}(\text{NO})(\text{CH}_2\text{CMe}_3)(\text{H})(\text{PPh}_3)$



Unfortunately, this synthesis is unsuccessful and results in mixtures of intractable decomposition products. No *ortho*-metalated complexes form from the reaction. The decomposition of the organometallics probably occurs in the final steps of the synthesis since the formation of $\text{Cp}^*\text{W}(\text{NO})(\text{Cl})(\text{CH}_2\text{CMe}_3)$ has been invoked previously in related studies.^{29,67} Due to the difficulty of synthesizing $\text{Cp}^*\text{W}(\text{NO})(\text{CH}_2\text{CMe}_3)(\text{H})(\text{PPh}_3)$ and the previously reported C–H activation of benzene by **3.1**, complex **3.1** is used instead for reactions with hydrocarbon substrates.

3.2.3 Thermolysis of **3.1** in Hydrocarbons

The C–H activation ability of **3.1** has been seen in one previous example but has not been expanded upon.⁵⁹ Consequently, during the current study a range of hydrocarbon substrates varying in both size and hybridization has been used in these thermolysis reactions. The hydrocarbon substrates include methane, pentane, octane, benzene, and mesitylene. The reactions of **3.1** with hydrocarbon substrates are performed at 50 °C and 80 °C in neat solutions of the substrate, with the exception of methane which is carried out in cyclohexane at 750 psig of methane.

3.2.3.1 Thermolysis reactions at 80 °C

Reactions of methane, pentane, octane, and mesitylene with **3.1** have been carried out at 80 °C overnight. In all of these experiments, the reaction mixtures turn from a clear yellow solution to a cloudy brown mixture the following day. All of the reactions proceed similarly, and this is confirmed via NMR analyses of the reaction mixtures which show no C–H activation products of the hydrocarbon substrate. Instead, upon heating, complex **3.1** isomerizes to form *trans*-Cp*W(NO)(H)(κ^2 -PPh₂(C₆H₄)) (**3.2**) as the major product. Cp*W(NO)(PPh₃)₂, a disproportionation product, uncoordinated PPh₃ proligand, and intractable decomposition products are also present in minor amounts in the final reaction mixtures. The isomerization of **3.1** into **3.2** is unexpected since the isomerized product is not observed in the previously reported thermal C–H activation of benzene at 50 °C by **3.1**.⁵⁹

3.2.3.2 Thermolysis reactions at 50 °C

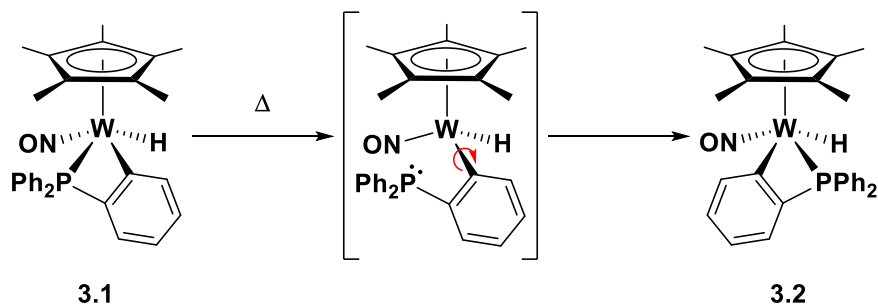
Reactions of **3.1** with methane, pentane, benzene, and mesitylene have been performed at 50 °C in order to inhibit *cis*–*trans* isomerization into **3.2**. Consistent with previous results, the activation of benzene by **3.1** is successful and the activated product, *cis*-Cp*W(NO)(C₆H₅)(H)(PPh₃), is the only complex formed. Reactions of methane, pentane, and mesitylene show no evidence for products resulting from the C–H activation of the hydrocarbon substrates. Instead, all of these experiments contain unreacted **3.1** as the major component, evident from the C₆D₆ ¹H NMR spectra of the reaction mixtures. Minor amounts of **3.2**, Cp*W(NO)(PPh₃)₂, and decomposition products are also present in all of the reaction mixtures, thereby indicating that **3.1** undergoes a minor amount of isomerization at 50 °C as well.

3.2.4 Thermal Isomerization of **3.1** into *trans*-Cp*W(NO)(H)(κ²-PPh₂(C₆H₄)) (**3.2**)

In the absence of a suitable hydrocarbon substrate, the predominant pathway at temperatures above 50 °C is the *cis* to *trans* isomerization of **3.1** into **3.2** (Scheme 3.5). This isomerization process as well as the amount of Cp*W(NO)(PPh₃)₂, uncoordinated PPh₃ proligand, and decomposition products formed in the reactions provide insight into the lability of the PPh₃ ligand. The labile nature of PPh₃ is also shown from the isolation of the PMe₃-trapped intermediate complex, Cp*W(NO)(κ¹-C₆H₄(PPh₂))(H)(PMe₃).⁵⁸ The *cis* to *trans* isomerization probably occurs in order to achieve a more thermodynamically favourable orientation of the ligands, with the σ-donating phosphine ligand being *trans* to the π-accepting nitrosyl ligand. The ν_{NO} of **3.2** is 1552 cm⁻¹, which is similar to that of **3.1**. Complex **3.2** does not perform C–H

activation chemistry at 80 °C in neat hydrocarbon solutions, and this suggests that the isomerization pathway impedes the desired reaction pathway because it produces a thermodynamically favoured product that halts any further reactivity. It is also important to note that the reductive elimination of the phenyl and hydrido ligands to form the 16e reaction intermediate needed to effect the C–H activation of hydrocarbons is only possible when the two ligands are *cis* to one another. In addition to this isomerization, the formation of disproportionation and decomposition products also provide undesired pathways for the organometallic complex that complicate the reactivity of these systems.

Scheme 3.5. Possible isomerization pathway of 3.1 into 3.2 upon heating



The spectroscopic data are fully consistent with the structure depicted above. The ^1H NMR spectrum of complex **3.2** in C_6D_6 displays a resonance at δ 2.28 ppm with a $^2J_{\text{HP}}$ of 70.2 Hz attributable to the hydrido ligand (Figure B.3). During this study, it has been found that the *cis* and *trans* isomers of these complexes, such as **3.1** and **3.2**, can be distinguished by their $^2J_{\text{HP}}$ or $^2J_{\text{PH}}$ values in their ^1H or ^{31}P NMR spectra, respectively.⁶⁰ For instance, in complex **3.2**, the *trans* configuration of the alkyl and hydrido ligands manifests in a much larger $^2J_{\text{HP}}$ coupling constant value of the hydride resonance compared to that of complex **3.1** (Figure 3.1). This

observed trend allows for easy assignments of *trans* or *cis* configurations without the need of solid-state molecular structures.

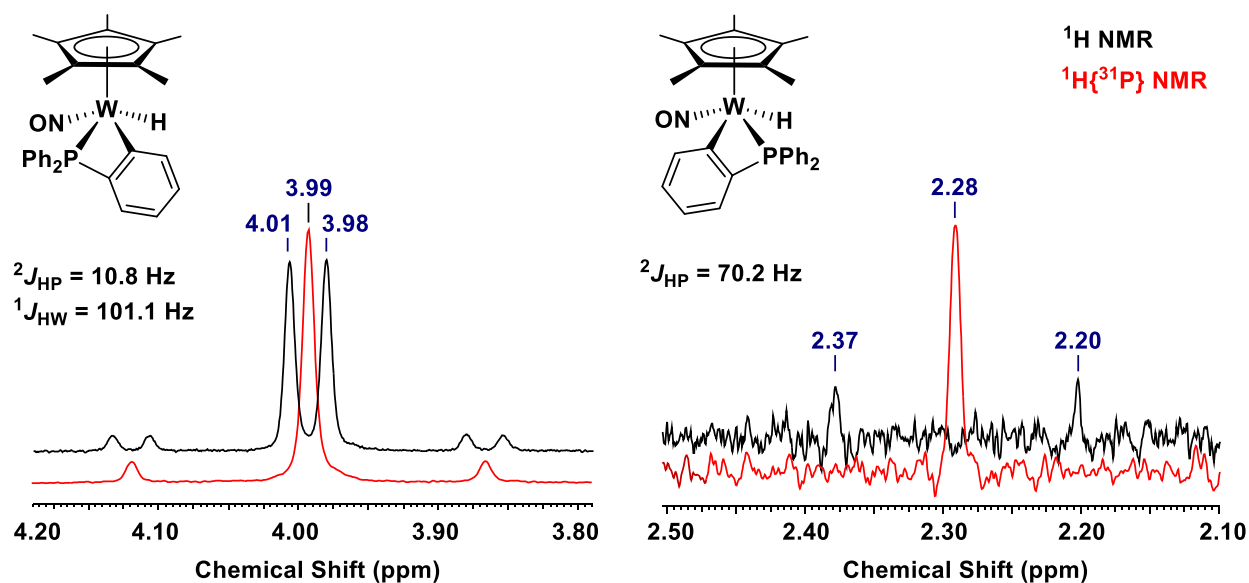


Figure 3.1. (a) Expansions of ^1H (black) and $^1\text{H}\{^{31}\text{P}\}$ (red) NMR spectra (400 MHz, C_6D_6) from δ 3.79 to 4.20 ppm showing the hydride resonance of complex **3.1**. (b) Expansions of the ^1H (black) and $^1\text{H}\{^{31}\text{P}\}$ (red) NMR spectra (400 MHz, C_6D_6) from δ 2.10 to 2.50 ppm showing the hydride resonance of complex **3.2**.

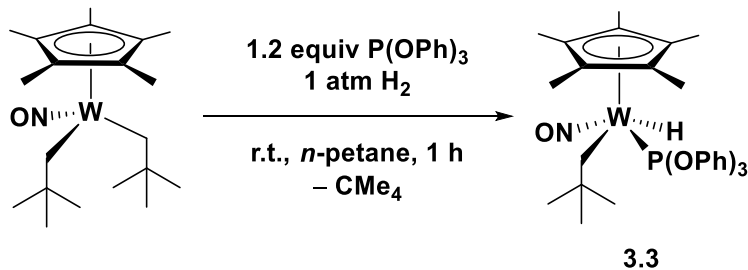
Attempts to recrystallize **3.2** from solutions of Et_2O or *n*-pentane at $-30\text{ }^\circ\text{C}$ in order to obtain single-crystals of sufficient quality for an X-ray diffraction analysis have been unsuccessful. However, this *cis*–*trans* isomerization is also seen in an analogous complex, *trans*- $\text{Cp}^{i\text{-Pr}}\text{W}(\text{NO})(\text{H})(\kappa^2\text{-PPh}_2(\text{C}_6\text{H}_4))$ [$\text{Cp}^{i\text{-Pr}} = \eta^5\text{-C}_5\text{H}_4i\text{-Pr}$], which has been synthesized by Ms. Diana Fabulyak. Crystals of this complex suitable for single-crystal X-ray analysis have been obtained and the solid-state molecular structure confirms the *trans* orientation of the

ligands.⁶⁰ The synthesis of this complex is carried out in a similar manner compared to **3.1**, except that $\text{Cp}^{i\text{-Pr}}\text{W}(\text{NO})(\text{CH}_2\text{CMe}_3)_2$ is used as the initial reactant. From this reaction, only the *trans* isomer is observed probably due to the *cis* isomer undergoing isomerization into *trans* as soon as it forms in solution. As expected, the ^1H NMR spectrum of *trans*- $\text{Cp}^{i\text{-Pr}}\text{W}(\text{NO})(\text{H})(\kappa^2\text{-PPh}_2(\text{C}_6\text{H}_4))$ in C_6D_6 , displays a resonance attributable to the hydride ligand at δ 2.27 ppm with a $^2J_{\text{HP}}$ of 70.6 Hz, which is comparable to that of **3.2** and is consistent with the observation that $^2J_{\text{HP}}$ or $^2J_{\text{PH}}$ values are indicative of the *cis* or *trans* orientation of the alkyl and hydrido ligands.

3.2.5 Synthesis of *trans*- $\text{Cp}^*\text{W}(\text{NO})(\text{CH}_2\text{CMe}_3)(\text{H})(\text{P}(\text{OPh})_3)$ (**3.3**)

The synthesis and isolation of *trans*- $\text{Cp}^*\text{W}(\text{NO})(\text{CH}_2\text{CMe}_3)(\text{H})(\text{P}(\text{OPh})_3)$ (**3.3**) has been performed in order to investigate its C–H activation chemistry with hydrocarbon substrates. $\text{P}(\text{OPh})_3$ has a Tolman cone angle of 128° , indicating a smaller steric demand when compared to PPh_3 which has a Tolman cone angle of 145° .^{68,69} $\text{P}(\text{OPh})_3$ also has a pK_a of -2.00 , signifying a decrease in the σ -donation capability of the proligand.⁶² This Lewis base is a direct comparison to the PPh_3 systems, and should result in the formation of *ortho*-metalated products being less likely due to the *ortho* C–H bonds of the phenyl substituents being further removed from the metal centre. As shown in Scheme 3.6, the synthesis of complex **3.3** is performed by a reaction of $\text{Cp}^*\text{W}(\text{NO})(\text{CH}_2\text{CMe}_3)_2$, $\text{P}(\text{OPh})_3$, and H_2 in *n*-pentane for 1 hour at ambient temperatures.

Scheme 3.6. Synthesis of complex 3.3



The synthesis of **3.3** likely follows a similar mechanism as seen with complex **3.1**, except that only one equivalent of neopentane is eliminated from the reaction. The *trans* orientation of ligands in complex **3.3** is confirmed by a solid-state molecular structure. No evidence is seen for the formation of the *cis* isomer of **3.3**, suggesting that the mechanism for the formation of this complex differs from that of **3.2** in that it does not form from a *cis*–*trans* isomerization, but instead results directly from the reaction. Additionally, it is important to note that signals due to Cp*W(NO)(κ²-P(OPh)₂(OC₆H₄)), the *ortho*-metalated product, are not observed in the NMR or MS data of the reaction mixture, hence a *cis*–*trans* isomerization pathway as depicted in Scheme 2.5 is not possible. The use of P(OPh)₃ also successfully inhibits the formation of disproportionation products since no Cp*W(NO)(P(OPh)₃)₂ is formed from the reaction.

The NMR and IR data of the complex are fully consistent with the structure drawn above in Scheme 3.6. Consistent with previous observations, the ¹H NMR spectrum of complex **3.3** in C₆D₆ displays a resonance attributable to the hydride ligand at δ -2.42 ppm that exhibits a ²J_{HP} coupling constant of 117.4 Hz, indicative of a *trans* configuration of ligands (Figure B.7). Complex **3.3** displays a ν_{NO} of 1591 cm⁻¹ in the IR spectrum, which signifies a smaller amount of electron density existing on the metal centre when compared to **3.1** and **3.2**. This decrease in electron density is probably due to the less σ-donating P(OPh)₃ ligand. Purification attempts of

3.3 via column chromatography over basic alumina are unsuccessful at completely isolating the complex since the complex requires a high polarity solvent to be eluted, at which point impurities from the reaction co-elute with the product.

Recrystallization of **3.3** from an Et₂O solution at -30 °C results in crystals suitable for single-crystal X-ray diffraction analysis, and a solid-state molecular structure has been obtained (Figure 3.2). This complex is a four-legged piano-stool molecule capped by a Cp* ring in which the hydride ligand is situated in a *trans* orientation to the alkyl ligand. Even though the hydride ligand in Figure 3.2 has not been located, the analysis has revealed a “vacant” coordination slot between the phosphite and nitrosyl ligands at which it probably coordinates to the tungsten centre (Figure 3.3). This complex has an essentially linear nitrosyl ligand with a W(1)–N(1)–O(1) angle of 169.9(3)°, and the W(1)–P(1) bond length is similar to those found in related four-legged piano-stool molecules.^{41,58,70}

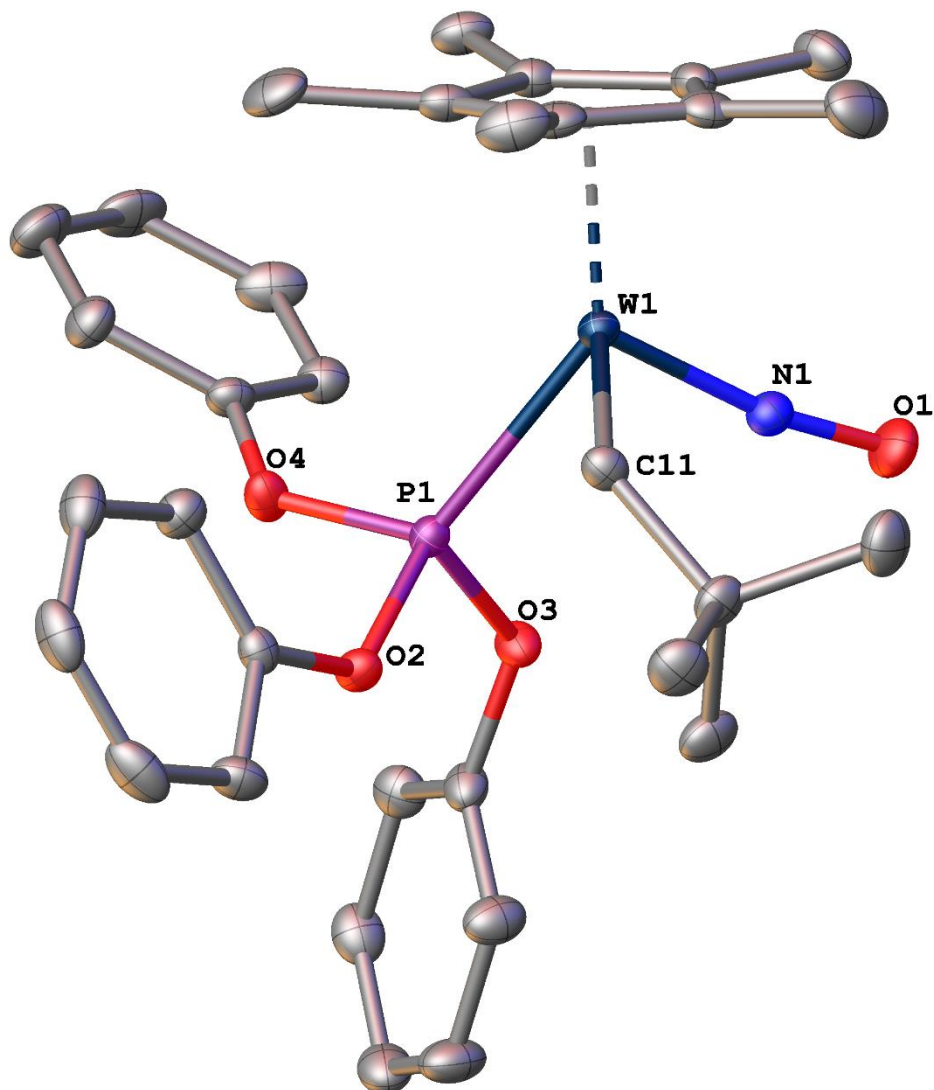


Figure 3.2. Solid-state molecular structure of **3.3** with 50% probability thermal ellipsoids shown.

Hydrogen atoms have been omitted for the sake of clarity. Selected bond lengths (Å) and angles (deg): W(1)–N(1) = 1.783(3), W(1)–P(1) = 2.4216(9), W(1)–C(11) = 2.274(4), N(1)–O(1) = 1.225(4), P(1)–O(2) = 1.611(3), P(1)–O(3) = 1.611(3), P(1)–O(4) = 1.626(3), W(1)–N(1)–O(1) = 169.9(3), N(1)–W(1)–C(11) = 94.77(14), C(11)–N(1)–P(1) = 82.55(9), N(1)–W(1)–P(1) = 95.43(10).

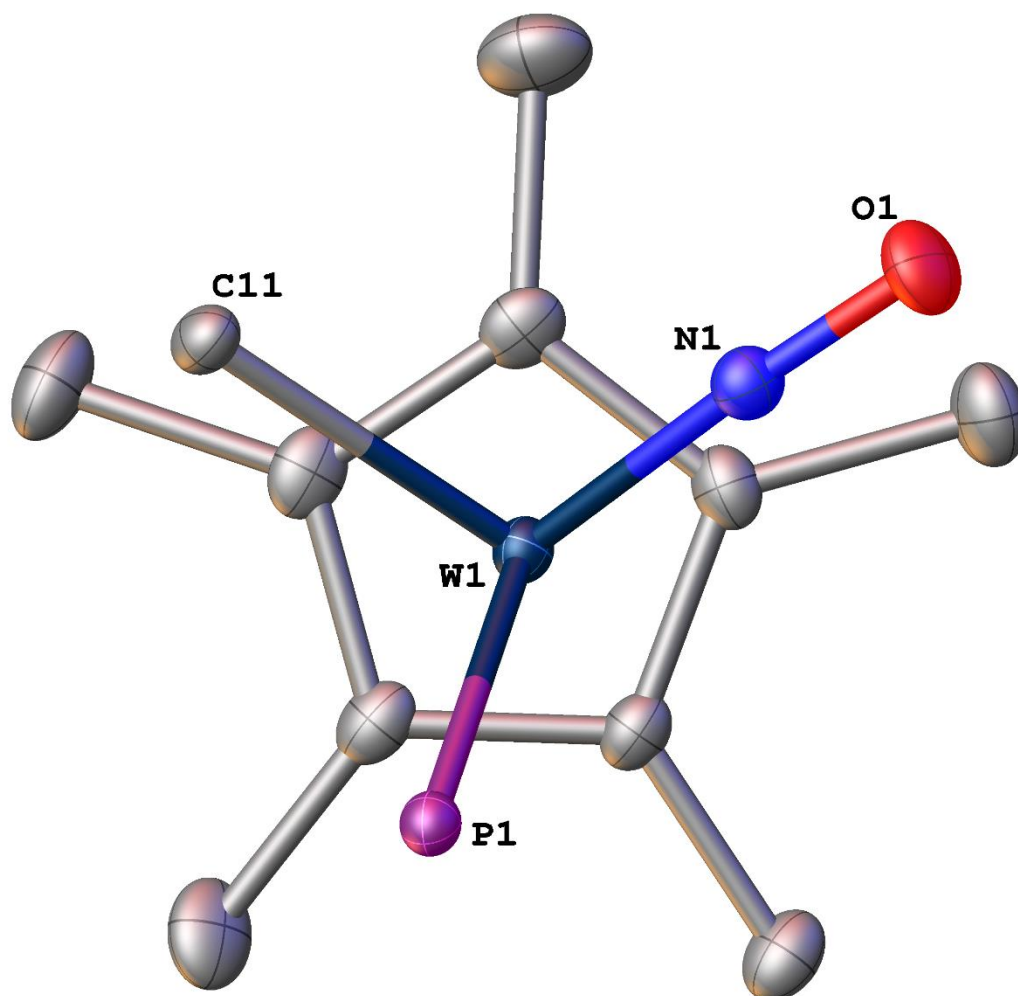


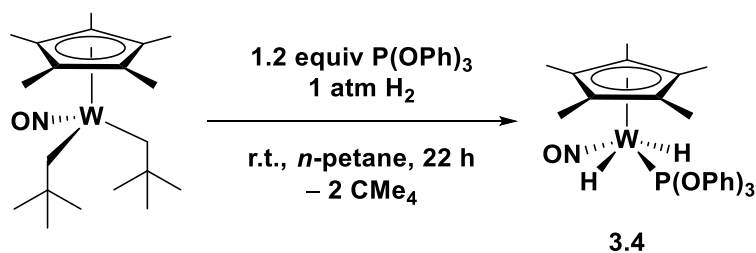
Figure 3.3. View of the solid-state molecular structure of **3.3** along the W–Cp* axis displaying the vacant coordination slot between the phosphite and nitrosyl ligands where the hydride ligand resides. The carbon atoms of the neopentyl ligand other than C11, the OPh substituents of the phosphite ligand, and the hydrogen atoms of the complex have been omitted for the sake of clarity.

Unfortunately, heating of **3.3** at 50 °C in neat solutions of C₆H₆ or *n*-pentane results in the elimination of neopentane, release of proligand P(OPh)₃, and subsequent decomposition of the remaining organometallic fragment into mixtures of intractable products. Even at ambient temperatures the organometallic complex slowly eliminates neopentane, releases proligand, and undergoes decomposition. Interestingly, when the same synthesis for **3.3** is carried out but with CpW(NO)(CH₂SiMe₃)₂ [Cp = η⁵-C₅H₅] as the initial reactant, the product formed is CpW(NO)(CH₂SiMe₃)(H)(P(OPh)₃) which, upon heating at 50 °C in neat C₆D₆, forms the *ortho*-metalated complex CpW(NO)(H)(κ²-P(OPh)₂(OC₆H₄)).⁵⁵

3.2.6 Synthesis of *trans*-Cp*W(NO)(H)₂(P(OPh)₃) (**3.4**)

Curiously, if the exact reaction mentioned above for the formation of **3.3** from Cp*W(NO)(CH₂CMe₃)₂, P(OPh)₃, and H₂ is left for 22 hours rather than 1 hour, a completely different complex is formed, namely *trans*-Cp*W(NO)(H)₂(P(OPh)₃) (**3.4**) (Scheme 3.7). This complex probably results from further hydrogenation and neopentane elimination of the initially formed *trans*-Cp*W(NO)(CH₂CMe₃)(H)(P(OPh)₃).

Scheme 3.7. Synthesis of complex 3.4



The spectroscopic properties of the complex are consistent with the structure drawn above wherein the two hydride ligands are located in a *trans* orientation. For instance, in the ^1H NMR spectrum in C_6D_6 , the signal attributable to the hydride ligands exhibits a $^2J_{\text{HP}}$ coupling constant of 85.9 Hz, indicating that the hydride ligands are located *trans* to one another (Figure B.11). Additionally, the hydride resonance in the $^1\text{H}\{^{31}\text{P}\}$ NMR spectrum is a sharp singlet with ^{183}W satellites that has a relative integration of 2, indicating that the hydride ligands of **3.4** are in an identical chemical environment. Complex **3.4** exhibits a ν_{NO} in the IR spectrum at 1591 cm^{-1} , which indicates that it has a similar amount of electron density on the metal centre when compared to complex **3.3**, its mononeopentyl analogue. Purification attempts of **3.4** via column chromatography over basic alumina are unsuccessful in completely isolating the complex since the complex requires a high polarity solvent to be eluted, at which point impurities co-elute with the product.

3.2.7 Related $\text{Cp}^*\text{W}(\text{NO})(\text{R})(\text{H})(\text{L})$ Systems within the Research Group

Other related complexes have been synthesized within the research group that utilize other L proligands that vary by size and donor capability. The other Lewis bases used include NPh_3 , PMe_3 , $\text{P}(\text{OMe})_3$, $\text{P}(\text{Mes})_3$, $\text{P}(\text{C}_6\text{F}_5)_3$, and $\text{P}(\text{OCH}_2)_3\text{CMe}$. Novel complexes have been synthesized utilizing these proligands, with the exception of NPh_3 and $\text{P}(\text{Mes})_3$, which did not form organometallic complexes, and PMe_3 , which has been reported previously.^{56,60} The complexes *trans*- $\text{Cp}^*\text{W}(\text{NO})(\text{CH}_2\text{CMe}_3)(\text{H})(\text{P}(\text{OMe})_3)$ and *trans*- $\text{Cp}^*\text{W}(\text{NO})(\text{CH}_2\text{CMe}_3)(\text{H})(\text{P}(\text{OCH}_2)_3\text{CMe})$ can successfully effect the C–H activation of benzene and form the corresponding phenyl hydrido complexes, but with all other compounds,

any attempts to further C–H activation chemistry beyond that which is previously reported have been unsuccessful. In all cases, the C–H activation experiments in neat hydrocarbon solvents result in disproportionation products, decomposition products, and/or the formation of an inactive species.

3.3 Summary

The complex *cis*-Cp*W(NO)(H)(κ^2 -PPh₂(C₆H₄)) (**3.1**) is known to effect the intermolecular C–H activation of benzene in neat solutions at 50 °C. Attempts to expand this reactivity to encompass other hydrocarbon substrates that contain C(*sp*²)–H and C(*sp*³)–H bonds are unsuccessful and do not result in the desired η^1 -hydrocarbyl complexes. Instead, at increased temperatures, **3.1** undergoes *cis*–*trans* isomerization into *trans*-Cp*W(NO)(H)(κ^2 -PPh₂(C₆H₄)) (**3.2**), and also forms Cp*W(NO)(PPh₃)₂, a disproportionation product. A spectroscopic trend in the ¹H and ³¹P NMR spectra is observed, and the *cis* and *trans* isomers are found to be discernable from one another by the magnitude of the coupling constants attributable to their hydride or phosphorus ligands in ¹H or ³¹P NMR spectra, respectively. In an attempt to circumvent the problems of isomerization and disproportionation that result in inactive species being formed, P(OPh)₃ is used to synthesize the complexes *trans*-Cp*W(NO)(CH₂CMe₃)(H)(P(OPh)₃) (**3.3**) and *trans*-Cp*W(NO)(H)₂(P(OPh)₃) (**3.4**). Complex **3.3** successfully overcomes the problems of isomerization and disproportionation since no *ortho*-metalated or disproportionation products are formed. However, **3.3** does not effect any C–H activation chemistry in hydrocarbon solutions at elevated or ambient temperatures. Instead, the

elimination of neopentane, release of P(OPh)₃, and subsequent decomposition of the organometallic fragment are prevalent and even occur at ambient temperatures, albeit slowly.

3.4 Experimental Section

3.4.1 General Procedures

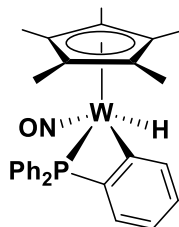
All reactions and subsequent manipulations involving organometallic reagents were performed under anhydrous and anaerobic conditions except where noted. High-vacuum and inert-atmosphere techniques were performed using double-manifold Schlenk lines or in Innovative Technologies LabMaster 100 and MS-130 BG dual-station gloveboxes equipped with freezers maintained at $-30\text{ }^{\circ}\text{C}$. Preparative scale reactions were performed with Schlenk or round bottom flasks; reactions were performed in thick-walled glass reaction flasks (larger scale) or J. Young NMR tubes (smaller scale), both of which were typically sealed with Kontes greaseless stopcocks. Tetrahydrofuran (THF) and diethyl ether (Et₂O) were dried over sodium/benzophenone ketyl and freshly distilled prior to use; *n*-pentane was dried over calcium hydride and freshly distilled prior to use; all other solvents were dried according to standard procedures. Complexes Cp*W(NO)Cl₂³² and Cp*W(NO)(CH₂CMe₃)₂⁶⁷ were prepared according to the published procedures. Pentamethylcyclopentadiene was obtained from the Boulder Scientific Co. All other chemicals and reagents were ordered from commercial suppliers and used as received. Unless otherwise specified, all IR samples were prepared as Nujol mulls sandwiched between NaCl plates, and their spectra were recorded on a Thermo Nicolet model 4700 FT-IR spectrometer. Except where noted, all NMR spectra were recorded at room

temperature on Bruker AV-400 instruments (direct and indirect probes), and all chemical shifts are reported in parts per million and coupling constants in hertz. ^1H NMR spectra were referenced to the residual protio isotopomer present in C_6D_6 (7.16 ppm). ^{13}C NMR spectra were referenced to C_6D_6 (128.39 ppm). ^{31}P NMR spectra were externally referenced to 85% H_3PO_4 . For the characterization of most complexes, two-dimensional NMR experiments, $\{^1\text{H}-^1\text{H}\}$ COSY, $\{^1\text{H}-^{13}\text{C}\}$ HSQC, $\{^1\text{H}-^{31}\text{P}\}$ HMBC, and $\{^1\text{H}-^{13}\text{C}\}$ HMBC, were performed to correlate and assign ^1H , ^{13}C , and ^{31}P NMR signals and establish atom connectivity. Low- and high-resolution mass spectra (EI, 70 eV) and MALDI-TOF spectra were recorded by M. Lapawa of the UBC mass spectrometry facility using a Kratos MS-50 spectrometer and a Bruker Autoflex spectrometer, respectively. M. Yeung recorded ESI mass spectra on a Bruker HCT spectrometer, and elemental analyses were performed by D. Smith of the UBC microanalytical facility. X-ray crystallographic data collection, solution, and refinement were performed by Dr. B. O. Patrick of the UBC X-ray crystallography facility.

3.4.2 Synthesis of *cis*- $\text{Cp}^*\text{W}(\text{NO})(\kappa^2\text{-PPh}_2(\text{C}_6\text{H}_4))(\text{H})$ (3.1)

In a glovebox, a thick-walled flask was charged with $\text{Cp}^*\text{W}(\text{NO})(\text{CH}_2\text{CMe}_3)_2$ (0.495 g, 1.007 mmol) and a magnetic stir bar. On a double-manifold, the flask was then charged with PPh_3 (0.320 g, 1.220 mmol) and *n*-pentane (ca. 50 mL) to obtain a dark red solution. In a fume hood, H_2 was bubbled through the reaction mixture for 5 min, and the flask was then sealed under 1 atm of H_2 . The reaction mixture was stirred at room temperature overnight, whereupon it developed a green colour and a yellow precipitate was deposited. The solvent was removed from the final reaction mixture by cannulation and the remaining precipitate was washed with *n*-

pentane (10 × 10 mL) before being dried in vacuo to obtain *cis*-Cp*W(NO)(H)(κ²-PPh₂(C₆H₄)) (**3.1**) as a yellow solid (0.249 g, 0.407 mmol, 40% yield).

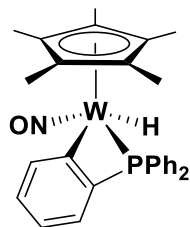


Characterization data for *cis*-Cp*W(NO)(H)(κ²-PPh₂(C₆H₄)) (**3.1**). IR (cm⁻¹): 1545 (s, ν_{NO}). ¹H NMR (400 MHz, C₆D₆): δ 1.79 (s, 15H, C₅Me₅), 4.00 (d, ¹J_{HW} = 101.1, ²J_{HP} = 10.8, 1H, WH), 7.49 (t, ²J_{HH} = 8.2, 1H, aryl H), 7.85 (m, 1H, aryl H), 7.95 (m, 2H, aryl H), 8.09 (d, ²J_{HH} = 7.2, 1H, aryl H). ³¹P{¹H} NMR (162 MHz, C₆D₆): δ -48.6 (s, ¹J_{PW} = 168.4, WP). This data matches previously reported spectroscopic data.⁵⁷

3.4.3 Isomerization of *cis*-Cp*W(NO)(κ²-PPh₂(C₆H₄))(H)

In a glovebox, a thick-walled flask was charged with *cis*-Cp*W(NO)(H)(κ²-PPh₂(C₆H₄)) (0.064 g, 0.100 mmol), *n*-pentane (ca. 20 mL), and a magnetic stir bar to produce a dark yellow solution. The reaction mixture was heated overnight at 80 °C while being stirred, whereupon it became yellow-brown in colour. The solvent was removed from the final reaction mixture in vacuo to produce a yellow solid whose ¹H NMR spectrum in C₆D₆ showed it to consist of a 3:1 mixture of *trans*-Cp*W(NO)(H)(κ²-PPh₂(C₆H₄)) (**3.2**) and *cis*-Cp*W(NO)(H)(κ²-PPh₂(C₆H₄))

(3.1). Attempts at separating the two isomers of $\text{Cp}^*\text{W}(\text{NO})(\text{H})(\kappa^2\text{-PPh}_2(\text{C}_6\text{H}_4))$ have been unsuccessful.

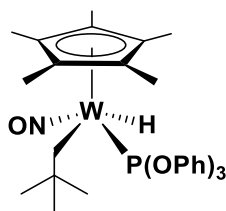


Partial characterization data for *trans*- $\text{Cp}^*\text{W}(\text{NO})(\text{H})(\kappa^2\text{-PPh}_2(\text{C}_6\text{H}_4))$ (3.2). IR (cm^{-1}): 1552 (s, ν_{NO}). MS (LREI, m/z , probe temperature of 150 °C): 611 [M^+ , ^{184}W]. HRMS-EI m/z : [M^+ , ^{182}W] calcd for $\text{C}_{28}\text{H}_{30}\text{NOP}^{182}\text{W}$, 609.15510; found, 609.15473. ^1H NMR (400 MHz, C_6D_6): δ 1.75 (s, 15H, C_5Me_5), 2.29 (d, $^2J_{\text{HP}} = 70.2$, 1H, WH), 6.88 (m, 1H, aryl H), 7.00 (m, 2H, aryl H), 7.05 (m, 4H, aryl H), 7.29 (m, 1H, aryl H), 7.37 (m, 4H, aryl H), 7.78 (m, 1H, aryl H), 8.01 (dd, $^3J_{\text{HP}} = 11.5$, $^3J_{\text{HH}} = 7.2$, 1H, aryl H). ^{13}C APT NMR (100 MHz, C_6D_6): δ 11.0 (C_5Me_5), 106.1 (C_5Me_5), 128.9 (aryl C), 129.1 (aryl C), 129.2 (aryl C), 132.6 (m, aryl C), 132.8 (m, aryl C), 134.5 (m, aryl C), 135.2 (m, aryl C), 138.4 (m, aryl C), 152.3 (m, aryl C), 167.8 (m, aryl C). ^{31}P NMR (162 MHz, C_6D_6): δ -39.5 (d, $^1J_{\text{PW}} = 148.5$, $^2J_{\text{PH}} = 38.5$, WP).

3.4.4 Synthesis of *trans*- $\text{Cp}^*\text{W}(\text{NO})(\text{CH}_2\text{CMe}_3)(\text{H})(\text{P}(\text{OPh})_3)$ (3.3)

In a glovebox, a thick-walled flask was charged with $\text{Cp}^*\text{W}(\text{NO})(\text{CH}_2\text{CMe}_3)_2$ (0.266 g, 0.519 mmol), *n*-pentane (ca. 20 mL), and a magnetic stir bar, resulting in a dark red solution. On a double-manifold, $\text{P}(\text{OPh})_3$ (0.164 mL, 0.623 mmol) was added to the reaction vessel. In a

fume hood, H₂ was flushed through the vessel for 15 minutes before the flask was sealed under 1 atm of H₂. After being stirred at room temperature for 1 h, the reaction mixture consisted of a dark turquoise solution and a yellow precipitate. The supernatant solution was removed via filter cannulation, and the precipitate was washed with *n*-pentane (4 × 10 mL) to obtain Cp*W(NO)(CH₂CMe₃)(H)(P(OPh)₃) (**3.3**) as a light yellow solid (0.100 g, 0.137 mmol, 27% yield). Crystals suitable for single-crystal X-ray diffraction analysis were obtained by maintaining an Et₂O solution of the compound at -30 °C for several days. As of yet, an analytically pure sample of **3.3** has not been obtained.



Characterization data for Cp*W(NO)(CH₂CMe₃)(H)(P(OPh)₃) (**3.3**). IR (cm⁻¹): 1878 (vw, ν_{WH}), 1590 (s, ν_{NO}). MS (LREI, *m/z*, probe temperature of 150 °C): 659 [M⁺ - CMe₄, ¹⁸⁴W]. ESI(+)-MS (40 V, *m/z*): 731.3 for C₃₃H₄₂NO₄PW ([M]⁺, ¹⁸⁴W). ¹H NMR (400 MHz, C₆D₆): δ -2.42 (ddd, ²J_{HP} = 117.4, ¹J_{HW} = 47.2, ³J_{HH} = 8.2, 5.4, 1H, WH), 0.78 (ddd, ²J_{HH} = 12.9, ³J_{HP} = 11.7, ³J_{HH} = 5.3, 1H, CH₂Me₃), 1.59 (s, 9H, CH₂CMe₃), 1.60 (s, 15H, C₅Me₅), 2.38 (ddd, ³J_{HP} = 33.1, ²J_{HH} = 13.3, ³J_{HH} = 8.2, 1H, CH₂CMe₃), 6.82 (t, ³J_{HH} = 7.4, 3H, *p*-aryl H), 7.00 (t, ³J_{HH} = 7.6, 6H, *m*-aryl H), 7.28 (d, ³J_{HH} = 8.4, 6H, *o*-aryl H). ¹³C APT NMR (100 MHz, C₆D₆): δ 10.8 (C₅Me₅), 27.9 (d, ²J_{CP} = 20.4, CH₂CMe₃), 35.4 (CH₂CMe₃), 38.8 (d, ³J_{CP} = 1.5, CH₂CMe₃), 106.6 (d, ²J_{CP} = 2.3, C₅Me₅), 121.8 (d, ³J_{CP} = 4.5, *o*-aryl C), 124.8 (*p*-aryl C) 130.1

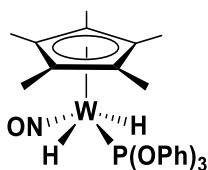
(*m*-aryl C), 153.0 (ipso C). ^{31}P NMR (162 MHz, C_6D_6): δ 120.0 (ddd, $^1J_{\text{PW}} = 361.6$, $^2J_{\text{PH}} = 116.9$, $^3J_{\text{PH}} = 33.7$, 11.4, WP).

3.4.5 Synthesis of *trans*-Cp*W(NO)(H)₂(P(OPh)₃) (3.4)

The reaction involving Cp*W(NO)(CH₂CMe₃)₂ (0.256 g, 0.521 mmol), P(OPh)₃ (0.164 mL, 0.626 mmol), H₂, and *n*-pentane was performed as outlined in the preceding section.

However, in this instance the reaction mixture was stirred for 22 h at room temperature to obtain a dark green solution with green precipitate. The supernatant solution was removed via filter cannulation, and the precipitate was washed with cold *n*-pentane (4 × 10 mL) to obtain *trans*-Cp*W(NO)(H)₂(P(OPh)₃) (3.4) as a yellow-green solid (0.055 g, 0.083 mmol, 16% yield).

Attempts to effect further purification of this solid by column chromatography on basic alumina or by crystallization from Et₂O or Et₂O/*n*-pentane solutions were unsuccessful. Consequently, as of yet, an analytically pure sample of 3.4 has not been obtained.



Characterization data for Cp*W(NO)(H)₂(P(OPh)₃) (3.4). IR(cm^{-1}): 1591 (s, ν_{NO}). MS (LREI, m/z , probe temperature 150 °C): 659 [$\text{M}^+ - \text{H}_2$, ^{184}W]. HRMS-EI m/z : [$\text{M}^+ - \text{H}_2$, ^{182}W] calcd for $\text{C}_{28}\text{H}_{30}\text{NO}_4\text{P}^{182}\text{W}$, 657.13947; found, 657.14009. ^1H NMR (400 MHz, C_6D_6): δ -0.94 (d, $^1J_{\text{HW}} = 90.6$, $^2J_{\text{HP}} = 85.9$, 2H, WH), 1.86 (s, 15H, C_5Me_5), 6.88 (t, $^3J_{\text{HH}} = 7.4$, 3H, *p*-aryl H),

7.07 (t, $^3J_{\text{HH}} = 7.8$, 6H, *m*-aryl H), 7.35 (d, $^3J_{\text{HH}} = 8.2$, 6H, *o*-aryl H). ^{13}C APT NMR (100 MHz, C_6D_6): δ 11.7 (C_5Me_5), 105.7 (C_5Me_5), 122.5 (d, $^3J_{\text{CP}} = 4.6$, *o*-aryl C), 125.3 (*p*-aryl C), 130.5 (*m*-aryl C), 153.2 (ipso C). ^{31}P NMR (162 MHz, C_6D_6): δ 142.7 (t, $^1J_{\text{PW}} = 281.9$, $^2J_{\text{PH}} = 86.0$, WP).

3.4.6 X-ray Crystallography

Data collection was carried out at -173.0 ± 2 °C on a Bruker X8 APEX II diffractometer with cross-coupled multilayer optics Mo-K α radiation.

The data for **3.3** were collected to a maximum 2θ value of 60.2° in 0.5° oscillations using 10.0-second exposures. The crystal-to-detector distance was 60.12 mm. The material crystallizes as a two-component ‘split-crystal’ with components one and two related by a 2.6° rotation about the $(-0.222 \ 0.017 \ 1)$ reciprocal crystal axis. Data were integrated for both twin components, including both overlapped and non-overlapped reflections. The structure was solved by direct methods⁷¹ using non-overlapped data from the major twin component and expanded using Fourier techniques. Subsequent refinements were carried out using a HKLF 5 format data set, containing data from both twin components. The material crystallizes with two crystallographically independent molecules in the asymmetric unit. All non-hydrogen atoms were refined anisotropically. All hydrogen atoms were included in calculated positions but not refined. The final cycle of full-matrix least-squares refinement was based on 37919 reflections and 738 variable parameters.

Neutral atom scattering factors were taken from Cromer and Waber.⁷² Anomalous dispersion effects were included in F_{calc}^{73} ; the values for $\Delta f'$ and $\Delta f''$ were those of Creagh and

McAuley.⁷⁴ The values for the mass attenuation coefficients are those of Creagh and Hubbell.⁷⁵

All refinements were performed using the SHELXL-2014⁷⁶ via the OLEX2⁷⁷ interface.

Table 3.1. X-ray crystallographic data for complex **3.3**.

Complex	3.3
Empirical Formula	C ₃₃ H ₄₁ NO ₄ PW
Formula Weight	731.24
Crystal Colour, Habit	yellow, irregular
Crystal Size (mm)	0.14 × 0.20 × 0.52
Crystal System	monoclinic
Space Group	<i>P</i> 2 ₁ / <i>n</i>
Volume (Å ³)	6159.6(4)
a (Å)	22.8828(9)
b (Å)	9.1026(3)
c (Å)	29.5801(12)
α (°)	90
β (°)	91.369(2)
γ (°)	90
Z	8
Density, ρ (calculated) (g/cm ³)	1.575
Absorption Coefficient, μ (mm ⁻¹)	3.84
F ₀₀₀	2936.0
Measured Reflections: Total	181939
Measured Reflections: Unique	37919
Final R Indices ^a	R ₁ = 0.042 wR ₂ = 0.099
Goodness-of-fit on F ² , ^b	1.05
Largest diff. peak/hole (e ⁻ Å ⁻³)	3.90/-0.67

$${}^a\text{R1 on F} = \sum ||F_o| - |F_c|| / \sum |F_o| ; \text{wR2} = \sqrt{\sum ((F_o^2 - F_c^2)^2) / \sum w(F_o^2)^2} ; w = (\sigma^2 F_o^2)^{-1}$$

$${}^b\text{GOF} = \sqrt{\sum (w (|F_o| - |F_c|)^2) / \text{degrees of freedom}}$$

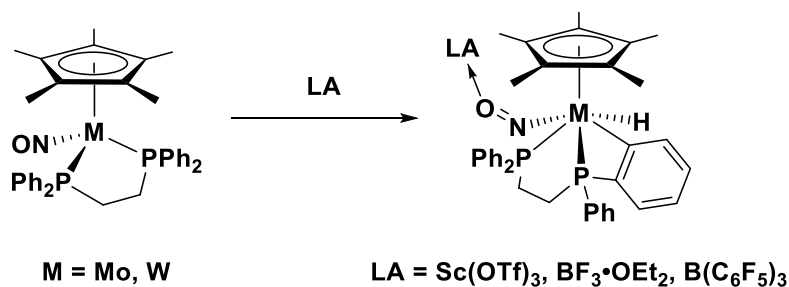
Chapter 4: Synthesis and Reactivity of

Cp*Mo(NO)(κ^2 -dmpe) Systems

4.1 Introduction

In the investigations of the $\text{Cp}^*\text{W}(\text{NO})(\text{R})(\text{H})(\text{L})$ systems, the lability of the L phosphine or phosphite ligands result in unwanted isomerization and disproportionation reaction pathways. Hence, $\text{Cp}^*\text{M}(\text{NO})$ -containing systems utilizing bisphosphine ligands have been investigated since these bidentate ligands impede these unwanted reactions. The use of bidentate bisphosphine ligands is common in the literature. For instance, these ligands are used in metal catalyzed transformations such as borylation,^{78,79} Suzuki cross-coupling,⁸⁰⁻⁸² C–N amination,⁸³⁻⁸⁶ or C–H functionalization.⁸⁷⁻⁹⁰ We have recently extended our investigations to compounds that possess electron-rich metal centres such as $\text{Cp}^*\text{M}(\text{NO})(\kappa^2\text{-dppe})$ [dppe = 1,2-bis(diphenylphosphino)ethane] that should, in principle, facilitate the oxidative addition of hydrocarbon C–H bonds to them. Interestingly, the $\text{Cp}^*\text{W}(\text{NO})(\kappa^2\text{-dppe})$ compounds are rendered prone to effecting C–H activation reactions not by thermolyses, but by treatment with equimolar amounts of appropriate Lewis acids (LA) which readily form adducts with the basic O-termini of their nitrosyl ligands (Scheme 4.1).⁹¹

Scheme 4.1. Lewis-Acid Induced Intramolecular C–H Activation



Regrettably, these systems only promote intramolecular C–H activations, presumably because steric factors in the metal’s coordination sphere bring one of the phenyl substituents of the dppe ligand into a position in which it can readily undergo *ortho*-metalation. The related and less sterically bulky Cp*M(NO)(κ²-dmpe) [dmpe = 1,2-bis(dimethylphosphino)ethane] complexes were then used in order to overcome this mode of reactivity. Unfortunately, treatment of the dmpe compounds with Lewis acids does not result in the desired intermolecular C–H activations.⁹² Consequently, we have extended our investigations to encompass other reactants in order to establish the characteristic chemical properties of one of the Cp*M(NO)(κ²-dmpe) complexes. In this chapter, investigations into the reactivity of the molybdenum complex towards the C–H activation of hydrocarbon substrates are described, and have been extended to investigate the novel reactivity of the complex with elemental sulfur and organic halides. Molybdenum is used instead of tungsten for these investigations to aid in the efficiency of the study, since we have found that tungsten complexes and their molybdenum analogues tend to act similarly with the exception that the molybdenum analogues generally react faster and produce cleaner results with fewer byproducts.

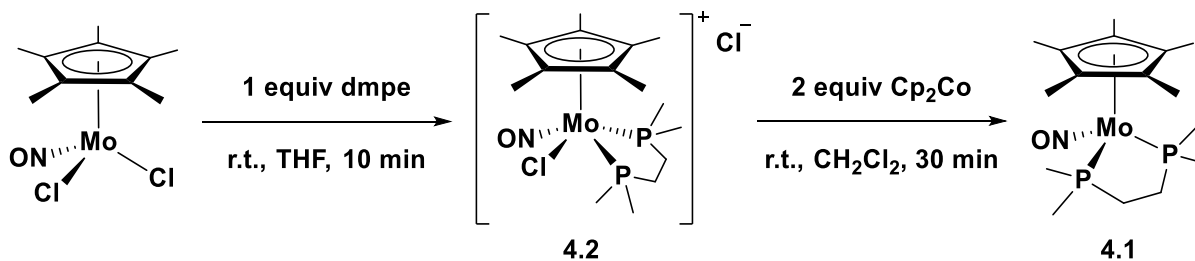
4.2 Results and Discussion

4.2.1 Synthesis of Cp*Mo(NO)(κ²-dmpe) (4.1)

The synthesis of Cp*Mo(NO)(κ²-dmpe) (**4.1**) is performed from a two-step reaction of Cp*Mo(NO)Cl₂, 1 equivalent of dmpe, and 2 equivalents of Cp₂Co at ambient temperatures. The first reaction of Cp*Mo(NO)Cl₂ with dmpe in THF solvent results in the formation of the

intermediate complex, $[\text{Cp}^*\text{Mo}(\text{NO})(\text{Cl})(\kappa^2\text{-dmpe})]\text{Cl}$ (**4.2**). After removal of the THF solvent, the intermediate complex is redissolved in CH_2Cl_2 , in which it is readily soluble, and forms a yellow solution. The second step involves the reduction of the molybdenum centre in **4.2** by cobaltocene in CH_2Cl_2 , and this results in the formation of complex **4.1**. The CH_2Cl_2 solvent is removed in vacuo from the now red solution, and Et_2O extractions are carried out to remove the desired product from the $[\text{Cp}_2\text{Co}]\text{Cl}$ byproducts. The product is then purified via recrystallization from Et_2O at $-30\text{ }^\circ\text{C}$ and is isolated as analytically pure dark orange crystals in a 36% yield. The complete synthesis of **4.1** is depicted in Scheme 4.2.

Scheme 4.2. Two-step synthesis of 4.1



The spectroscopic properties are fully consistent with the structures depicted above in Scheme 4.2. Complex **4.1** has an IR ν_{NO} frequency of 1535 cm^{-1} , which is a manifestation of the significant electron density in existence on the metal centre due to the strongly-donating dmpe ligand that in turn results in considerable $\text{Mo}\rightarrow\text{NO}$ π backbonding. This indicates a large overall increase in the amount of electron density extant on the metal centre when compared to the initial reactant, $\text{Cp}^*\text{Mo}(\text{NO})\text{Cl}_2$, which has a ν_{NO} frequency in its IR spectrum at 1647 cm^{-1} . This large increase in electron density is attributed to the removal of the weaker-donating chloro ligands and the incorporation of a stronger-donating bisphosphine ligand.

Interestingly, the infrared spectrum of the intermediate complex **4.2** displays a ν_{NO} frequency at 1661 cm^{-1} , indicative of an overall decrease in the amount of electron density backbonding from the metal centre to the nitrosyl ligand when compared to $\text{Cp}^*\text{Mo}(\text{NO})\text{Cl}_2$. This is interesting because the coordination of a stronger donating ligands should necessarily result in an increase of electron density on the metal centre, but that does not seem to be the case in complex **4.2**. There are two probable explanations for the large difference in ν_{NO} frequencies between complexes **4.1** and **4.2**, and these may also help explain the increase in ν_{NO} stretching frequency between the $\text{Cp}^*\text{Mo}(\text{NO})\text{Cl}_2$ starting reactant and **4.2**. First, complex **4.2** is a salt wherein the organometallic fragment is a cation with an overall charge of +1, whereas **4.1** is a neutral molecule, and this may cause the large difference in nitrosyl stretching frequencies. Second, the two complexes differ in formal oxidation state of the metal centres. The molybdenum centre in **4.2** has a formal oxidation state of +2, and in **4.1** has a formal oxidation state of 0. This difference in oxidation states may explain the greater amount $\text{Mo}\rightarrow\text{NO}$ π backbonding seen in complex **4.1**, therefore resulting in a lower ν_{NO} , when compared to **4.2**. This second point may also explain why $\text{Cp}^*\text{Mo}(\text{NO})\text{Cl}_2$ and **4.2** have much closer ν_{NO} frequencies (1647 and 1661 cm^{-1} , respectively), wherein both of these compounds have Mo^{II} centres.

The ^1H , ^{13}C APT, $^{31}\text{P}\{^1\text{H}\}$ NMR spectra of complex **4.1** in C_6D_6 display chemical shifts that are as expected. The ^1H NMR spectrum displays two sets of doublets that are attributable to the two methyl groups pointing towards or the two pointing away from the Cp^* ring, two multiplets that are attributable to the four methylene protons, and a singlet attributable to the Cp^* ligand (Figure C.1). Consistent with these data, the $^{31}\text{P}\{^1\text{H}\}$ NMR spectrum of **4.1** in C_6D_6 consists of one sharp singlet due to the chemically equivalent phosphorus atoms in the dmpe ligand (Figure C.3). These chemical shifts reflect the C_s symmetry of the molecule. In

comparison, the NMR spectra of **4.2** in CD₂Cl₂ differ immensely due to the loss of symmetry in the molecule. In the ¹H NMR spectrum of **4.2**, four doublets are attributable to the four chemically inequivalent methyl groups and four multiplets arise from the four different methylene protons (Figure C.4). The ³¹P{¹H} NMR spectrum of **4.2** in CD₂Cl₂ consists of two doublets with similar chemical shifts that are attributable to the two chemically inequivalent phosphorus atoms on the dmpe ligand (Figure C.6).

Recrystallization of complex **4.1** from the slow evaporation of an Et₂O solution at ambient temperatures results in the deposition of orange crystals of sufficient quality for a single-crystal X-ray diffraction analysis. From this analysis, a solid-state molecular structure has been obtained and is shown in Figure 4.1. Complex **4.1** is a three-legged piano-stool complex capped by a Cp* ring. This complex has a linear nitrosyl ligand with a Mo(1)–N(1)–O(1) angle of 177.33(11)°. Complex **4.1** also has two essentially equal in length molybdenum–phosphorus bonds, with a Mo(1)–P(1) bond length of 2.3884(4) Å and a Mo(1)–P(2) bond length of 2.3866(4) Å. These bond lengths are similar to the molybdenum–phosphorus bond lengths found in other related three-legged piano-stool complexes.^{60,91}

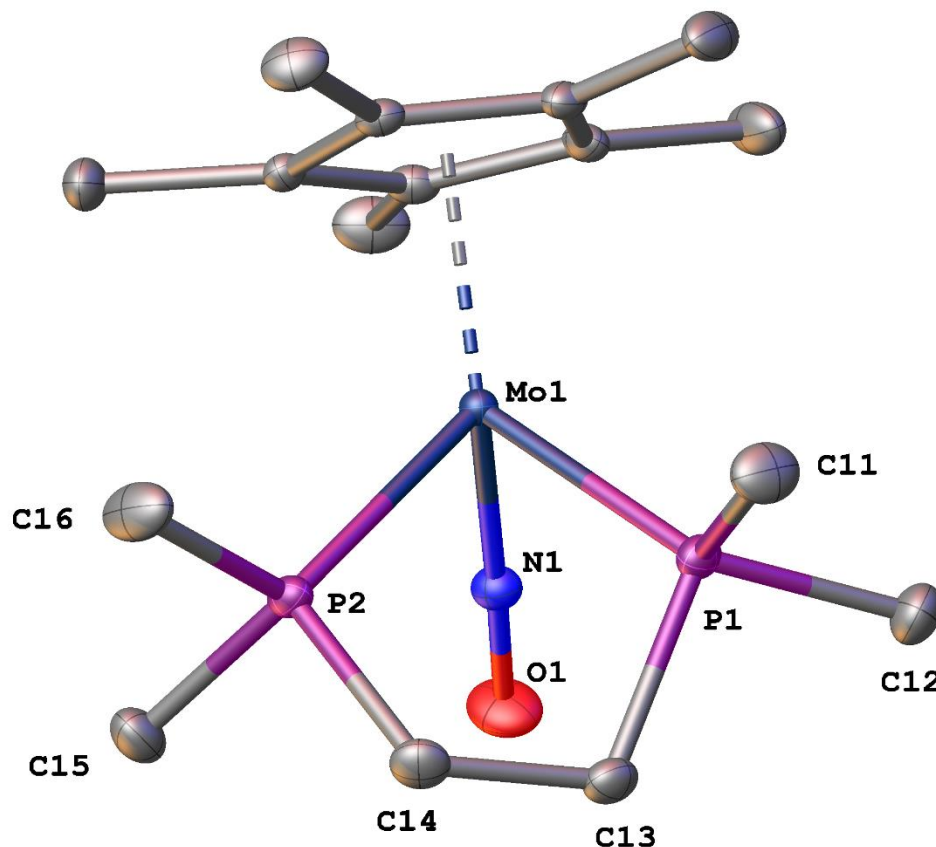


Figure 4.1. Solid-state molecular structure of **4.1** with 50% probability thermal ellipsoids shown. Hydrogen atoms have been omitted for the sake of clarity. Selected bond lengths (Å) and angles (deg): Mo(1)–P(1) = 2.3884(4), Mo(1)–P(2) = 2.3866(4), Mo(1)–N(1) = 1.7864(11), N(1)–O(1) = 1.2243(14), P(1)–C(11) = 1.8284(14), P(1)–C(12) = 1.8270(14), P(1)–C(13) = 1.8439(14), P(2)–C(14) = 1.8556(13), P(2)–C(15) = 1.8217(14), P(2)–C(16) = 1.8287(14), C(13)–C(14) = 1.5288(19), Mo(1)–N(1)–O(1) = 177.33(11), N(1)–Mo(1)–P(1) = 87.45(4), N(1)–Mo(1)–P(2) = 87.31(4), P(1)–Mo(1)–P(2) = 79.813(13).

The intermediate complex **4.2** is formed as a yellow precipitate after the addition of dmpe to the Cp*Mo(NO)Cl₂ solution and is purified by THF washes of precipitate. Recrystallization of **4.2** from CH₂Cl₂/hexanes at ambient temperatures in an aerobic environment results in the deposition of small yellow crystals suitable for single-crystal X-ray diffraction analysis, and a solid-state molecular structure of **4.2**·2H₂O is shown in Figure 4.2. The molecule is a salt dihydrate wherein the cation is a four-legged piano-stool complex capped by a Cp* ring with a chloride anion. The nitrosyl ligand in **4.2** has a Mo(1)–N(1)–O(1) angle of 171.82(16) and is essentially linear. The two molybdenum–phosphorus bonds are similar in length, with Mo(1)–P(1) being 2.5447(5) Å and Mo(1)–P(2) being 2.5537(5) Å, with the slightly closer phosphorus terminus of the dmpe ligand located *trans* to the chloro ligand. Both of these molybdenum–phosphorus bonds are much longer in length than those in **4.1**, and this may be attributable to the different oxidation states of the metal centres in the two complexes, and may also be an effect of the increased number of coordinated ligands in **4.2**.

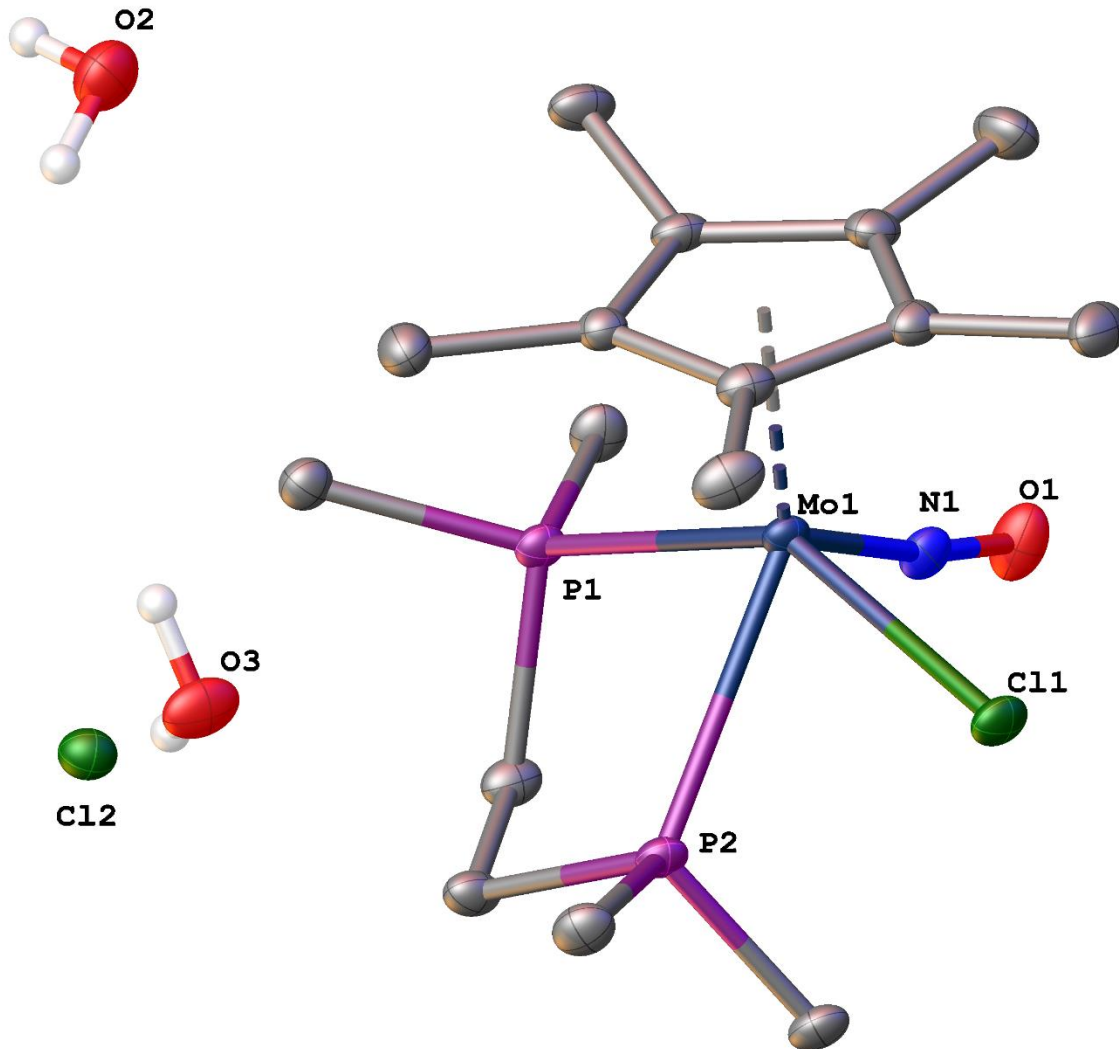


Figure 4.2. Solid-state molecular structure of **4.2** as its dihydrate with 50% probability thermal ellipsoids shown. Most hydrogen atoms have been omitted for the sake of clarity. Selected bond lengths (Å) and angles (deg): Mo(1)–P(1) = 2.5447(5), Mo(1)–P(2) = 2.5537(5), Mo(1)–Cl(1) = 2.4785(5), Mo(1)–N(1) = 1.7889(18), N(1)–O(1) = 1.201(2), Mo(1)–N(1)–O(1) = 171.82(16), P(1)–Mo(1)–P(2) = 74.840(17), P(2)–Mo(1)–Cl(1) = 72.186(16), Cl(1)–Mo(1)–N(1) = 91.76(6), N(1)–Mo(1)–P(1) = 80.89(5).

4.2.2 Reactions of **4.1** with Hydrocarbons

It has been thought that **4.1** could effect the C–H activation of hydrocarbon substrates via the dissociation of one terminus of the dmpe ligand followed by the oxidative addition of a C–H bond of the hydrocarbon substrate. Ideally, heating of **4.1** in neat solutions of a hydrocarbon substrate can hopefully cause the partial dissociation of the κ^2 -dmpe ligand into a κ^1 -dmpe ligand and form a 16e reactive intermediate in situ, which could then effect C–H activation chemistry.

Solutions of **4.1** in neat *n*-pentane or benzene-*d*₆ are heated at 40 °C and maintained at that temperature for 24 hours. After 24 hours, the reaction vessels are removed from the heat source and there are no observable changes in appearance. Further analysis by ¹H and ³¹P{¹H} NMR spectroscopy in C₆D₆ of the reaction mixtures, after removal of volatiles, reveals that no chemical transformations have occurred. Both the *n*-pentane and benzene-*d*₆ experiments contain unreacted **4.1** as their sole product. Increasing the temperature to 80 °C and maintaining solutions of **4.1** in neat *n*-pentane or benzene-*d*₆ at that temperature for 24 hours does not result in any new products being formed, and this is also confirmed via NMR analyses of the reaction mixtures after the removal of volatiles. Due to these results, heating of complex **4.1** probably does not cause the partial dissociation of the κ^2 -dmpe ligand into a κ^1 bonding mode, nor does it occur transiently in the solution upon heating since no colour change of the solution is observed. It has also been found that the addition of acetonitrile to complex **4.1** at room temperature does not cause the partial dissociation of the dmpe ligand and the formation of Cp*Mo(NO)(NCCH₃)(κ^1 -dmpe), which we have seen occur readily in other related chelating systems.⁹²

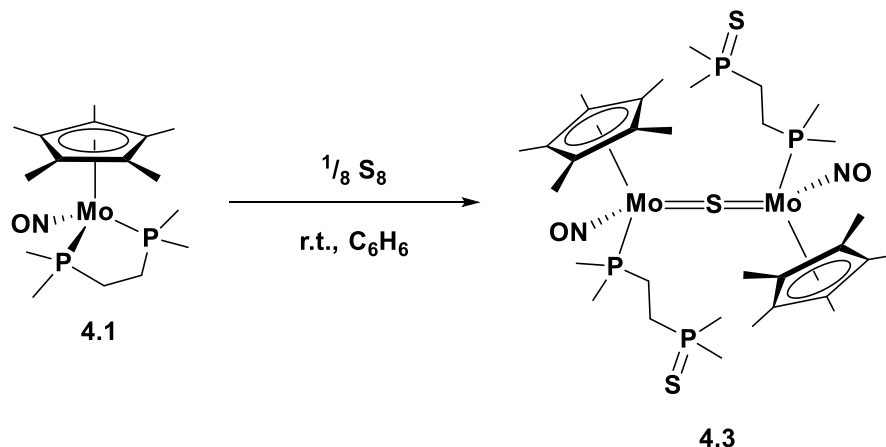
4.2.3 Reactions of 4.1 with Chalcogens

4.2.3.1 Synthesis of $(\mu\text{-S})[\text{Cp}^*\text{Mo}(\text{NO})(\kappa^1\text{-dmpeS})]_2$ (4.3)

A plethora of transition metal–sulfur complexes are found in the literature, and these complexes can effect chemical transformations and have applications that are of significance in both biological and industrial settings.⁹³ Reactions of **4.1** with stoichiometric amounts of elemental sulfur have been performed to garner insight into the reactivity it exhibits with elemental sulfur, and subsequently, what kind of chemistry the formed transition metal-sulfur complexes can effect with other reagents.

As summarized in Scheme 4.3, the addition of 1 mole equivalent S to **4.1** in C₆H₆ results in the formation of $(\mu\text{-S})[\text{Cp}^*\text{Mo}(\text{NO})(\kappa^1\text{-dmpeS})]_2$ (**4.3**) [dmpeS = PMe₂CH₂CH₂P(=S)Me₂]. This sulfur-bridged complex forms immediately upon the addition of sulfur and is accompanied by an instantaneous colour change from a clear orange solution to a brown solution with precipitate. Removal of volatiles in vacuo results in the deposition of **4.3** as a brown precipitate at the bottom of the flask. Further purification is carried out by column chromatography over basic alumina wherein the complex in THF elutes as an intensely dark blue solution. The removal of solvent from the eluate solution results in $(\mu\text{-S})[\text{Cp}^*\text{Mo}(\text{NO})(\kappa^1\text{-dmpeS})]_2$ being obtained as a blue residue in a 34% yield. Additionally, approximately half of the initial reactant **4.1** in Et₂O elutes as an orange solution from the column chromatography.

Scheme 4.3. Reaction of 4.1 with a stoichiometric amount of elemental sulfur



The spectroscopic properties of complex **4.3** are consistent with the molecular structure drawn in Scheme 4.3. A solid-state molecular structure of the complex has been obtained, confirming its identity. The two halves of the bimetallic complex are found to be chemically equivalent in solution in the ^1H , ^{13}C , and $^{31}\text{P}\{^1\text{H}\}$ NMR spectra in C_6D_6 . Thus, the ^1H NMR spectrum consists of four doublets attributable to the inequivalent methyl groups, four multiplets due to the four methylene protons, and a singlet attributable to the Cp* ring (Figure C.8). Consistent with this data, the $^{31}\text{P}\{^1\text{H}\}$ NMR spectrum consists of two doublets at δ 22.7 and 39.2 ppm, each displaying a coupling constant of $^3J_{\text{PP}} = 47.6$ Hz (Figure C.10). The correct assignment of the two phosphorus resonances being attributable to either the P(III) or P(V) atom is corroborated by comparison to the spectroscopic data for complex **4.1** and $\text{Me}_3\text{P}=\text{S}$.

Complex **4.3** displays an interesting trend in the ^1H and ^{13}C APT NMR spectra regarding the chemical shifts and coupling constants of the nuclei in the κ^1 -dmpeS ligands (Figure 4.3). The chemical shifts attributable to carbon and hydrogen nuclei 1–3 bonds away from the P(V) atom are more downfield than those attributed to nuclei 1–3 bonds away from the P(III) atom.

This difference is more apparent in the ^{13}C APT spectrum where, for example, the chemical shifts of resonances attributable to the two methyl groups bound to the P(V) atom are both around δ 21 ppm while those of the two methyl groups bound to the P(III) atom are around δ 15 ppm (Figure C.9). An even more significant disparity is seen in the coupling constants of the carbon and hydrogen nuclei. Those nuclei whose resonances show coupling to the P(V) nucleus in the NMR spectra are significantly larger in magnitude compared to nuclei that couple with the P(III) atom. For instance, in the ^{13}C APT spectrum the resonances attributable to the methyl substituents on the P(III) atom display $^1J_{\text{CP}}$ values of 23.9 and 27.9 Hz while those of the methyl substituents on the P(V) atom exhibit $^1J_{\text{CP}}$ values of 53.3 and 55.5 Hz. This trend in chemical shifts and coupling constants must be a manifestation of the different oxidation states of the phosphorus nuclei wherein a more downfield chemical shift and a larger coupling constant is seen for hydrogen and carbon nuclei closer to the higher oxidation state, and thus more electron-withdrawing, phosphorus(V) atom as well as the more electron-withdrawing P=S linkage.

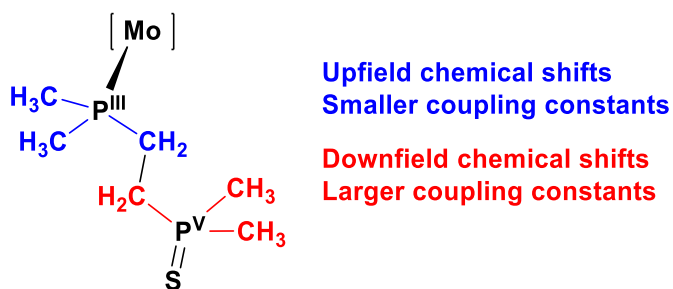


Figure 4.3. A portion of complex **4.3** displaying the κ^1 -dmpes ligand and indicating the trend observed in the ^1H and ^{13}C APT NMR spectra in C_6D_6 .

The IR spectrum of **4.3** shows a ν_{NO} band at 1562 cm^{-1} , which is similar to other $\text{Cp}^*\text{Mo}(\text{NO})$ complexes. This nitrosyl frequency indicates a decrease in electron density on the metal centre compared to the initial reactant, complex **4.1**, and this can be attributed to the dissociation of one of the phosphorus donor termini of the dmpe ligand and the oxidation of the molybdenum centre.

The overall mechanism for this transformation is not obvious. A possible mechanism for the formation of **4.3** involves the initial step being the insertion of sulfur into the W–P linkage, thereby oxidizing one end of the dmpe ligand and transiently forming $[\text{Cp}^*\text{Mo}(\text{NO})(\kappa^2\text{-dmpeS})]$ which contains a hemilabile dmpeS ligand.⁹⁴ Dissociation of the sulfur donor site from the molybdenum's coordination sphere then generates the 16e $[\text{Cp}^*\text{Mo}(\text{NO})(\kappa^1\text{-dmpeS})]$ complex. Interestingly, this intermediate complex does not activate the benzene solvent to form 18e $\text{Cp}^*\text{Mo}(\text{NO})(\text{Ph})(\text{H})(\kappa^1\text{-dmpeS})$, but rather incorporates another sulfur atom on the way to forming the Mo=S=Mo bridge in the final complex **4.3**. That this second addition of sulfur forms a bridge between two identical metal centres is an unexpected and surprising result since preliminary NMR and MS data reaction had hinted that the product was a monometallic species.⁹⁵ It is important to note that approximately half of the initial reactant **4.1** is recovered from the reaction, indicating that the formation of this 3:2 sulfur–molybdenum complex is favoured over the formation of other monometallic molybdenum complexes incorporating one or two sulfur atoms.

This reaction highlights the successful dissociation of one of the phosphorus termini of the $\kappa^2\text{-dmpe}$ ligand from the molybdenum's coordination sphere achieved through the formation of a phosphine–sulfide linkage. Interestingly, the formation of bimetallic organometallic complexes bridged by a single sulfur atom alone are highly uncommon, and complex **4.3** is an

example of one such complex, and additionally, to the best of my knowledge, the only example wherein the bridged fragment is a M=S=M fragment rather than M≡S≡M.^{96–98} The vast majority of sulfur-bridged organometallic complexes, specifically molybdenum complexes, incorporate multiple bridging sulfur atoms in addition to a metal–metal bond.^{99,100}

Recrystallization from a 1:10 *n*-pentane/benzene solution left at room temperature for 15 days affords small blue crystals of (μ-S)[Cp*Mo(NO)(κ¹-dmpeS)]₂ of sufficient quality for single-crystal X-ray diffraction analysis, and a solid-state molecular structure has been obtained (Figure 4.4). The complex is a bimetallic molecule in which both molybdenum centres are in a three-legged piano-stool configuration capped by Cp* rings. In the solid-state two halves of **4.3** are crystallographically equivalent and are related by a C₂ rotation axis (Figure 4.5). There are no other symmetry elements, except for identity, present in the solid-state molecular structure of **4.3**, and therefore the complex belongs in the C₂ symmetry point group. The bridging sulfur atom in **4.3** forms an Mo=S=Mo bridge that allows each metal centre to attain the favoured 18e configuration, and this is evident from the Mo(1)–S(2)–Mo(1') bond angle of 151.93(5)°, which is a larger angle than what would be expected of a sp³ hybridized sulfur singly bonded to the two metal centres. It is also important to note that this angle is much lower than those found in M≡S≡M complexes which are essentially linear.^{96,98} The molybdenum–sulfur bond length of 2.2965(4) Å is intermediate between those reported for Mo=S (~2.10–2.20 Å) and Mo–S (~2.35–2.45 Å) linkages,^{101–104} and there is no Mo–Mo bond since the separation of 4.4559(10) Å precludes a significant interaction between the two metal centres.^{105,104} In addition, the P=S distance of 1.9647(12) Å is as expected for such a bond.¹⁰⁶ The nitrosyl ligand is essentially linear with a Mo(1)–N(1)–O(1) bond angle of 172.6(3)°. The Mo(1)–P(1) bond length is

2.4550(8) Å, which is longer than that found in the initial reactant **4.1**, and is probably an effect of the ligand being a κ^1 ligand in **4.3** rather than a bidentate ligand, as is the case in **4.1**.

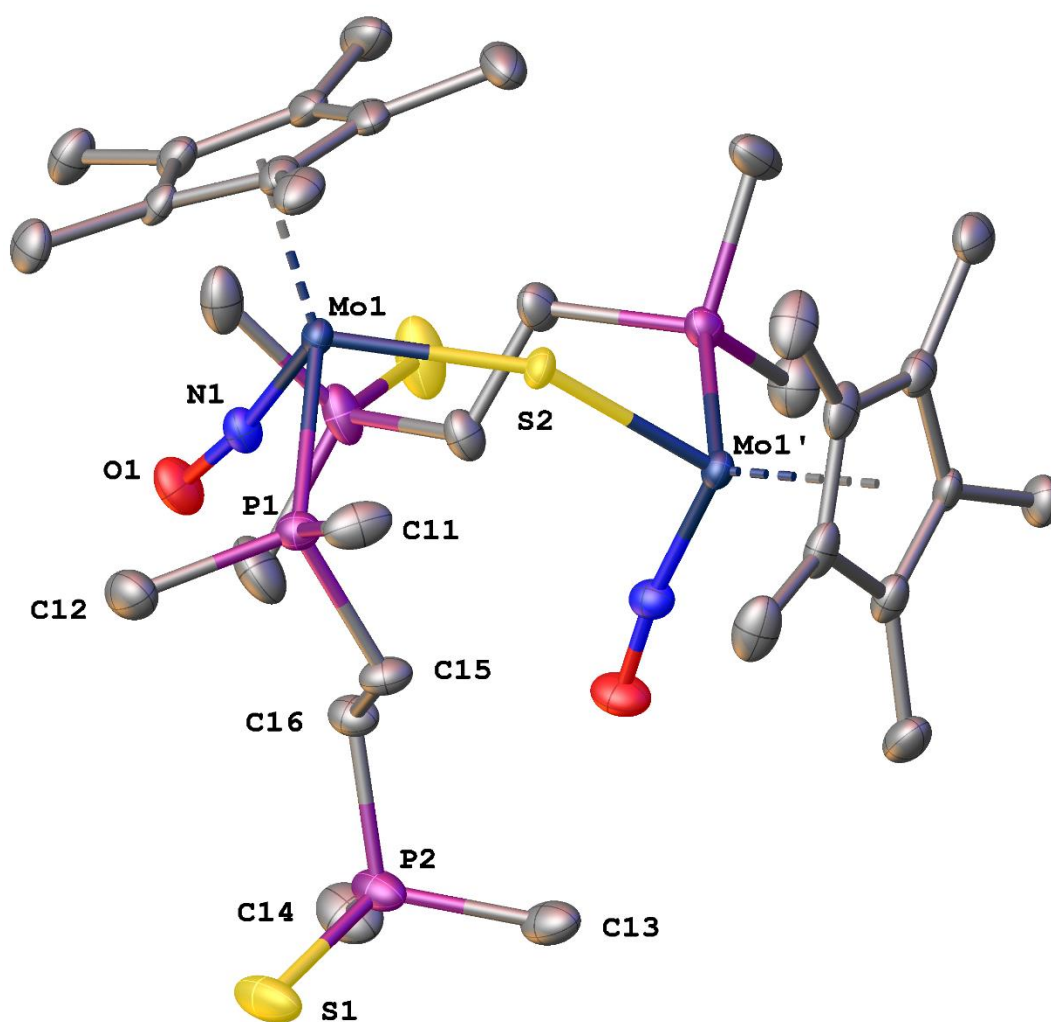


Figure 4.4. Solid-state molecular structure of **4.3** with 50% probability thermal ellipsoids shown.

Hydrogen atoms have been omitted for the sake of clarity. Only half of the molecule has been fully labelled for the sake of clarity. Selected bond lengths (Å) and angles (deg): Mo(1)–S(2) = 2.2965(4), Mo(1)–P(1) = 2.4550(8), Mo(1)–N(1) = 1.781(3), N(1)–O(1) = 1.226(3), P(1)–C(11) = 1.820(3), P(1)–C(12) = 1.827(4), P(1)–C(15) = 1.832(3), P(2)–C(13) = 1.793(4), P(2)–C(14) = 1.798(4), P(2)–C(16) = 1.816(3), P(2)–S(1) = 1.9647(12), C(15)–C(16) = 1.531(4), Mo(1)–N(1)–O(1) = 172.6(3), S(2)–Mo(1)–P(1) = 91.57(2), P(1)–Mo(1)–N(1) = 87.98(8), N(1)–Mo(1)–S(2) = 105.68(9), Mo(1)–S(2)–Mo(1') = 151.93(5).

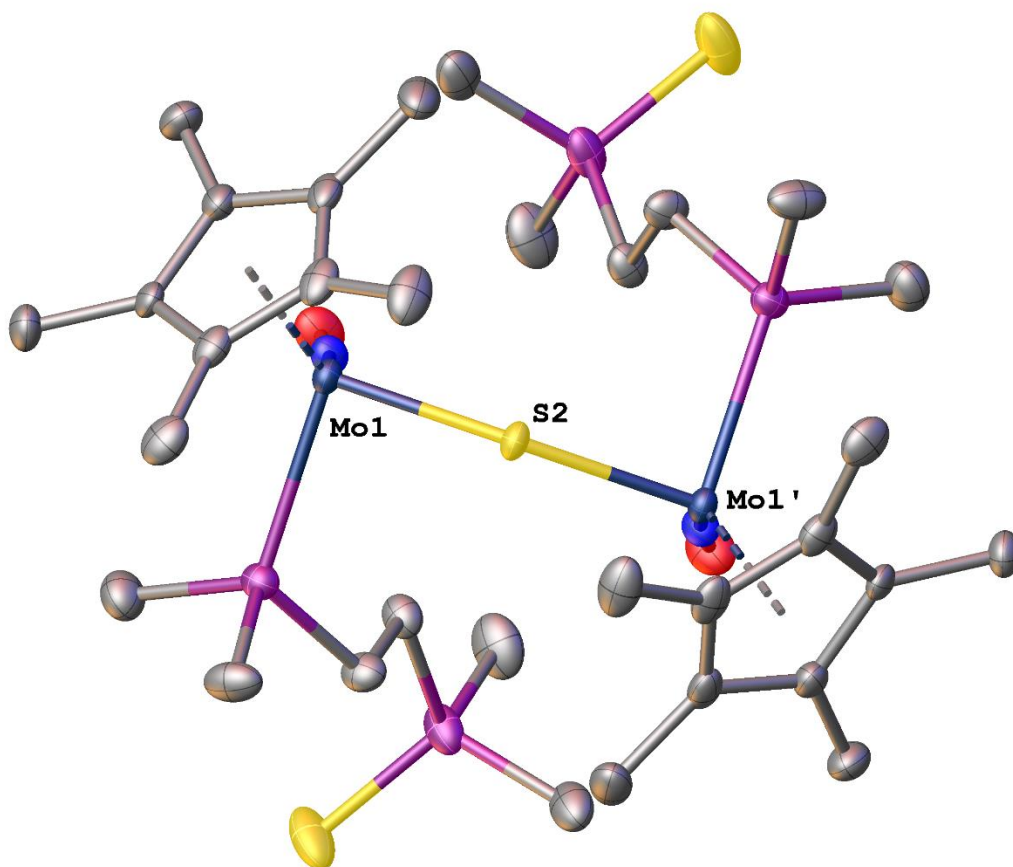


Figure 4.5. View of the solid-state molecular structure of **4.3** along the C_2 axis of symmetry that relates the two crystallographically equivalent halves of the bimetallic molecule. Hydrogen atoms have been omitted for the sake of clarity.

Complex **4.3** is a vibrant blue colour in solution and even at low concentrations the solution appears almost opaque because of the intensity of the colour. Complex **4.3** is extremely air and moisture sensitive and will decompose immediately in undried solvent or in an aerobic environment, and this is marked by an instantaneous colour change into a clear yellow solution.

The sensitivity of the complex to react readily (in this case, with O₂ or H₂O) shows that the complex is relatively unstable and should easily form complexes with appropriate reactants. Due to its reactivity, the complex's ability to effect C–H activation chemistry has been subsequently investigated.

Complex **4.3** in neat C₆D₆ or *n*-pentane forms a clear dark blue solution. These solutions are heated at temperatures up to 150 °C and are maintained at these temperatures for more than 16 hours, after which the solutions do not appear to have changed. NMR analyses in C₆D₆ of the reaction mixtures after the removal of volatiles show that no products resulting from the C–H activation of the hydrocarbon substrates had been formed. Instead, only resonances attributable to complex **4.3** and solvent molecules are observed in the ¹H and ³¹P{¹H} NMR spectra, indicating, surprisingly, that complex **4.3** is extremely thermally stable. Furthermore, the addition of NO⁺ from [NO]BF₄ to **4.3** in C₆D₆ has also been performed to see if the sulfur bridge can be cleaved, but the complex is unreactive to NO⁺ and remains intact after 4 days at ambient temperatures with a stoichiometric amount of [NO]BF₄.

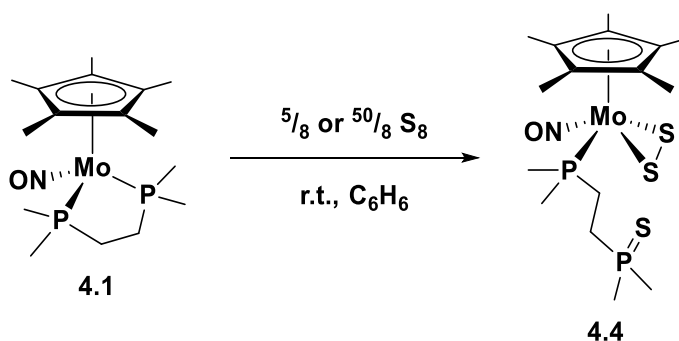
Examples of complexes with bisphosphine monooxide hemilabile ligands are found in the literature, and these complexes have been found act as catalysts to mediate chemical transformations, such as alkene polymerization and Cu-mediated enantioselective reduction.^{107–111} These complexes use an already monooxidized bisphosphine proligand which then function as hemilabile ligands on the active catalyst. This differs from complex **4.3** because the bisphosphine ligand is oxidized in situ by elemental sulfur. Recently, successful C–H functionalization mediated by a Pd-catalyst utilizing an in situ monooxidized bisphosphine ligand has been reported.⁹⁴ In the presence of a base and water in solution, the bisphosphine containing precatalyst complex, PdCl₂(κ²-Xantphos) [Xantphos = 4,5-Bis(diphenylphosphino)-

9,9-dimethylxanthene], rapidly undergoes monooxidation of one of the phosphorus termini in the κ^2 -Xantphos ligand into a P=O linkage, thereby forming a hemilabile κ^2 -P,O ligand in situ. This active catalyst then goes on to effect C–H functionalization. In the study, the in situ formation of the hemilabile ligand is found to be essential for the reactivity of the complex. This is akin to what is observed in complex **4.3** since the monooxidation of the κ^2 -dmpe ligand into a hemilabile ligand occurs in situ, but unfortunately, the complex does not react further to perform any comparable chemical transformations.

4.2.3.2 Synthesis of $\text{Cp}^*\text{Mo}(\text{NO})(\eta^2\text{-S}_2)(\kappa^1\text{-dmpeS})$ (**4.4**)

Addition of an excess of elemental sulfur to a solution of complex **4.1** in C_6H_6 results in the formation of $\text{Cp}^*\text{Mo}(\text{NO})(\eta^2\text{-S}_2)(\kappa^1\text{-dmpeS})$ (**4.4**) (Scheme 4.4). The red-brown crude product is then purified via column chromatography and complex **4.4** in solvent elutes as a dark red band. Removal of volatiles results in **4.4** as a red powder in a 41% yield.

Scheme 4.4 Reaction of **4.1** with an excess of elemental sulfur



Since treatment of **4.3** with additional sulfur also results in the production of **4.4**, it is likely that the reaction of $\text{Cp}^*\text{Mo}(\text{NO})(\kappa^2\text{-dmpe})$ (**4.1**) with elemental sulfur proceeds in a stepwise manner wherein **4.3** is formed initially. The last step to form complex **4.4** involves the cleavage of the $\text{Mo}=\text{S}=\text{Mo}$ bridge by the additional sulfur with concomitant formation of the $\eta^2\text{-S}_2$ ligand at each molybdenum so that the favored 18e configuration can be maintained. This complex is also formed upon the addition of 50 mol equivalents S to **4.1**, indicating that complex **4.4** does not show any further reactivity with elemental sulfur. Multiple examples of $\eta^2\text{-S}_2$ transition metal complexes can be found in the literature, and they can be synthesized in a variety of ways such as addition of elemental sulfur, sulfide reagents, or through oxidation of sulfur-containing ligands.¹¹²

The spectroscopic data are fully consistent with the complex depicted above. In the IR spectrum, complex **4.4** displays a nitrosyl stretching frequency at 1593 cm^{-1} , indicating that there is less electron density extant on the metal centre when compared to complex **4.3**. The same trend in the ^1H and ^{13}C NMR resonances attributable to nuclei in the $\kappa^1\text{-dmpeS}$ ligand seen in complex **4.3** (Figure 4.3) is also seen in complex **4.4** (Figures C.12 and C.13).

Recrystallization of the complex is performed at ambient temperatures via vapour diffusion of Et_2O into a C_6H_6 solution of **4.4** in an inert atmosphere. Small red crystals of suitable quality for single-crystal X-ray diffraction were deposited on the sides of the vial after 3 d, from which a solid-state molecular structure was obtained (Figure 4.6). The complex is a four-legged piano-stool complex capped with a Cp^* ring. The $\text{Mo}(1)\text{-S}(1)$ and $\text{Mo}(1)\text{-S}(2)$ linkages are both single bonds, as indicated by their bond lengths of 2.450(5) and 2.459(4) Å, respectively, and the $\text{S}(1)\text{-S}(2)$ linkage in the $\eta^2\text{-S}_2$ ligand has a bond length of 2.059(4) Å, as expected of a S-S single bond.^{113,114} Finally, complex **4.4** has a $\text{Mo}(1)\text{-P}(1)$ bond length of

2.4696(13) Å which is similar to that extant in **4.3**, and has an essentially linear Mo(1)–N(1)–O(1) linkage with a bond angle of 170.1(5)°.

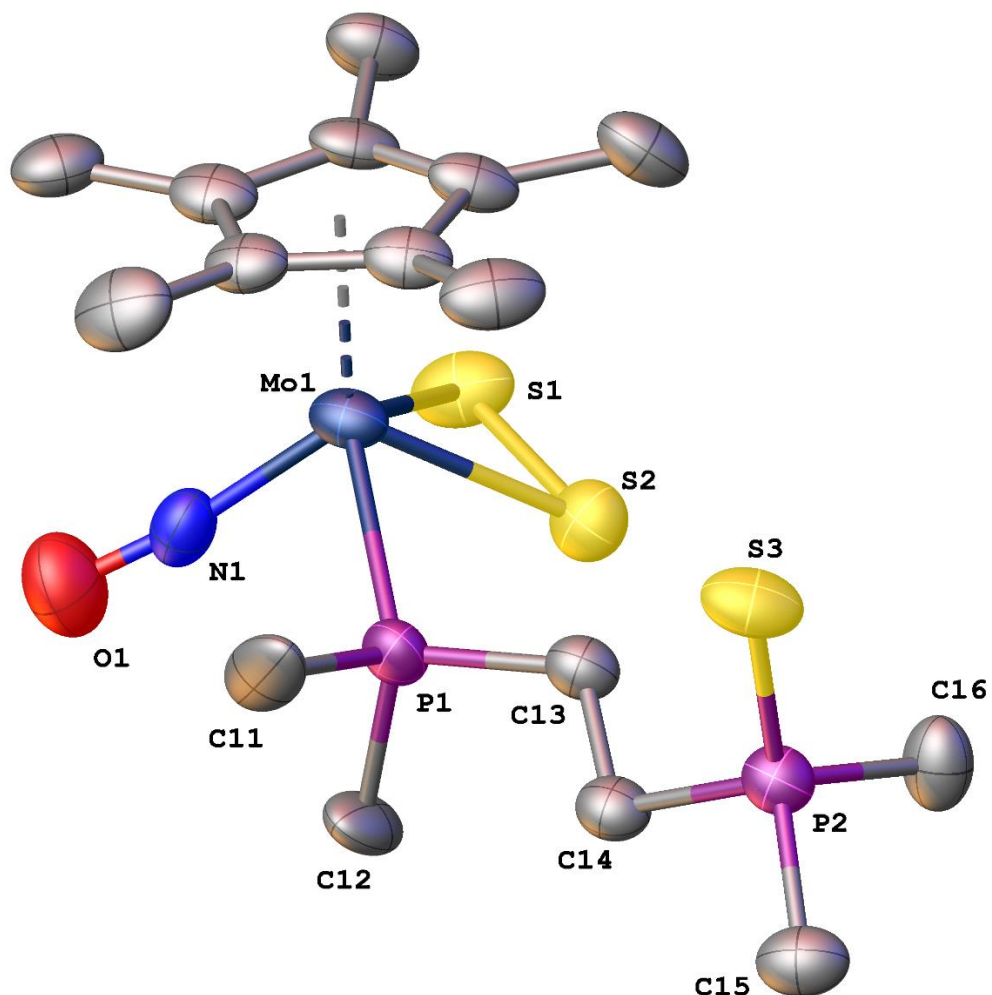


Figure 4.6. Solid-state molecular structure of **4.4** with 50% probability thermal ellipsoids shown. Hydrogen atoms have been omitted for the sake of clarity. Selected bond lengths (Å) and angles (deg): Mo(1)–S(1) = 2.450(5), Mo(1)–S(2) = 2.459(4), Mo(1)–P(1) = 2.4696(13), Mo(1)–N(1) = 1.825(5), N(1)–O(1) = 1.172(6), S(1)–S(2) = 2.059(4), P(1)–C(11) = 1.843(8), P(1)–C(12) = 1.797(7), P(1)–C(13) = 1.834(5), C(13)–C(14) = 1.523(7), P(2)–S(3) = 1.962(2), P(2)–C(14) = 1.807(5), P(2)–C(15) = 1.817(6), P(2)–C(16) = 1.792(5), Mo(1)–N(1)–O(1) = 170.1(5), S(1)–Mo(1)–S(2) = 49.61(9), S(2)–Mo(1)–P(1) = 76.00(8), P(1)–Mo(1)–N(1) = 82.20(14), N(1)–Mo(1)–S(1) = 95.55(19), S(1)–S(2)–Mo(1) = 64.98(16), S(2)–S(1)–Mo(1) = 65.41(18).

4.2.3.3 Reaction of 4.1 with Oxygen

In an attempt to isolate the analogous peroxide complex, an Et₂O solution of **4.1** has been exposed to an oxygen atmosphere which causes the immediate formation of a yellow precipitate. The precipitate has only been partially characterized as all attempts to purify it by chromatography or recrystallization have been unsuccessful to date. Nevertheless, NMR and MS data are consistent with the yellow solid being formed by the incorporation of 1 or 2 equivalents of oxygen by the initial reactant, resulting in either an oxo or peroxide complex, respectively. For example, the ³¹P{¹H} NMR spectrum of the yellow solid in C₆D₆ (Figure 4.7) exhibits two doublets at chemical shifts comparable to those in the analogous spectra of **4.3** and **4.4**, thereby indicating the formation of an organometallic complex wherein the two phosphorus atoms in the possibly modified dmpe ligand are no longer chemically equivalent (Figure C.17), and the ¹H NMR resonances (Figure C.16) are also similar to those seen in complexes **4.3** and **4.4**.

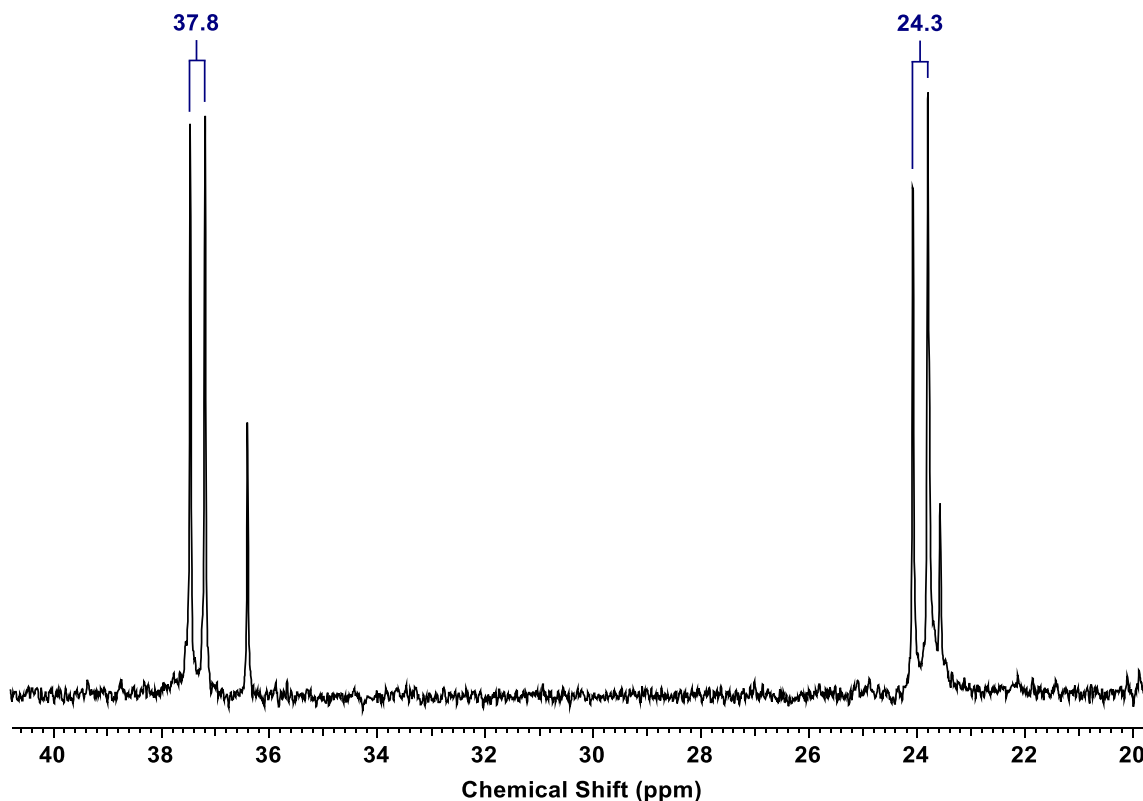


Figure 4.7. Expansion of the $^{31}\text{P}\{^1\text{H}\}$ NMR spectrum (162 MHz, C_6D_6) from 19.8 to 40.8 ppm showing the two doublets attributable to the two chemically inequivalent phosphorus nuclei in the possibly modified dmpe ligand of the complex resulting from the exposure of **4.1** to O_2 . Both doublets have a coupling constant of $J_{\text{PP}} = 44.6$ Hz.

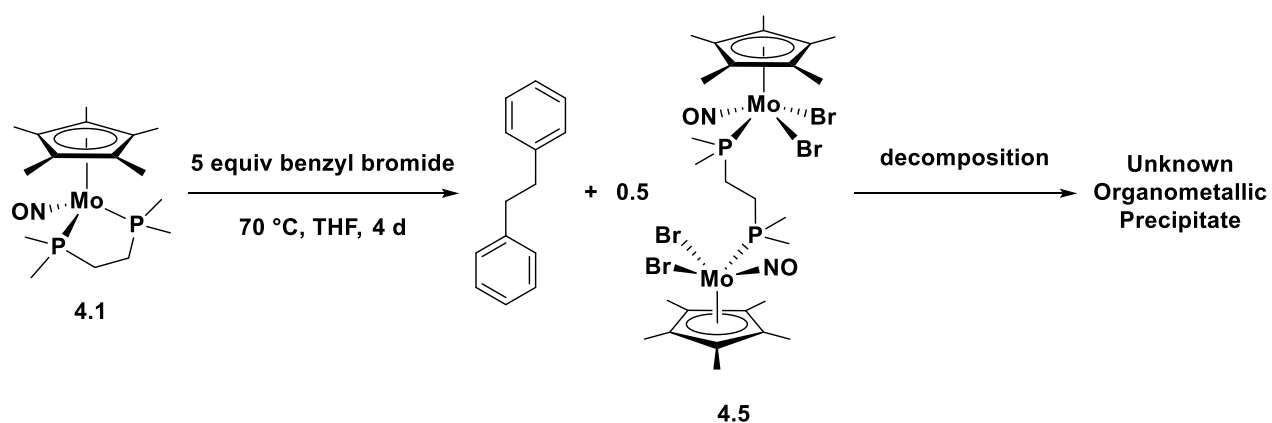
4.2.4 Reactions of **4.1** with Organic Halides

4.2.4.1 Reaction of **4.1** with Benzyl Bromide

Reaction of **4.1** with 5 equivalents of benzyl bromide in THF results in the formation of $(\mu\text{-dmpe})[\text{Cp}^*\text{Mo}(\text{NO})\text{Br}_2]_2$ (**4.5**) and bibenzyl after 4 d at 70 °C (Scheme 4.5). The reaction

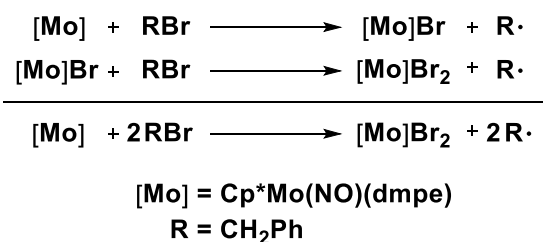
solution changes from a clear bright orange to a dark orange solution containing a beige precipitate. The beige precipitate's identity is unknown, but it is found to contain molybdenum, evident from a combustion test of a sample of precipitate wherein the residue appears yellow. The bibenzyl product can be isolated via flash silica column chromatography and is recovered in a 71% yield. Crystals of the organometallic product, **4.5**, were obtained from the slow cooling of the reaction mixture wherein a small amount of orange crystals are deposited on the sides of the flask after 4 d. Unfortunately, subsequent reactions with benzyl bromide following the same procedure have not resulted in more crystals of complex **4.5** being formed in solution. Purification attempts of **4.5** from the THF supernatant solution via column chromatography or recrystallization is unsuccessful. Addition of pentane to the THF supernatant solution results in the immediate precipitation of the beige solid that is initially formed from the reaction, suggesting that complex **4.5** is an unstable intermediate complex that is formed upon thermolysis but does not persist in solution, and instead forms this unknown organometallic precipitate.

Scheme 4.5. Reaction of **4.1** with benzyl bromide



The formation of the bibenzyl product suggests a possible mechanism for the reaction that involves radical processes wherein benzyl radical species are produced. In the reaction outlined above, the homolytic cleavage of the benzyl bromide reagent results in the formation of benzyl and bromo radicals and occurs concomitantly with atom transfer processes resulting in the intermediate complex $\text{Cp}^*\text{Mo}(\text{NO})(\text{Br})_2(\kappa^1\text{-dmpe})$, wherein the partial dissociation of the dmpe ligand has occurred and the metal centre is formally oxidized (Scheme 4.6). Finally, two of these intermediate complexes dimerize with the loss of one of the dmpe ligands in order to form complex **4.5** as the organometallic product of the reaction.

Scheme 4.6. Reaction of complex 4.1 with two equivalents of benzyl bromide



The precipitate that forms in this reaction displays a broad band in the IR spectrum at 1635 cm^{-1} , indicating that it contains nitrosyl ligands. The ^1H NMR spectrum of the precipitate is uninformative as it consists of a few broad resonances as well as multiplets in the alkane region of the spectrum, from which conclusions regarding its exact identity cannot be made (Figure C.18). The product obtained from the purification of the supernatant solution is also this unknown precipitate as it produces similar IR and NMR spectra. This unknown product is obtained in a large amount, indicating it to be the major product of the reaction and suggesting that it is the decomposition product of **4.5**.

Many examples of reactions involving the homolytic cleavage of alkyl–halide bonds and atom transfer processes resulting in the formation of alkyl radicals and metal halides have been described in the literature.^{115–120} For instance, in a manner analogous to that depicted in Scheme 4.6, reaction of the monoanionic pincer complex, $[\text{PCP-Pt}^0]^-$ [$\text{PCP} = \text{C}_6\text{H}_3(\text{CH}_2\text{Pt-Bu}_2)_2$], with benzyl chloride in THF results in the formation of PCP-PtCl and bibenzyl.¹²¹

The slow cooling of the reaction mixture results in X-ray-quality crystals, and a solid-state molecular structure of complex **4.5** has been obtained from single-crystal X-ray diffraction analysis. The two halves of the bimetallic complex are related by a centre of inversion, and both molybdenum centres are in four-legged piano-stool geometries capped by Cp* rings (Figure 4.8). A single dmpe ligand forms the bridge between the two metal centres. The nitrosyl ligands are essentially linear and have Mo(1)–N(1)–O(1) bond angles of $165.5(7)^\circ$, and the molybdenum–phosphorus bonds have bond lengths of $2.492(7) \text{ \AA}$, which is comparable to other bond lengths of other such linkages.

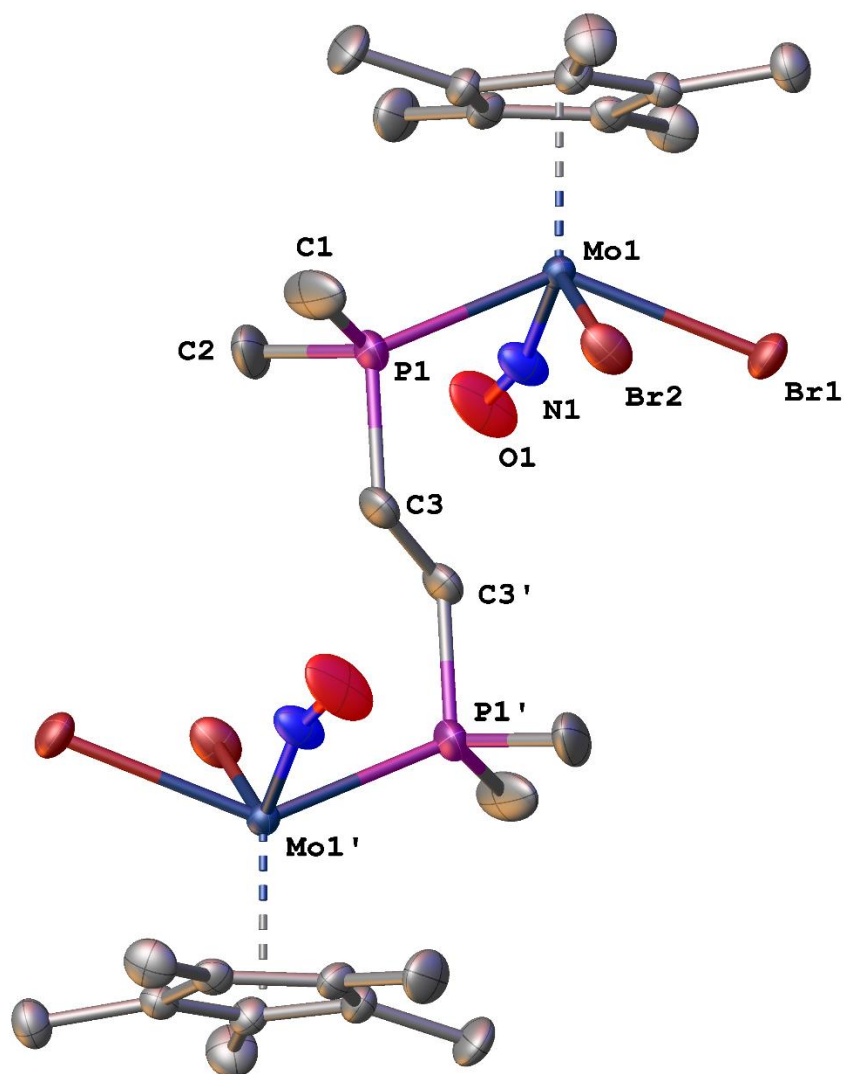


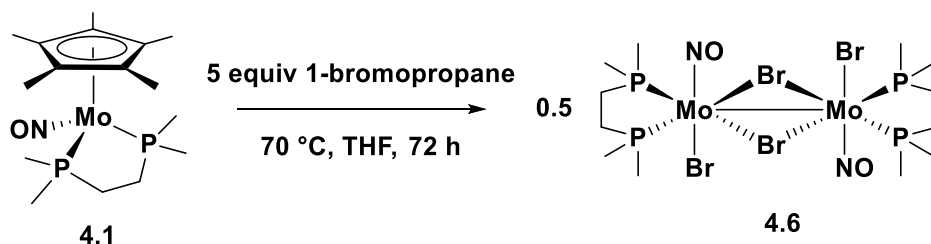
Figure 4.8. The major disordered fragment of the solid-state molecular structure of **4.5** with 50% probability thermal ellipsoids shown. Hydrogen atoms have been omitted for the sake of clarity.

Only half of the molecule has been fully labelled for the sake of clarity. Selected bond lengths (Å) and angles (deg): Mo(1)–Br(1) = 2.6068(6), Mo(1)–Br(2) = 2.6014(8), Mo(1)–P(1) = 2.492(7), Mo(1)–N(1) = 1.806(8), N(1)–O(1) = 1.144(9), P(1)–C(1) = 1.810(9), P(1)–C(2) = 1.841(8), P(1)–C(3) = 1.837(7), C(3)–C(3)' = 1.532(15), Br(1)–Mo(1)–Br(2) = 80.79(3), Br(2)–Mo(1)–P(1) = 74.39(18), P(1)–Mo(1)–N(1) = 82.8(3), N(1)–Mo(1)–Br(1) = 82.08(19), Mo(1)–N(1)–O(1) = 165.5(7).

4.2.4.2 Reaction of 4.1 with 1-Bromopropane

A THF solution of complex **4.1** containing 5 equivalents of 1-bromopropane results in the deposition of a large red crystalline precipitate and the formation of a pale yellow supernatant solution after 72 hours at 70 °C. The crystals that form from the reaction are of sufficient quality for a single-crystal X-ray diffraction analysis, and a solid-state structure has been obtained, revealing the complex to be $[\text{Mo}(\text{NO})(\text{Br})_2(\kappa^2\text{-dmpe})]_2$ (**4.6**). This reaction is shown in Scheme 4.7. The crystalline product can be isolated in 69% yield by decanting the supernatant solution and washing the crystals with THF.

Scheme 4.7. Reaction of 4.1 with 1-bromopropane



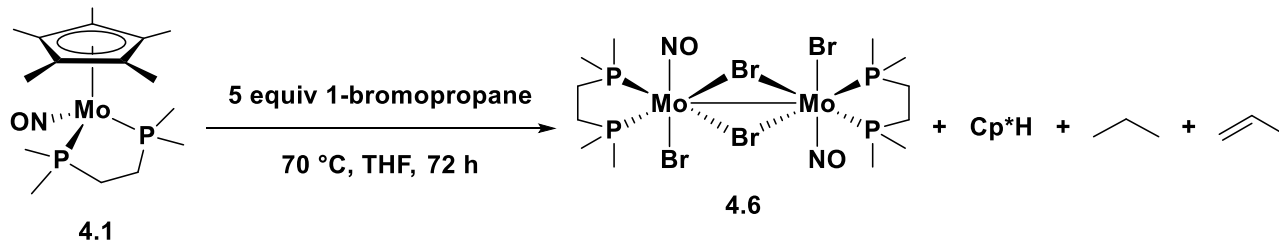
This transformation involves the loss of the Cp* ligand and the incorporation of two bromine atoms per metal centre from the bromoalkane reagent. A metal–metal bond is invoked in the complex to allow both metal centres to attain a favourable 18e count.

All spectroscopic evidence is consistent with the structure depicted above in Scheme 4.7. The bimetallic complex exhibits a ν_{NO} band in the IR spectrum at 1619 cm^{-1} with a shoulder at 1577 cm^{-1} attributable to the asymmetric stretch of the nitrosyl ligands. The complex is completely insoluble in most NMR solvents and is only sparingly soluble in CD_2Cl_2 . The ^1H ,

$^{13}\text{C}\{^1\text{H}\}$, and $^{31}\text{P}\{^1\text{H}\}$ NMR spectra in CD_2Cl_2 are as expected and indicate that the nuclei in the two κ^2 -dmpe ligands are in chemically equivalent environments. The ^1H NMR spectrum consists of four resonances attributable to the two groups of methyl protons and methylene protons pointing either above or below the Mo- μ -Br₂-Mo plane (Figure C.19). The $^{31}\text{P}\{^1\text{H}\}$ NMR spectrum displays a lone singlet at δ 35.4 ppm (Figure C.21), which is consistent with the nuclei of the κ^2 -dmpe ligands being chemically equivalent.

The reaction shown in Scheme 4.7 depicts the transformation of the organometallic fragment but does not address the outcome of the organic portions of the reactants. NMR analysis of the supernatant solution after the removal of volatiles has provided insight into their identities. Interestingly, in the ^1H NMR spectra, the observable products of the reaction are Cp*H and propene, suggesting that the reaction performed by **4.1** is a dehydrohalogenation reaction wherein 1-bromopropane is transformed into propene, and additionally results in the transfer of hydrogen from 1-bromopropane to the Cp* ring. GCMS analysis of the supernatant solution has identified more of the organic products of this reaction. In addition to the Cp*H and propene products, propane is also observed in the GCMS chromatogram. Shown below in Scheme 4.8 are all the major products of the reaction that have been identified. Due to the volatility of both the propane and propene products as well as the unreacted 1-bromopropane left in solution that dominates certain regions in the ^1H NMR spectrum, NMR analysis is unable to quantify the relative amounts of the organic products. Additionally, GCMS analysis is unable to correctly quantify the relative amounts of the products, even when accounting for the volatility of some of the products, since the propene and propane products cannot be successfully separated from one another.

Scheme 4.8. Identified products of the reaction of 4.1 with 5 equiv 1-bromopropane



A notable feature of the transformation depicted above in Scheme 4.8 is the loss of the Cp* ligand from the metal's coordination sphere in **4.1**. The Cp* ligand is ubiquitous in transition-metal organometallic chemistry, and when coordinated to a transition-metal centre, it often remains as a spectator ligand. For example, in the chemistry exhibited by Cp*M(NO)-containing complexes (M = Mo, W) the 14e fragment remains intact throughout all of the chemical transformations.¹⁹ However, seen in Scheme 4.8 is a rare example wherein the Cp* ligand is not only a participant in the characteristic reactivity of a Cp*M(NO) scaffold complex (**4.1**), but is subsequently lost from the transition-metal's coordination sphere as free Cp*H. Rarely has it been found that the Cp* ligand can also be a participant in the chemistry exhibited by its molecular scaffolds while remaining coordinated to the metal centre. For instance, under a variety of experimental conditions the C–H bond activation of a methyl group in coordinated Cp* ligands has been shown to result in the formation of either $\eta^2:\eta^4$ or $\eta^1:\eta^5$ tetramethylfulvene-like ligands via H-atom abstraction.¹²² Recently, it has also been reported that treatment of 18e Cp*Rh(bpy) [bpy = κ^2 -2,2'-bipyridine] with a protonic acid initially affords the 16e pentamethylcyclopentadiene-containing cation, $[(\eta^4\text{-Cp}^*\text{H})\text{Rh}(\text{bpy})]^+$, which is believed to result from C–H bond-forming reductive elimination from the transient rhodium hydrido complex, $[\text{Cp}^*\text{Rh}(\text{bpy})\text{H}]^+$.^{123,124} Even more rare is the case in which Cp*H is also liberated as the free

diene, which has been seen in the reported solvent-induced elimination of Cp*H from Cp*Ir(H)₃(PPh₃),¹²⁵ and also the reported elimination of Cp*H from Cp*Rh(H)₂(PMe₃) induced by phosphine coordination.¹²⁶ The exact mechanism of the transformation seen in the reaction of **4.1** with bromoalkanes that results in the liberation of Cp*H— whether it involves the reductive elimination of a hydrido and Cp* ligand from the transition-metal's coordination sphere or radical processes wherein hydrogen radicals and the Cp* rings couple, or some other mechanism entirely— remains to be ascertained, and more work is required to fully elucidate it.

A solid-state molecular structure has been obtained for complex **4.6** from a single-crystal X-ray diffraction analysis of the red crystalline precipitate resulting from the reaction (Figure 4.8). The structure is that of a bimetallic complex wherein the two halves of the molecule are related by an inversion centre with the molybdenum centres in an octahedral-like geometry (Figure 4.9). Two bromine atoms form bridging linkages between the molybdenum centres with molybdenum–bromine bond lengths of that are essentially the same. A metal–metal bond exists in the structure and the metal–metal bond length is 2.9819(10) Å, which is comparable to other molybdenum–molybdenum bonds in other bimetallic structures described in the literature.^{105,127,128} The nitrosyl ligands are linear and have Mo(1)–N(1)–O(1) bond angles of 175.2(13)°. The molybdenum–phosphorus bonds have bond lengths of 2.4790(17) and 2.4825(17) Å and are similar in length compared to other molybdenum–phosphorus linkages seen in related systems.

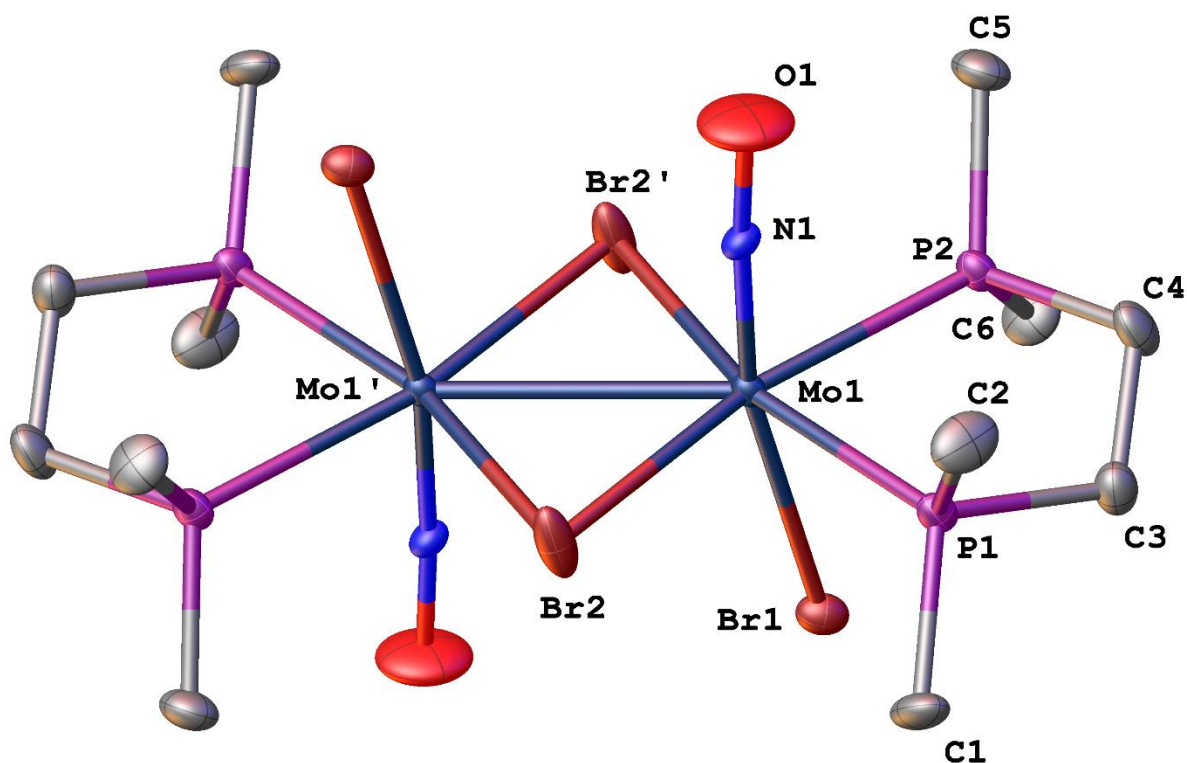


Figure 4.9. The major component of the solid-state molecular structure of **4.6** with 50% probability thermal ellipsoids shown. Hydrogen atoms have been omitted for the sake of clarity. Only half of the molecule has been fully labelled for the sake of clarity. Selected bond lengths (Å) and angles (deg): Mo(1)–Mo(1)' = 2.9819(10), Mo(1)–Br(1) = 2.6315(19), Mo(1)–Br(2) = 2.5847(9), Mo(1)–Br(2)' = 2.5871(9), Mo(1)–P(1) = 2.4790(17), Mo(1)–P(2) = 2.4825(17), Mo(1)–N(1) = 1.776(13), N(1)–O(1) = 1.35(2), P(1)–C(1) = 1.811(7), P(1)–C(2) = 1.801(7), P(1)–C(3) = 1.824(7), P(2)–C(4) = 1.834(7), P(2)–C(5) = 1.804(7), P(2)–C(6) = 1.821(7), C(3)–C(4) = 1.525(10), Mo(1)–N(1)–O(1) = 175.2(13), Mo(1)–Br(2)–Mo(1)' = 70.42(3), Mo(1)'–Mo(1)–N(1) = 94.0(3), Mo(1)'–Mo(1)–Br(1) = 98.64(4), P(1)–Mo(1)–P(2) = 80.53(6), Br(2)–Mo(1)–Br(2)' = 109.58(3), P(1)–Mo(1)–Br(2) = 85.58(4), P(2)–Mo(1)–Br(2)' = 84.35(4).

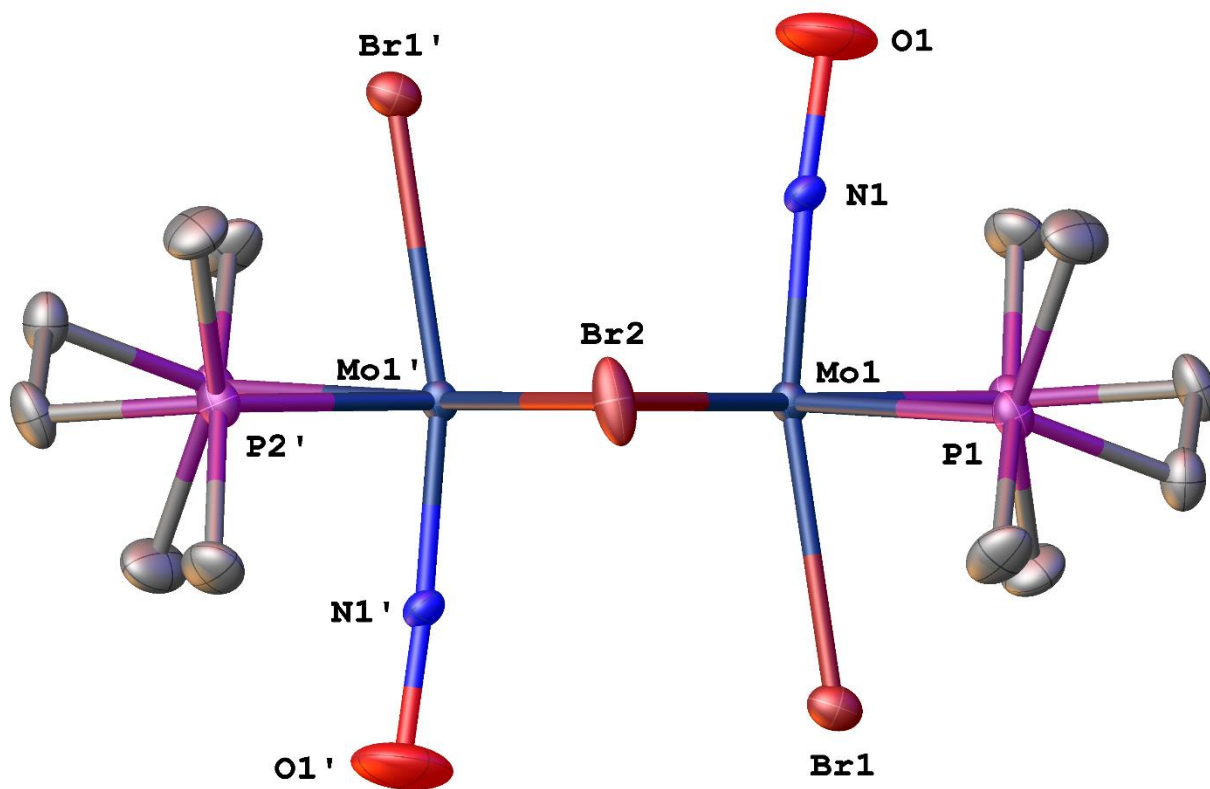


Figure 4.10. View of the major component of the solid-state molecular structure of complex **4.6** along the Br(2)–Br(2)' axis showing the inversion centre symmetry that relates the two halves of the bimetallic molecule. Hydrogen atoms have been omitted for the sake of clarity.

4.2.4.3 Reaction of 4.1 with 1-Bromooctane

In lieu of 1-bromopropane, 1-bromooctane is used as the alkyl halide reactant in order to successfully quantify the relative amounts of the products of the reaction. Reaction of 5 equivalents 1-bromooctane with complex **4.1** in a THF solution results in a pale yellow supernatant solution and a large red crystalline precipitate after 16 hours. The identity of these

crystals being $[\text{Mo}(\text{NO})(\text{Br})_2(\kappa^2\text{-dmpe})]_2$ (**4.6**) is confirmed via spectroscopic evidence, namely, an identical IR spectrum displaying a band at 1619 cm^{-1} with a shoulder at 1577 cm^{-1} is obtained. A mass spectrum of the product also confirms its identity to be that of **4.6**.

GCMS analysis of the supernatant solution shows that the organic products of the reaction are octane, Cp^*H , and isomers of octene, which mirror the products identified in the 1-bromopropane experiments. The GCMS analysis identifies the octene isomers to be 1-octene, *trans*-2-octene, and *cis*-2-octene. In order to discern the relative amounts of products formed in the solution, the experiment was replicated on the NMR scale in C_6D_6 in a J-Young tube. Interestingly, in the ^1H NMR spectrum resonances attributable to *2-trans*-octene are observed, but no resonances belonging to other isomers of octene are seen, indicating that the 1-octene and *cis*-2-octene are probably formed in negligible amounts. Shown in Figure 4.8, the ^1H NMR spectrum of the supernatant solution shows that *2-trans*-octene and Cp^*H are present in a 3:2 ratio, respectively. The relative amount of octane produced is unable to be ascertained from the NMR data since the 1-bromooctane dominates the regions of the NMR spectrum wherein the resonances of octane would appear.

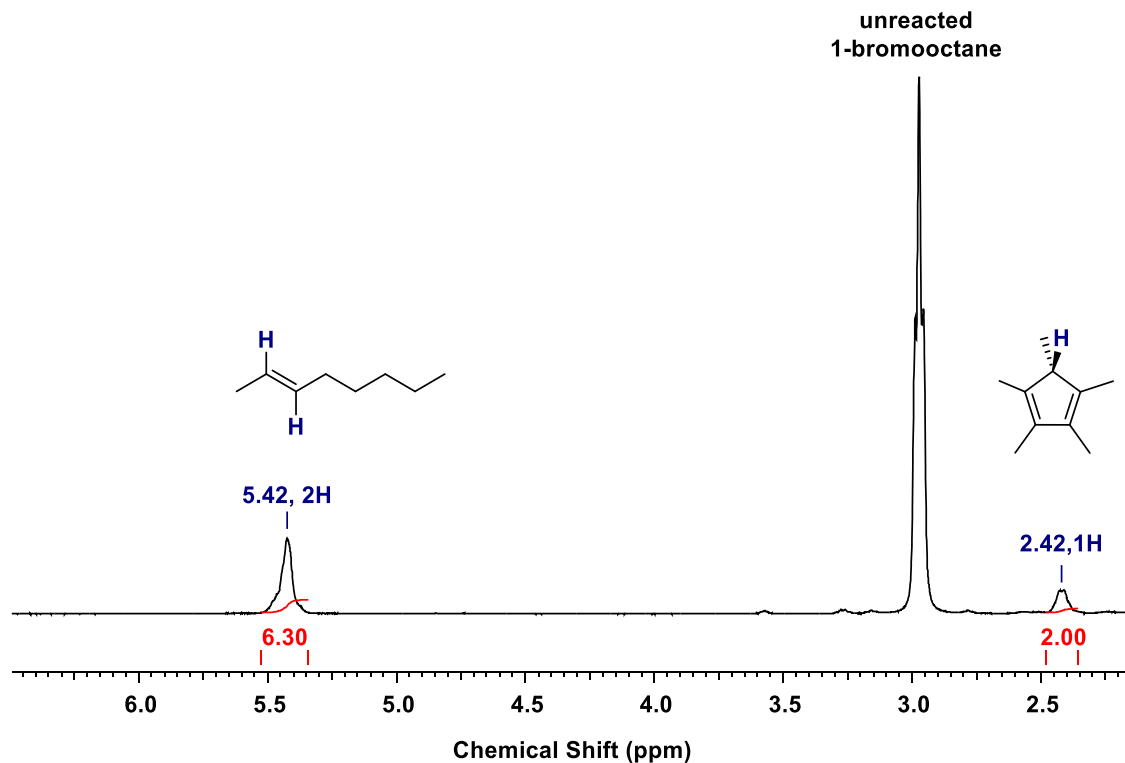
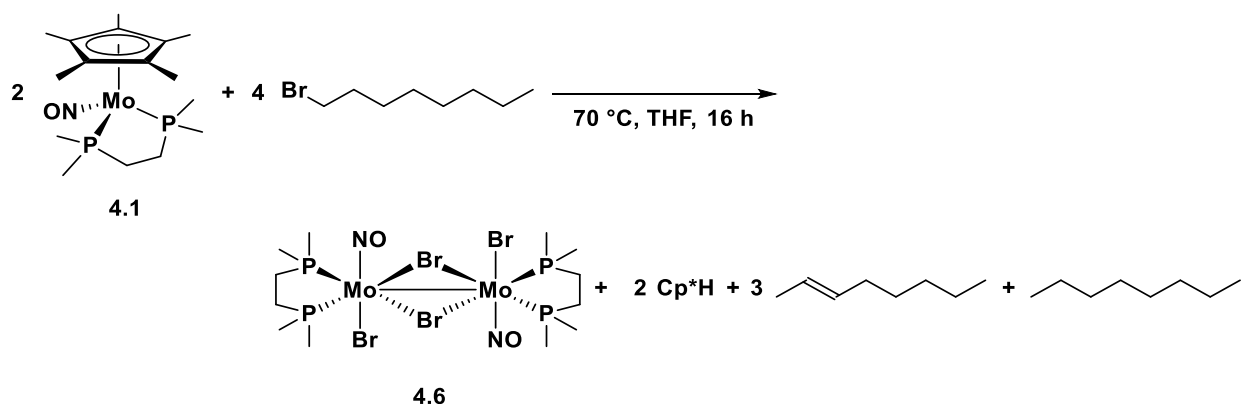


Figure 4.11. Expansion of the ^1H NMR spectrum (400 MHz, C_6D_6) from δ 2.14 to 6.44 ppm showing the resonances attributable to the two methine protons of *trans*-2-octene and the single non-methyl proton of pentamethylcyclopentadiene and their relative integrations.

From this data, a balanced chemical equation can be written and is shown below in Scheme 4.9, wherein two equivalents of **4.1** and four equivalents of 1-bromooctane are consumed in order to form the dimeric complex accompanied by three equivalents of *trans*-2-octene and 1 equivalent of octane. Akin to what we see with in the comparable reaction of **4.1** with benzyl bromide, the mechanism in this reaction probably involves radical alkyl species being produced in situ. However, in the experiment with benzyl bromide the benzyl radical produced is much more stable than alkyl radicals and favours the formation of bibenzyl as the major product. In the reactions with alkyl bromides, the radical species are much more unstable

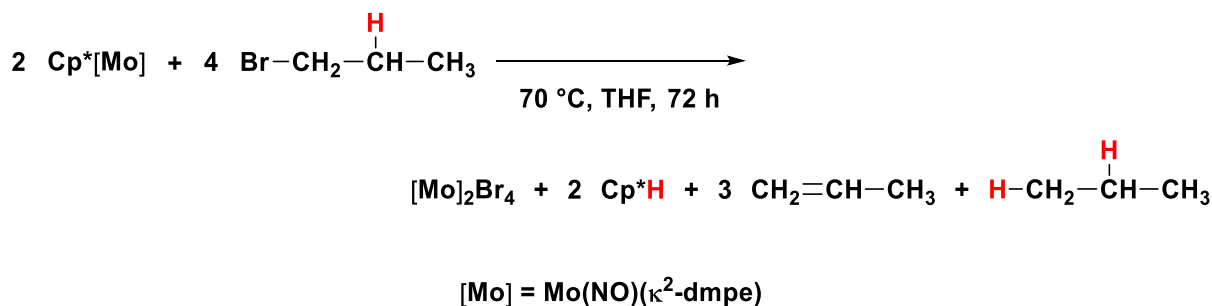
and cause the dehydrohalogenation of the alkyl bromide reagent and the atom transfer of hydrogen to the Cp* ligand to occur, resulting in the observed organic products. Similar reactivity is probably not seen in the reaction with benzyl bromide due to the lack of β -hydrogens on the organic halide reagent.

Scheme 4.9. Reaction of 4.1 with 1-bromooctane



A more general chemical equation showing this interesting reactivity is illustrated in Scheme 4.10 wherein the reaction of **4.1** with 1-bromopropane is used as an example and the hydrogen atoms that are transferred are shown in red.

Scheme 4.10. General reaction of complex 4.1 with 1-bromopropane



4.2.4.4 Reaction of 4.1 with Bromobenzene

As a direct comparison to the above experiments, 5 equivalents of bromobenzene have been reacted with **4.1** in a THF solution. After 3 d of heating at 70 °C no reaction occurs. The appearance of the solution before and after is the same, and analysis of the reaction mixture after the removal of volatiles confirms that the only contents of the mixture are initial reactant **4.1** and bromobenzene. This is probably a result of the sp^2 hybridized C–Br bond in bromobenzene which is stronger than the sp^3 C–Br bonds in bromoalkanes and benzyl bromide and thus inhibits the homolytic cleavage and formation of radical species.

4.2.4.5 Reactions of 4.1 with Other Organic Halides

In addition to the reactions with bromoalkanes, benzyl bromide, and bromobenzene, reactions with chloro- and iodoalkanes have been performed. The reactions of complex **4.1** with chloroalkanes result in no reactivity after heating at 70 °C for prolonged periods, and the reactions with iodoalkanes result in very messy reaction mixtures after heating for prolonged periods. Thus, investigations into the reactivity of complex **4.1** with organic chlorine or iodine reagents have not been pursued further.

4.3 Summary

Reaction of $Cp^*Mo(NO)Cl_2$ with 1 equivalent of dmpe in THF forms the complex $[Cp^*Mo(NO)(Cl)(\kappa^2\text{-dmpe})]Cl$ (**4.2**) which is isolable as an analytically pure yellow powder.

Further addition of 2 equivalents of Cp_2Co to **4.2** in CH_2Cl_2 results in the formation of $\text{Cp}^*\text{Mo}(\text{NO})(\kappa^2\text{-dmpe})$ (**4.1**), which is isolable as an analytically pure red powder. The ability of complex **4.1** to effect C–H activation of hydrocarbon substrates has been investigated and it has been found that it does not effect the desired chemistry. Subsequently, the reactivity of **4.1** towards oxidants, such as elemental sulfur, has been investigated, and reaction of **4.1** with 1 mol equivalent of S in benzene has been performed and results in the formation of $(\mu\text{-S})[\text{Cp}^*\text{Mo}(\text{NO})(\kappa^1\text{-dmpeS})]_2$ (**4.3**). Complex **4.3** is a rare example of a bimetallic transition-metal complex bridged by a single sulfur atom, and to the best of my knowledge is the only example wherein the bridging linkage involves $\text{M}=\text{S}=\text{M}$ bonding rather than $\text{M}=\text{S}\equiv\text{M}$. Reaction of **4.1** with 5 mol equivalents of S in benzene results in the formation of $\text{Cp}^*\text{Mo}(\text{NO})(\eta^2\text{-S}_2)(\kappa^1\text{-dmpeS})$ (**4.4**). Complex **4.4** can also be formed from the addition of elemental sulfur to complex **4.3**, indicating that **4.3** is an intermediate complex leading to the formation of **4.4**. Reaction of **4.1** with organic halide reagents has also been investigated, and bromine reagents are found to be the most productive. Reaction of **4.1** in THF with 5 equivalents of benzyl bromide results in the formation of $(\mu\text{-dmpe})[\text{Cp}^*\text{Mo}(\text{NO})\text{Br}_2]_2$ (**4.5**) and bibenzyl after heating at 70 °C. This probably results from radical processes in the reaction wherein benzyl radicals undergo homolytic coupling and form bibenzyl. The organometallic product, complex **4.5**, undergoes decomposition readily and forms an unknown organometallic precipitate. In comparison to the reaction with benzyl bromide, reaction of **4.1** with 5 equivalents of 1-bromopropane or 1-bromooctane after heating at 70 °C results in the formation of $[\text{Mo}(\text{NO})(\text{Br})_2(\kappa^2\text{-dmpe})]_2$ (**4.6**), olefin, alkane, and Cp^*H . Similar to the benzyl bromide reaction, the mechanism of the reaction most likely involves radical processes in order to form the observed products. A more in depth study is required to further elucidate the reactivity of complex **4.1** towards alkyl bromides; thus

far all observations point towards a radical pathway occurring. Complex **4.1** does not display any reactivity with bromobenzene after maintaining the reaction solution at 70 °C for multiple days, suggesting that this unique reactivity is limited to organic bromine reagents with a C(*sp*³)-Br linkage. Further investigations into this chemistry are needed to fully explore this interesting mode of reactivity.

4.4 Experimental Section

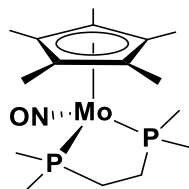
4.4.1 General Methods

All reactions and subsequent manipulations involving organometallic reagents were performed under anhydrous and anaerobic conditions except where noted. High-vacuum and inert-atmosphere techniques were performed using double-manifold Schlenk lines or in Innovative Technologies LabMaster 100 and MS-130 BG dual-station gloveboxes equipped with freezers maintained at -30 °C. Preparative scale reactions were performed with Schlenk or round bottom flasks; reactions were performed in thick-walled glass reaction flasks (larger scale) or J. Young NMR tubes (smaller scale), both of which were typically sealed with Kontes greaseless stopcocks. Tetrahydrofuran (THF) and diethyl ether (Et₂O) were dried over sodium/benzophenone ketyl and freshly distilled prior to use; *n*-pentane was dried over calcium hydride and freshly distilled prior to use; all other solvents were dried according to standard procedures.¹²⁹ Cp*Mo(NO)Cl₂ was prepared according to the published procedures.³² Pentamethylcyclopentadiene was obtained from the Boulder Scientific Co. All other chemicals and reagents were ordered from commercial suppliers and used as received. Unless otherwise

specified, all IR samples were prepared as Nujol mulls sandwiched between NaCl plates, and their spectra were recorded on a Thermo Nicolet model 4700 FT-IR spectrometer. Except where noted, all NMR spectra were recorded at room temperature on Bruker AV-400 instruments (direct and indirect probes), and all chemical shifts are reported in parts per million and coupling constants in hertz. ^1H NMR spectra were referenced to the residual protio isotopomer present in C_6D_6 (7.16 ppm), CD_2Cl_2 (5.32 ppm), or CDCl_3 (7.26 ppm). ^{13}C NMR spectra were referenced to C_6D_6 (128.39 ppm), CD_2Cl_2 (53.84 ppm), or CDCl_3 (77.16 ppm). ^{31}P NMR spectra were externally referenced to 85% H_3PO_4 . For the characterization of most complexes, two-dimensional NMR experiments, $\{^1\text{H}-^1\text{H}\}$ COSY, $\{^1\text{H}-^{13}\text{C}\}$ HSQC, $\{^1\text{H}-^{31}\text{P}\}$ HMBC, and $\{^1\text{H}-^{13}\text{C}\}$ HMBC, were performed to correlate and assign ^1H , ^{13}C , and ^{31}P NMR signals and establish atom connectivity. GC analyses were performed on an Agilent technologies 7890B GC equipped with a HP-5MS (30 m \times 0.250 mm \times 0.25 μm) capillary column coupled to an Agilent technologies 5977A MSD analyzer. Low- and high-resolution mass spectra (EI, 70 eV) and MALDI-TOF spectra were recorded by M. Lapawa of the UBC mass spectrometry facility using a Kratos MS-50 spectrometer and a Bruker Autoflex spectrometer, respectively. M. Yeung recorded ESI mass spectra on a Bruker HCT spectrometer, and elemental analyses were performed by D. Smith of the UBC microanalytical facility. GC analyses were performed by Dr. Y. Ling of the UBC microanalytical facility. X-ray crystallographic data collection, solution, and refinement were performed by Dr. B. O. Patrick of the UBC X-ray crystallography facility.

4.4.2 Synthesis of Cp*Mo(NO)(κ²-dmpe) (**4.1**)

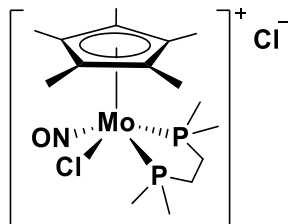
In a glovebox, a Schlenk flask was charged with Cp*Mo(NO)Cl₂ (1.002 g, 3.017 mmol) and a stir bar, a second Schlenk flask was charged with dmpe (0.51 mL, 3.0 mmol), and a third Schlenk flask was charged with Cp₂Co (1.142 g, 6.038 mmol). On a double-manifold, THF (ca. 50 mL) was cannulated into both flasks containing Cp*Mo(NO)Cl₂ and dmpe, affording a bright green solution and a colourless solution, respectively. The dmpe solution was then transferred by cannula into the flask containing the stirred Cp*Mo(NO)Cl₂ solution, whereupon the colour of the reaction mixture changed from green to yellow and a yellow precipitate formed. After 10 min the solvent was decanted, and the remaining solid was washed with THF (2 × 20 mL) before it was taken to dryness in vacuo to obtain [Cp*Mo(NO)(Cl)(κ²-dmpe)]Cl (**4.2**). CH₂Cl₂ (ca. 100 mL) was then cannulated into the flask to obtain a clear yellow solution. The Cp₂Co was dissolved in CH₂Cl₂ (ca. 30 mL), and this solution was then added dropwise to the yellow solution, whereupon it became black. The reaction mixture was stirred for 30 min to obtain a clear, dark red solution. Removal of the solvent in vacuo and recrystallization of the residue from Et₂O at -30 °C afforded Cp*Mo(NO)(κ²-dmpe) (**4.1**) as dark red crystals (0.449 g, 1.092 mmol, 36% yield). Single crystals suitable for an X-ray diffraction analysis were obtained by slow evaporation of an Et₂O solution of **4.1** at ambient temperatures.



Characterization data for Cp*Mo(NO)(κ^2 -dmpe) (**4.1**). IR(cm^{-1}): 1535 (s, ν_{NO}). MS (LREI, m/z , probe temperature 150 °C): 413 [M^+ , ^{98}Mo]. MS (HREI, m/z , ^{92}Mo): calcd 407.09449, found 407.09490. ^1H NMR (400 MHz, C_6D_6): δ 0.92 (d, $^2J_{\text{HP}} = 6.5$, 6H, *PMe*), 1.07 (m, 2H, *CH*₂), 1.29 (m, 2H, *CH*₂), 1.39 (d, $^2J_{\text{HP}} = 8.4$, 6H, *PMe*), 1.95 (s, 15H, *C*₅*Me*₅). ^{13}C APT NMR (100 MHz, C_6D_6): δ 12.2 (*C*₅*Me*₅), 16.7 (m, *PMe*), 19.2 (m, *PMe*), 31.9 (m, *PCH*₂), 101.2 (*C*₅*Me*₅). $^{31}\text{P}\{^1\text{H}\}$ NMR (162 MHz, C_6D_6): δ 57.1 (s, *MoP*). Anal. Calcd for $\text{C}_{16}\text{H}_{31}\text{MoNOP}_2$: C, 46.72; H, 7.60; N, 3.41. Found: C, 46.80; H, 7.37; N, 3.19.

4.4.3 Synthesis of [Cp*Mo(NO)(Cl)(κ^2 -dmpe)]Cl (**4.2**)

In a glovebox, a Schlenk flask was loaded with Cp*Mo(NO)Cl₂ (0.200 g, 0.602 mmol) and a stir bar. Also in the glovebox, another Schlenk flask was charged with dmpe (0.10 mL, 0.60 mmol). On a double-manifold, THF (ca. 50 mL) was cannulated into both flasks affording a bright green solution and a colourless solution, respectively. The dmpe solution was then transferred by cannula into the flask containing the stirred Cp*Mo(NO)Cl₂ solution, whereupon the colour of the reaction mixture changed from green to yellow and a yellow precipitate formed. After 10 min the solvent was decanted, and the remaining solid was washed with THF (2 \times 20 mL) before being taken to dryness in vacuo to obtain [Cp*Mo(NO)(Cl)(κ^2 -dmpe)]Cl (**4.2**) as a fine yellow powder (0.189 g, 0.392 mmol, 65% yield). Recrystallization of **4.2** from 1:1 CH₂Cl₂/hexanes in an aerobic environment afforded small yellow crystals of [Cp*Mo(NO)(Cl)(κ^2 -dmpe)]Cl \cdot 2H₂O that were subjected to an X-ray diffraction analysis.

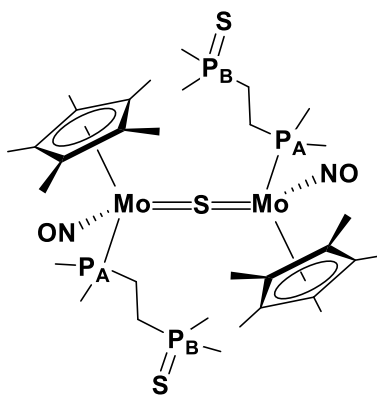


Characterization data for $[\text{Cp}^*\text{Mo}(\text{NO})(\text{Cl})(\text{dmpe})]\text{Cl}$ (**4.2**). IR(cm^{-1}): 1661 (s, ν_{NO}). MALDI-TOF (dtcb/ CDCl_3 , m/z): 448.2 for $\text{C}_{16}\text{H}_{31}\text{ClINOP}_2^{98}\text{Mo}$ ($[\text{M} - \text{Cl}]^+$, ^{98}Mo). HRMS-ESI(+) (40V, m/z): ($[\text{M} - \text{Cl}]^+$, ^{92}Mo) calcd for $\text{C}_{16}\text{H}_{31}\text{ClINOP}_2^{92}\text{Mo}$, 442.0638; found, 442.0633. ^1H NMR (400 MHz, CD_2Cl_2): δ 1.75 (d, $^2J_{\text{HP}} = 10.4$, 3H, *PMe*), 1.81 (d, $^2J_{\text{HP}} = 10.8$, 3H, *PMe*), 1.84 (d, $^2J_{\text{HP}} = 10.6$, 3H, *PMe*), 2.00 (s, 15H, C_5Me_5), 2.03–2.11 (overlapped m, 1H, $\text{PCH}_2\text{CH}_2\text{P}$), 2.19 (d, $^2J_{\text{HP}} = 10.0$, 3H, *PMe*), 2.40–2.49 (m, 1H, $\text{PCH}_2\text{CH}_2\text{P}$), 2.81–2.94 (overlapped m, 2H, $\text{PCH}_2\text{CH}_2\text{P}$). ^{13}C APT NMR (100 MHz, CD_2Cl_2): δ 10.6 (d, $^1J_{\text{CP}} = 28.8$, *PMe*), 11.4 (C_5Me_5), 12.9 (d, $^1J_{\text{CP}} = 28.0$, *PMe*), 15.4 (d, $^1J_{\text{CP}} = 21.5$, *PMe*), 17.6 (d, $^1J_{\text{CP}} = 36.8$, *PMe*), 25.4 (dd, $^1J_{\text{CP}} = 27.6$, $^2J_{\text{CP}} = 8.4$, $\text{PCH}_2\text{CH}_2\text{P}$), 33.7 (dd, $^1J_{\text{CP}} = 36.4$, $^2J_{\text{CP}} = 14.6$, $\text{PCH}_2\text{CH}_2\text{P}$), 117.2 (C_5Me_5). $^{31}\text{P}\{^1\text{H}\}$ NMR (162 MHz, CD_2Cl_2): δ 37.4 (d, $^3J_{\text{PP}} = 45.6$, *MoP*), 44.9 (d, $^3J_{\text{PP}} = 45.6$, *MoP*). Anal. Calcd for $\text{C}_{16}\text{H}_{31}\text{Cl}_2\text{NOP}_2\text{Mo}$: C, 39.85; H, 6.48; N, 2.90. Found: C, 39.77; H, 6.58; N, 2.62.

4.4.4 Synthesis of $(\mu\text{-S})[\text{Cp}^*\text{Mo}(\text{NO})(\kappa^1\text{-dmpeS})]_2$ (**4.3**)

In a glovebox, a thick-walled flask was charged with complex **4.1** (0.084 g, 0.205 mmol), C_6H_6 (ca. 20 mL), and a magnetic stir bar. On a double-manifold, elemental sulfur (0.007 g, 0.218 mmol) was added to the vessel, whereupon the stirred orange solution immediately

developed a brown colouration and a precipitate formed. The solvent was removed in vacuo to obtain a brown powder that was purified by column chromatography over basic alumina (1 × 4 cm) made up in Et₂O. Elution of the column with 1:1 THF/Et₂O resulted in a dark blue band that was eluted and collected. Removal of solvents from the eluate under reduced pressure afforded (μ-S)[Cp*Mo(NO)(κ¹-dmpeS)]₂ (**4.3**) as a dark blue solid (0.032 g, 0.035 mmol, 34% yield). Recrystallization of **4.3** from a 1:10 *n*-pentane/benzene solution left at ambient temperatures for 15 d afforded small blue crystals of sufficient quality for a single-crystal X-ray diffraction analysis.

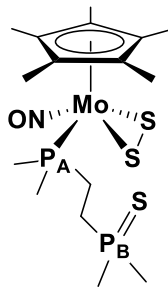


Characterization data for (μ-S)[Cp*Mo(NO)(κ¹-dmpeS)]₂ (**4.3**). IR(cm⁻¹): 1562 (s, ν_{NO}). ESI(+)-MS (40V, *m/z*): 918 for C₃₂H₆₂N₂O₂P₄S₃Mo₂, (M⁺, ⁹⁸Mo), 445 for C₁₆H₃₁NOP₂SMo, ([Cp*Mo(NO)(κ²-dmpeS)]⁺, ⁹⁸Mo). HRMS-ESI(+) (40V, *m/z*): ([Cp*Mo(NO)(κ²-dmpeS) + H]⁺, ⁹²Mo) calcd for C₁₆H₃₂NOP₂S⁹²Mo, 440.0748; found, 440.0748. ¹H NMR (400 MHz, C₆D₆): δ 1.07 (d, ²J_{HP} = 7.9, 3H, P_AMe), 1.36 (d, ²J_{HP} = 12.9, 3H, P_BMe), 1.37 (d, ²J_{HP} = 8.1, 3H, P_AMe), 1.39 (d, ²J_{HP} = 12.8, 3H, P_BMe), 1.87 (s, 15H, C₅Me₅), 1.88 (obscured m, 1H, P_ACH₂), 2.02 (m, 1H, P_BCH₂), 2.19 (m, 1H, P_ACH₂), 2.37 (m, 1H, P_BCH₂). ¹³C APT NMR (100 MHz, C₆D₆): δ

11.6 (C_5Me_5), 14.4 (d, $^1J_{CP} = 27.9$, P_AMe), 15.8 (d, $^1J_{CP} = 23.9$, P_AMe), 20.4 (d, $^1J_{CP} = 53.3$, P_BMe), 21.6 (d, $^1J_{CP} = 55.5$, P_BMe), 25.4 (d, $^1J_{CP} = 26.0$, P_ACH_2), 30.0 (d, $^1J_{CP} = 51.5$, P_BCH_2), 107.9 (C_5Me_5). $^{31}P\{^1H\}$ NMR (162 MHz, C_6D_6): δ 22.7 (d, $^3J_{PP} = 47.6$, MoP_A), 39.2 (d, $^3J_{PP} = 47.6$, SP_B).

4.4.5 Synthesis of $Cp^*Mo(NO)(\eta^2-S_2)(\kappa^1-dmpeS)$ (**4.4**)

In a glovebox, a thick-walled flask was charged with complex **4.1** (0.164 g, 0.400 mmol), C_6H_6 (ca. 30 mL), and a magnetic stir bar to afford a bright orange solution. To this vessel, elemental sulfur (0.064 g, 2.00 mmol) was added causing an instantaneous colour change of the solution to a dark red-brown colour. C_6H_6 was removed in vacuo, depositing a brown residue to the sides of the flask. Purification was carried out in an inert atmosphere via column chromatography over a basic alumina stationary phase (1 \times 4 cm) whereupon the complex $Cp^*Mo(NO)(\eta^2-S_2)(\kappa^1-dmpeS)$ (**4.4**) was eluted in 50% THF in Et_2O as a red band (0.083 g, 0.163 mmol, 41% yield). Recrystallization was performed at ambient temperatures via vapour diffusion of Et_2O into a C_6H_6 solution of **4.4** in an inert atmosphere. Small red crystals of suitable quality for single-crystal X-ray diffraction were deposited to the sides of the vial after 3 d, from which a solid-state molecular structure was obtained.



Characterization data for Cp*Mo(NO)(η^2 -S₂)(κ^1 -dmpeS) (**4.4**). IR(cm⁻¹): 1593 (s, ν_{NO}). MS (LREI, m/z , probe temperature 150 °C): 509 [M⁺, ⁹⁸Mo], 445 [M⁺ - S₂, ⁹⁸Mo]. MS (HREI, m/z , ⁹²Mo): calcd 503.01112, found 503.01123. ¹H NMR (400 MHz, C₆D₆): δ 1.03 (d, ²J_{HP} = 8.8, 3H, P_AMe), 1.07 (d, ²J_{HP} = 8.8, 3H, P_AMe), 1.12 (d, ²J_{HP} = 12.7, 3H, P_BMe), 1.17 (d, ²J_{HP} = 12.7, 3H, P_BMe), 1.62 (s, 15H, C₅Me₅), 1.71 (m, 1H, P_BCH₂), 1.82 (m, 1H, P_BCH₂), 2.27 (m, 1H, P_ACH₂), 2.35 (m, 1H, P_ACH₂). ¹³C APT NMR (100 MHz, C₆D₆): δ 10.7 (C₅Me₅), 12.5 (d, ¹J_{CP} = 26.0, P_AMe), 13.4 (d, ¹J_{CP} = 28.7, P_AMe), 20.4 (d, ¹J_{CP} = 54.0, P_BMe), 21.2 (d, ¹J_{CP} = 54.9, P_BMe), 28.5 (dd, ¹J_{CP} = 35.6, ²J_{CP} = 3.0, P_ACH₂), 29.5 (dd, ¹J_{CP} = 50.8, ²J_{CP} = 0.9, P_BCH₂), 110.8 (C₅Me₅). ³¹P{¹H} NMR (162 MHz, C₆D₆): δ 21.8 (d, ³J_{PP} = 48.5, MoP_A), 37.9 (d, ³J_{PP} = 49.5, SP_B). Anal. Calcd for C₁₆H₃₁MoNOP₂: C, 37.87; H, 6.16; N, 2.76; S, 18.95. Found: C, 40.16; H, 5.94; N, 2.23; S, 18.29. As of yet, an analytically pure sample of **4.4** has not been obtained.

4.4.6 Reaction of 4.1 with Oxygen

In a glovebox, a thick-walled flask was charged with complex **4.1** (0.191 g, 0.464 mmol), Et₂O (ca. 20 mL), and a magnetic stir bar, forming a bright orange solution. To this flask, 15 psig of O₂ was added. Immediately upon the O₂ addition, the initially clear bright orange

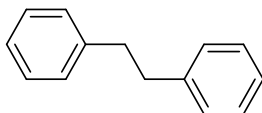
solution turned brown, and a yellow precipitate deposited. The Et₂O solvent was removed in vacuo, and Et₂O washes of the precipitate (6 × 10 mL) were performed before the crude product was brought to dryness and transferred into the glovebox for collection (0.123 g). Further purification of the crude product via column chromatography or recrystallization from mixtures of Et₂O, *n*-pentane, THF, and C₆H₆ were not successful.

Partial Characterization data of the product. ESI(+)-MS (40 V, *m/z*): 445.1 for C₁₆H₃₁MoNO₃P₂ ([Cp*Mo(NO)(dmpe) + O₂]⁺, ⁹⁸Mo), 429.2 for C₁₆H₃₁MoNO₂P₂ ([Cp*Mo(NO)(dmpe) + O]⁺, ⁹⁸Mo). ¹H NMR (400 MHz, C₆D₆): δ 1.04 (d, ²*J*_{HP} = 12.6, 3H, *PMe*), 1.06 (d, ²*J*_{HP} = 13.5, 3H, *PMe*), 1.11 (d, ²*J*_{HP} = 9.8, 3H, *PMe*), 1.21 (d, ²*J*_{HP} = 9.4, 3H, *PMe*), 1.72 (s, C₅Me₅, 15H). ³¹P{¹H} NMR (162 MHz, C₆D₆): δ 24.3 (d, *J*_{PP} = 44.6, MoP), 37.8 (d, *J*_{PP} = 44.6, MoP).

4.4.7 Reaction of 4.1 with Benzyl Bromide

In a glovebox a flask was charged with complex **4.1** (0.076 g, 0.185 mmol) and THF (ca. 10 mL), resulting in a clear bright orange solution. On a double-manifold, benzyl bromide (0.110 mL, 0.924 mmol) was added to the reaction flask via a micropipette. No immediate colour change occurred. The flask and its contents were maintained at 70 °C for 4 d, after which time a beige precipitate had deposited and the supernatant solution had darkened to a dark orange colour. Slow cooling of the supernatant solution to ambient temperatures resulted in the formation of orange crystals on the sides of the flask. Analysis of these red crystals determined their identity to be (μ-dmpe)[Cp*Mo(NO)(Br)₂]₂ (**4.5**). Unfortunately, characterization of the

complex was not possible as multiple attempts of repeating the reaction did not result in recrystallization of the complex, and purification methods attempted on the supernatant solution resulted in the isolation more of the unknown beige precipitate that formed initially in the reaction vessel. The isolation of bibenzyl was carried out from a separate reaction wherein complex **4.1** (0.076 g, 0.185 mmol) and benzyl bromide (0.110 mL, 0.924 mmol) in THF were reacted in a manner identical to that described above. The supernatant solution was decanted into a separate flask, and the THF solvent was removed in vacuo. Column chromatography on flash silica (3 × 15 cm) of the remaining residue with hexanes afforded bibenzyl as a colourless eluate. After the removal of volatiles, bibenzyl is obtained as a white crystalline solid (0.024 g, 0.132 mmol, 71% yield).

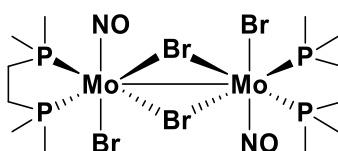


Partial characterization data for bibenzyl: MS (LREI, m/z , probe temperature 150 °C): 182 [M^+], 91 [$M^+ - CH_2Ph$]. 1H NMR (400 MHz, $CDCl_3$): δ 2.91 (s, 4H, CH_2), 7.17–7.29 (m, 10H, aryl H). These data match previously reported spectroscopic data.¹³⁰

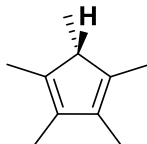
4.4.8 Reaction of **4.1** with 1-Bromopropane

In a glovebox, a thick-walled flask was charged with complex **4.1** (0.101 g, 0.246 mmol) and THF (ca. 10 mL), resulting in a clear dark orange solution. On a double-manifold Schlenk line, 1-bromopropane (0.112 mL, 1.228 mmol) was added to the reaction flask using a

micropipette. No colour change occurred. The flask was heated to 70 °C, and the temperature was maintained for 4 d, after which time large dark red crystals had deposited from the solution and the supernatant was a clear pale yellow solution. The supernatant solution was decanted from the flask, and the red crystals remaining were washed with THF (3 × 1 mL) before being dried in vacuo. [Mo(NO)(Br)₂(dmpe)]₂ (**4.6**) was collected as a red crystalline solid (0.074 g, 0.085 mmol, 69% yield). The red crystals from the reaction vessel were of suitable quality for single-crystal X-ray diffraction analysis, and a solid-state structure of the bimetallic complex was obtained.



Characterization data for [Mo(NO)(Br)₂(dmpe)]₂ (**4.6**). IR (cm⁻¹): 1619 (w, ν_{NO}). MALDI-TOF (LDI, *m/z*): 843.7 for C₁₂H₃₂Br₄NOP₄⁹⁸Mo₂ ([M - NO]⁺, ⁹⁸Mo), 792.8 for C₁₂H₃₂Br₃N₂O₂P₄⁹⁸Mo₂ ([M - Br]⁺, ⁹⁸Mo). HRMS-ESI(+) *m/z*: ([M - Br]⁺, ⁹²Mo) calcd for C₁₂H₃₂Br₃N₂O₂P₄⁹²Mo₂, 780.7106; found, 780.7101. ¹H NMR (400 MHz, CD₂Cl₂): δ 1.84 (d, ²J_{HP} = 9.6, 6H, *PMe*), 2.06 (d, ²J_{HP} = 10.8, 6H, *PMe*), 2.09–2.25 (m, 4H, *PCH*₂), 2.34–2.56 (m, 4H, *PCH*₂). ¹³C{¹H} NMR (100 MHz, CD₂Cl₂): δ 12.8 (m, *PMe*₃), 17.0 (m, *PMe*₃), 27.2 (m, *PCH*₂CH₂P). ³¹P{¹H} NMR (162 MHz, CD₂Cl₂): δ 35.4 (s, *MoP*). Anal. Calcd for C₁₂H₃₂Br₄N₂O₂P₄Mo₂: C, 16.53; H, 3.70; N, 3.21. Found: C, 18.75; H, 4.08; N, 3.04. As of yet, an analytically pure sample of **4.6** has not been obtained.



Partial characterization data for Cp*H: GC-MS m/z (% relative intensity, ion): 136 (95, M^+), 121 (100, $M^+ - CH_3$), 105 (88, $M^+ - C_2H_7$), 93 (71, $M^+ - C_3H_7$), 79 (79, $M^+ - C_4H_9$). 1H NMR (400 MHz, C_6D_6): δ 0.99 (d, $^3J_{HH} = 7.63$, 3H, CH_3), 1.74 (s, 6H, CH_3), 1.79 (s, 6H, CH_3), 2.42 (q, $^3J_{HH} = 7.63$, 1H, CH). These data matches spectroscopic data obtained from a sample of pure Cp*H in C_6D_6 .

4.4.9 Reaction of 4.1 with 1-Bromooctane

In a glovebox, a thick-walled flask was charged with complex **4.1** (0.101 g, 0.246 mmol) and THF (ca. 10 mL), resulting in a clear bright orange solution. On a double-manifold Schlenk line, 1-bromooctane (0.212 mL, 1.227 mmol) was added into the reaction flask via a micropipette. No colour change occurred. The flask was then heated to 70 °C, and the temperature was maintained for 16 h, after which time large dark red crystal had deposited around the sides of the flask and the supernatant solution had become pale yellow in colour. The supernatant solution was decanted from the flask, and the red crystals remaining were washed with THF (3×1 mL) before being dried in vacuo. $[Cp^*Mo(Br)_2(NO)(dmpe)]_2$ (**4.6**) was collected as a red crystalline solid (0.062 g, 0.071 mmol, 58% yield).

4.4.10 Reaction of 4.1 with Bromobenzene

In a glovebox, a thick-walled flask was charged with Cp*Mo(NO)(dmpe) (0.089 g, 0.216 mmol) and THF (ca. 10 mL), resulting in a clear dark orange solution. On a double-manifold, bromobenzene (0.1136 mL, 1.082 mmol) was added to the reaction flask using a micropipette. No immediate colour change occurred. The flask and its contents were heated to 70 °C and maintained at that temperature for 4 d, after which the solution had not changed in appearance. ¹H and ³¹P{¹H} NMR spectra (400 MHz, C₆D₆) of the reaction mixture after the removal of volatiles revealed that it was unchanged from the initial reactants.

4.4.11 X-ray Crystallography

Data collection was carried out at -173.0 ± 2 °C on a Bruker X8 APEX II diffractometer with cross-coupled multilayer optics Mo-K α radiation or at -183.0 ± 2 °C on a Bruker APEX DUO diffractometer equipped with a TRIUMPH curved-crystal monochromated Mo-K α radiation.

Data for **4.1** were collected to a maximum 2θ value of 60.4° in 0.5° oscillations using 3.0-second exposures. The crystal-to-detector distance was 40.05 mm. The structure was solved by direct methods⁷¹ and expanded using Fourier techniques. All non-hydrogen atoms were refined isotropically. All hydrogens atoms were placed in calculated positions. The final cycle of full-matrix least-squares refinement was based on 5650 reflections and 199 variable parameters.

Data for **4.2** were collected to a maximum 2θ value of 60.1° in 0.5° oscillations using 20.0-second exposures. The crystal-to-detector distance was 50.16 mm. The material crystallizes as a two-component ‘split-crystal’ with components one and two related by a 3.9° rotation about the (1.00 0.642 0.000) direct crystal axis. Data were integrated for both twin components, including both overlapped and non-overlapped reflections. The structure was solved by direct methods⁷¹ using non-overlapped data from the major twin component and expanded using Fourier techniques. Subsequent refinements were carried out using the same data set, containing all data from the major twin components. The material crystallizes with two water molecules and one free chloride in the asymmetric unit. All non-hydrogen atoms were refined anisotropically. All O–H hydrogen atoms were located in difference maps and refined isotropically. All other hydrogen atoms were included in calculated positions but not refined. The final cycle of full-matrix least-squares refinement was based on 6630 reflections and 251 variable parameters.

Data for **4.3** were collected to a maximum 2θ value of 55.8° in 0.5° oscillations using 20.0-second exposures. The crystal-to-detector distance was 60.21 mm. The material crystallizes as a two-component ‘split-crystal’ with components one and two related by a 1.7° rotation about the (0.029 -0.003 1) direct crystal axis. Data were integrated for both twin components, including both overlapped and non-overlapped reflections. The structure was solved by direct methods⁷¹ using non-overlapped data from the major twin component and expanded using Fourier techniques. The material crystallizes with one half-molecule in the asymmetric unit, with the bridging sulfur (S2) residing on a two-fold rotation axis. Subsequent refinements were carried out using a HKLF 5 format data set, containing all data from both twin components. All non-hydrogen atoms were refined anisotropically. All hydrogen atoms were

included in calculated positions but not refined. The final cycle of full-matrix least-squares refinement was based on 11361 reflections and 214 variable parameters.

Data for **4.4**: were collected to a maximum 2θ value of 50.8° in 0.5° oscillations using 60.0-second exposures. The crystal-to-detector distance was 40.18 mm. The material crystallizes as a two-component ‘split-crystal’ with components one and two related by a 3.5° rotation about the (1 0.100 0.013) direct crystal axis. Data were integrated for both twin components, including both overlapped and non-overlapped reflections. The structure was solved by direct methods⁷¹ using non-overlapped data from the major twin component and expanded using Fourier techniques. The material crystallizes with significant disorder. The Cp* ring, the disulfide group and two methyl groups are disordered and were modeled in two orientations. Subsequent refinements were carried out using a HKLF 4 format data set, containing all data from component one. All non-hydrogen atoms were refined anisotropically. All hydrogen atoms were included in calculated positions but not refined. The final cycle of full-matrix least-squares refinement was based on 4106 reflections and 337 variable parameters.

Data for **4.5** were collected to a maximum 2θ value of 60.2° in 0.5° oscillations using 10.0-second exposures. The crystal-to-detector distance was 50.22 mm. The structure was solved by direct methods.⁷¹ The material crystallizes with one half-molecule in the asymmetric unit, related to the other half-molecule by an inversion centre at (1-X, -Y, 1-Z). Additionally, there is significant disorder of the coordination around the Mo centre, with one bromine and the nitrosyl swapping positions. The bridging P-ligand is also disordered in two orientations. All non-hydrogen atoms were refined isotropically. All hydrogens atoms were placed in calculated positions. The scattering data and disorder make it impossible to locate hydrides on either Mo

atom. The final cycle of full-matrix least-squares refinement on F2 was based on 5103 reflections and 238 variable parameters.

Data for **4.6** were collected to a maximum 2θ value of 60.1° in 0.5° oscillations using 4.0-second exposures. The crystal-to-detector distance was 40.11 mm. The material crystallizes as a two-component twin with components one and two related by a 179.6° rotation about the (1 0 1) reciprocal axis. Data were integrated for both components, including both overlapped and non-overlapped reflections. The structure was solved by direct methods⁷¹ using non-overlapped data from the major twin component. Subsequent refinements were carried out using an HKLF 4 format data set containing complete data from component one. The molecule crystallizes with one half-molecule in the asymmetric unit, related to the other by an inversion centre at (1-X, 1-Y, 1-Z). Additionally, the bromo and nitrosyl substituents are positionally disordered in a 50/50 ratio. All non-hydrogen atoms were refined anisotropically. All hydrogen atoms were placed in calculated positions. The final cycle of full-matrix least-squares refinement was based on 3813 reflections and 139 variable parameters.

Neutral atom scattering factors were taken from Cromer and Waber.⁷² Anomalous dispersion effects were included in F_{calc} ⁷³; the values for $\Delta f'$ and $\Delta f''$ were those of Creagh and McAuley.⁷⁴ The values for the mass attenuation coefficients are those of Creagh and Hubbell.⁷⁵ All refinements were performed using the SHELXL-2014⁷⁶ via the OLEX2⁷⁷ interface.

Table 4.1. X-ray crystallographic data for complexes **4.1**, **4.2**, and **4.3**.

Complex	4.1	4.2	4.3
Empirical Formula	C ₁₆ H ₃₁ MoNOP ₂	C ₁₆ H ₃₁ MoNOP ₂ Cl ₂ •2H ₂ O	C ₃₂ H ₆₂ Mo ₂ N ₂ O ₂ P ₄ S ₃
Formula Weight	411.30	518.23	918.77
Crystal Colour, Habit	orange, irregular	yellow, needle	blue, blade
Crystal Size (mm)	0.12 × 0.21 × 0.23	0.02 × 0.08 × 0.22	0.07 × 0.18 × 0.45
Crystal System	orthorhombic	triclinic	monoclinic
Space Group	<i>Pbca</i>	<i>P</i> ₋₁	<i>C2/c</i>
Volume (Å ³)	3824.9(4)	1130.49(10)	4444.2(4)
a (Å)	13.6802(9)	8.393(4)	22.7280(10)
b (Å)	16.4231(11)	9.4840(5)	11.9139(5)
c (Å)	17.0245(12)	15.0666(7)	19.5595(10)
α (°)	90	86.290(3)	90
β (°)	90	84.030(3)	122.913(3)
γ (°)	90	63.175(3)	90
Z	8	2	4
Density, ρ (calculated) (g/cm ³)	1.428	1.522	1.373
Absorption Coefficient, μ (mm ⁻¹)	0.852	0.973	0.877
F ₀₀₀	1712	536	1904
Measured Reflections: Total	47214	50330	33932
Measured Reflections: Unique	5650	6630	11361
Final R Indices ^a	R ₁ = 0.020 wR ₂ = 0.047	R ₁ = 0.036 wR ₂ = 0.094	R ₁ = 0.042 wR ₂ = 0.117
Goodness-of-fit on F ^{2,b}	1.05	1.10	1.02
Largest diff. peak/hole (e ⁻ Å ⁻³)	0.45/-0.29	2.09/-0.98	2.23/-0.71

$$^a R_1 \text{ on } F = \sum ||F_o| - |F_c|| / \sum |F_o| ; wR_2 = \sqrt{\sum ((F_o^2 - F_c^2)^2) / \sum w(F_o^2)^2} ; w = (\sigma^2 F_o^2)^{-1}$$

$$^b \text{GOF} = \sqrt{\sum (w (|F_o| - |F_c|)^2) / \text{degrees of freedom}}$$

Table 4.2. X-ray crystallographic data for complexes **4.4**, **4.5**, and **4.6**.

Complex	4.4	4.5	4.6
Empirical Formula	C ₁₆ H ₃₁ MoNOP ₂ S ₃	C ₂₆ H ₄₆ Br ₄ Mo ₂ N ₂ O ₂ P ₂	C ₁₂ H ₃₂ Mo ₂ N ₂ O ₂ P ₄ Br ₄
Formula Weight	507.48	992.11	871.79
Crystal Colour, Habit	red, plate	orange, needle	red, plate
Crystal Size (mm)	0.02 × 0.12 × 0.25	0.07 × 0.14 × 0.35	0.09 × 0.18 × 0.20
Crystal System	triclinic	monoclinic	monoclinic
Space Group	<i>P</i> ₋₁	<i>P</i> 2 ₁ / <i>n</i>	<i>P</i> 2 ₁ / <i>n</i>
Volume (Å ³)	1121.45(18)	1735.5(4)	1308.82(11)
a (Å)	9.4988(9)	8.1677(11)	9.1639(4)
b (Å)	9.5065(9)	13.4105(19)	133.4852(7)
c (Å)	13.0367(12)	15.846(2)	10.6579(5)
α (°)	98.361(5)	90	90
β (°)	100.551(4)	90.937(2)	96.416(1)
γ (°)	99.770(5)	90	90
Z	2	2	2
Density, ρ (calculated) (g/cm ³)	1.503	1.899	2.212
Absorption Coefficient, μ (mm ⁻¹)	1.011	5.445	0.732
F ₀₀₀	524	972	836
Measured Reflections: Total	27459	18823	23972
Measured Reflections: Unique	4106	5103	3813
Final R Indices ^a	R ₁ = 0.056 wR ₂ = 0.166	R ₁ = 0.054 wR ₂ = 0.118	R ₁ = 0.061 wR ₂ = 0.118
Goodness-of-fit on F ² , ^b	1.10	1.03	1.33
Largest diff. peak/hole (e ⁻ Å ⁻³)	1.70/-1.04	1.94/-1.23	1.43/-1.47

$$^a R_1 \text{ on } F = \sum ||F_o| - |F_c|| / \sum |F_o| ; wR_2 = \sqrt{\sum ((F_o^2 - F_c^2)^2) / \sum w(F_o^2)^2} ; w = (\sigma^2 F_o^2)^{-1}$$

$$^b \text{GOF} = \sqrt{\sum (w (|F_o| - |F_c|)^2) / \text{degrees of freedom}}$$

Chapter 5: Conclusion and Future Works

5.1 Summary and Conclusions

The complex $\text{Cp}^*\text{W}(\text{NO})(\text{H})(\eta^3\text{-CH}_2\text{CHCHMe})$ (**2.1**) is readily synthesized from a sequential metatheses reaction involving $\text{Cp}^*\text{W}(\text{NO})\text{Cl}_2$, $\text{Mg}(\text{CH}_2\text{CH}=\text{CHMe})_2$, and LiBH_4 in THF solution. Complex **2.1** exists in solution as four different isomers that differ by the orientation of their η^3 -allyl ligands, either being in an endo or exo orientation, and by the position of the methyl substituent on the η^3 -allyl ligand being either proximal or distal with respect to the hydrido ligand. Under a high pressure of CO and in a solution of benzene, the complex mediates the formation of two ketones, 2-methyl-1-phenylbutan-1-one (**2.2a**) and 1-phenylpentan-1-one (**2.2b**), after heating at 80 °C for 18 hours. These ketones are formed in a 1:1 ratio, and they result from the $\text{C}(sp^2)\text{-H}$ activation and subsequent functionalization of benzene into acyl moieties before coupling with the coordinated η^3 -allyl ligands. Under a high pressure of CO and in a solution of mesitylene, the complex mediates the formation of two novel ketones, 1-(3,5-dimethylphenyl)-3-methylpentan-2-one (**2.3a**) and 1-(3,5-dimethylphenyl)hexan-2-one (**2.3b**), after heating at 80 °C for 18 hours. These ketones are formed in a ratio of 14:86, respectively, and they result from the $\text{C}(sp^3)\text{-H}$ activation and subsequent functionalization of mesitylene into an acyl ligand before coupling with the coordinated η^3 -allyl ligands. Additionally, both of these transformations result in $\text{Cp}^*\text{W}(\text{NO})(\text{CO})_2$ as the organometallic product, thus forming a complete synthetic cycle since $\text{Cp}^*\text{W}(\text{NO})(\text{CO})_2$ can be conveniently converted back into **2.1**. The proposed mechanistic pathway for these conversions has been corroborated via DFT calculations on a related system. Conveniently, these conversions of hydrocarbon and CO to ketones can be effected in the presence of air and water since both the initial and final organometallic complexes are oxidatively and hydrolytically stable. These

reactions highlight the successful C–H activation and functionalization of hydrocarbon substrates into unsymmetrical ketones in a complete synthetic cycle wherein the metal centre can be recycled and costly metals or highly reactive reagents are not required.

After the investigations into functionalization of hydrocarbons by **2.1**, the studies into C–H activation chemistry mediated by Cp*M(NO)-containing complexes have been extended to encompass Cp*W(NO)(R)(H)(L) complexes. *cis*-Cp*W(NO)(H)(κ^2 -PPh₂(C₆H₄)) (**3.1**) has been previously shown to effect the C–H activation of benzene in neat solutions upon heating at 50 °C. Attempts to expand this reactivity to encompass other hydrocarbon substrates that contain C(sp²)–H and C(sp³)–H bonds are unsuccessful and do not result in the desired η^1 -hydrocarbyl complexes. Instead, at increased temperatures complex **3.1** undergoes *cis*–*trans* isomerization into *trans*-Cp*W(NO)(H)(κ^2 -PPh₂(C₆H₄)) (**3.2**), and also forms Cp*W(NO)(PPh₃)₂, a disproportionation product. A spectroscopic trend in the ¹H and ³¹P NMR spectra is observed, and the *cis* and *trans* isomers are found to be discernable from one another by the magnitude of the coupling constants attributable to their hydride or phosphorus ligands in the ¹H or ³¹P NMR spectra, respectively. In an attempt to avoid the problem of forming isomerization and disproportionation products, which result in inactive species, P(OPh)₃ has been used to synthesize the complexes *trans*-Cp*W(NO)(CH₂CMe₃)(H)(P(OPh)₃) (**3.3**) and *trans*-Cp*W(NO)(H)₂(P(OPh)₃) (**3.4**). No *ortho*-metalated and disproportionation products are observed in the reaction mixtures. Unfortunately, complex **3.3** does not effect the C–H activation of hydrocarbon substrates in neat solutions at elevated temperatures. Instead, the elimination of neopentane, release of P(OPh)₃ as free proligand, and subsequent decomposition of the organometallic fragment are prevalent and even occur at ambient temperatures, albeit slowly.

As a direct transition from the research into Cp*W(NO)(R)(H)(L) complexes, the study has been expanded to that of systems using bidentate Lewis base ligands. Reaction of Cp*Mo(NO)Cl₂ with dmpe in THF forms the complex [Cp*Mo(NO)(Cl)(κ²-dmpe)]Cl (**4.2**) which is isolable as an analytically pure yellow powder. Further addition of 2 equivalents of Cp₂Co to **4.2** in CH₂Cl₂ results in the formation of Cp*Mo(NO)(κ²-dmpe) (**4.1**), which is isolable as an analytically pure red powder. The ability of complex **4.1** to effect the C–H activation of hydrocarbon substrates has been investigated, and it has been found that it does not effect the desired chemistry. Subsequently, the chemistry of **4.1** towards oxidants, such as elemental sulfur, has been studied, and reaction of **4.1** with 1 mol equivalent of S in benzene results in the formation of (μ-S)[Cp*Mo(NO)(κ¹-dmpeS)]₂ (**4.3**). Complex **4.3** is a rare example of a bimetallic transition-metal complex wherein the bridging linkage consists of only a single sulfur atom, and additionally, to the best of my knowledge, this is the only example wherein the bridging linkage involves M=S=M bonding rather than M≡S≡M. Reaction of **4.1** with an excess of elemental sulfur in benzene results in the formation of Cp*Mo(NO)(η²-S₂)(κ¹-dmpeS) (**4.4**). Complex **4.4** can also be formed by the addition of elemental sulfur to complex **4.3**, indicating that **4.3** is an intermediate complex leading to the formation of **4.4**. Reaction of **4.1** with organic halide reagents has also been investigated, and bromine reagents were found to be the most productive. Reaction of **4.1** in THF with 5 equivalents of benzyl bromide results in the formation of (μ-dmpe)[Cp*Mo(NO)Br₂]₂ (**4.5**) and bibenzyl after heating at 70 °C. This probably results from radical processes in the reaction wherein benzyl radicals undergo homolytic coupling and form bibenzyl. In comparison, reaction of **4.1** with 5 equivalents of 1-bromopropane or 1-bromooctane after heating at 70 °C results in the formation of [Mo(NO)(Br)₂(κ²-dmpe)]₂ (**4.6**), olefin, alkane, and Cp*H. These reactions are rare examples in

organometallic chemistry wherein the Cp* ligand is not only a participant in the characteristic reactivity of a Cp*M(NO) scaffold complex, but is also subsequently lost from the transition-metal's coordination sphere as free Cp*H. Similar to the benzyl bromide reaction, the mechanism of the reaction most likely involves radical processes in order to form the observed products. Complex **4.1** does not display any reactivity with bromobenzene after maintaining the reaction solution at 70 °C for multiple days, suggesting that this unique reactivity is limited to organic bromine reagents with a C(sp³)-Br linkage.

5.2 Future Directions

5.2.1 Optimization of the Conversion of Hydrocarbons and CO into Unsymmetrical Ketones as well as an Investigation of an Expanded Scope of Substrates

The work in Chapter 2 describes the successful C-H activation and functionalization of benzene and mesitylene into ketones mediated by complex **2.1**. Studies are needed to find the optimal pressure of CO and heating temperature required to maximize the amount of ketone formation. Additionally, the purification methods for the ketone and dicarbonyl products require more investigation in order to determine a better purification and isolation method that does not compromise the yield. The two reactions show that complex **2.1** can facilitate both C(sp²)-H and C(sp³)-H bond activation of hydrocarbon substrates, so investigation into an expanded scope of substrates is required. For instance, two related complexes, Cp*W(NO)(CH₂CMe₃)(η³-CH₂CHCMe₂) and Cp*W(NO)(CH₂CMe₃)(η³-CH₂CHCHPh), are able to effect the C-H activation of methane and other small molecule *n*-alkanes,^{47,48} therefore the expansion of the

chemistry exhibited by **2.1** to include methane and other *n*-alkanes as possible hydrocarbon substrates is attractive. Additionally, it would be interesting to investigate this chemistry utilizing substrates that contain other functional groups, such as ethers or amines, and functionalizing them into larger unsymmetrical ketones that contain multiple functional groups.

5.2.2 Investigation of Cp'M(NO)(R)(H)(L) Utilizing Bound Cyclopentadienyl-Phosphine Ligands

The work with Cp*W(NO)(R)(H)(L) complexes unfortunately did not show the desired C-H activation chemistry. Instead, these systems show a tendency to undergo other modes of reactivity that result in inactive species, namely isomerization and disproportionation products, due to the lability of their L ligands. The work described in Chapter 4 is a direct transition from these RHL systems since the bidentate L systems are investigated because they impede isomerization and disproportionation reactions. Another interesting possible route is the investigation of systems utilizing bidentate cyclopentadienyl-phosphine ligands, wherein the L ligand is bound to the Cp' ring. This would hopefully result in systems that may effect the C-H activation of hydrocarbons but do not follow the unwanted reactivity pathways because of the Cp-bound L ligands that cannot readily interact with other metal centres. There is precedence in the literature for such complexes,^{131,132} and shown in Figure 5.1 are examples of such complexes using zirconium¹³³ and ruthenium¹³⁴ transition-metal centres. The syntheses of these types of complexes on the Cp'M(NO) scaffold would involve the cyclopentadienyl-phosphine ligands having been prepared as lithium salts before coordinating them to a metal centre in a manner similar to that of the dicarbonyl precursor complexes currently used.³²

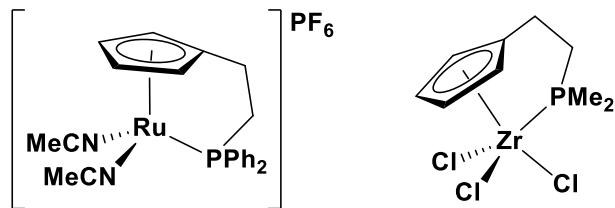


Figure 5.1. Examples found in the literature of complexes possessing a bidentate cyclopentadienyl-phosphine ligand.

5.2.3 Mechanistic Investigations into the Reaction of **4.1** with Organic Halides as well as an Investigation of an Expanded Scope of Substrates

Further elucidation of the interesting chemistry displayed by complex **4.1** towards organic halide reactants is required. The reactions of **4.1** with benzyl bromide, 1-bromopropane, and 1-bromooctane show curious results and further study is needed to fully understand the transformations that result in the observed products. Namely, it remains to be ascertained how the loss of the Cp* ring in the reactions with bromoalkanes occurs, and how the resulting coupled products in the reaction with benzyl bromide are formed. Labelling studies utilizing deuterium-labelled organic bromide reagents would further corroborate the hypothesis that the hydrogen atom transfer processes that result in the loss of the coordinated Cp* rings originates from the bromide reagents. Mechanistic studies into this transformation would also be interesting as this is a rare example of an organometallic reaction that results in the complete loss of Cp* from the metal's coordination sphere. Also, expanding this chemistry to include more substrates and more exotic organic bromide reagents would be of interest. For example, the

results of the reaction of **4.1** with 1-bromoalkanes show that two equivalents of bromine reagent per metal centre are consumed to produce the final product, complex **4.6**. Thus, would a reaction of complex **4.1** with a stoichiometric amount of a linear dibromoalkane reagent with the bromine substituents on both termini of the alkyl chain result in the formation of cyclic hydrocarbon products? For instance, would a reaction of **4.1** with 1,6-dibromohexane result in the formation of cyclohexane?

These outlined future works present possible avenues of research that would yield some interesting compounds and chemistry and would build upon the current research described within this thesis.

References

1. Richter-Addo, G. B.; Legzdins, P. *Metal Nitrosyls*. Oxford University Press: New York, 1992.
2. *Nitrosyl Complexes in Inorganic Chemistry, Biochemistry and Medicine, Parts I and II*; Mingos, D. M. P., Ed.; Springer: New York, 2014.
3. *Methods in nitric oxide research*; Feelisch, M., Stamler, J., Eds.; Wiley: 1996.
4. Lee, D.-H.; Mondal, B.; Karlin, K. D. In *Activation of Small Molecules*; Tolman, W. B., Ed., Wiley-VCH: Weinheim, 2006.
5. Wang, P. G.; Xian, M.; Tang, X. P.; Wu, X. J.; Wen, Z.; Cai, T. W.; Janczuk, A. J. *Chem. Rev.* **2002**, *102*, 1091–1134.
6. Nagano, T.; Yoshimura, T. *Chem. Rev.* **2002**, *102*, 1235–1269.
7. For instance, there is an entire journal that focuses exclusively on nitric oxide research and is the official journal of the Nitric Oxide Society.
<https://www.journals.elsevier.com/Nitric-Oxide>.
8. Hayton, T. W.; Legzdins, P.; Sharp, W. B. *Chem. Rev.* **2002**, *102*, 935–991.
9. Chin, T. T.; Hoyano, J. K.; Legzdins, P.; Malito, J. T. *Inorg. Synth.* **1990**, *28*, 196–198.
10. Legzdins, P.; Malito, J. T. *Inorg. Chem.* **1975**, *14*, 1875–1878.
11. Kolthammer, B. W. S.; Legzdins, P.; Malito, J. T. *Inorg. Chem.* **1977**, *16*, 3173–3178.
12. Greenhough, T. J.; Kolthammer, B. W. S.; Legzdins, P.; Trotter, J. *Acta Crystallogr., Sect. B* **1980**, *36*, 795–799.
13. Hoyano, J. K.; Legzdins, P.; Malito, J. T. *J. Chem. Soc., Dalton Trans.* **1975**, No. 11, 1022–1025.

14. Legzdins, P.; Martin, D. T. *Inorg. Chem.* **1979**, *18*, 1250–1254.
15. Legzdins, P.; Martin, D. T. *Organometallics* **1983**, *2*, 1785–1791.
16. Legzdins, P.; Veltheer, J. E. *Acc. Chem. Res.* **1993**, *26*, 41–48.
17. Blackmore, I. J.; Jin, X.; Legzdins, P. *Organometallics* **2005**, *24*, 4088–4098.
18. Herring, F. G.; Legzdins, P.; Richter-Addo, G. B. *Organometallics* **1989**, *8*, 1485–1493.
19. Baillie, R. A.; Legzdins, P. *Coord. Chem. Rev.* **2016**, *309*, 1–20.
20. Shree, M. V.; Fabulyak, D.; Baillie, R. A.; Lefèvre, G. P.; Dettelbach, K.; Béthegnies, A.; Patrick, B. O.; Legzdins, P.; Rosenfeld, D. C. Multiple C–H Activations of Linear Alkanes by Various (η^5 -Cyclopentadienyl)W(NO)(CH₂CMe₃)₂ Complexes. *Organometallics* [Online early access]. DOI: 10.1021/acs.organomet.7b00034. Published online: June 7, 2017. <http://pubs.acs.org/doi/abs/10.1021/acs.organomet.7b00034> (accessed June 24, 2017).
21. *Chem. Rev.* **2010**, *110* (2). (Special issue on selective functionalization of C–H bonds)
22. *Chem. Soc. Rev.* **2011**, *40* (4). (Special issue on C–H functionalization in organic synthesis)
23. *Acc. Chem. Res.* **2012**, *45* (6). (Special issue on C–H functionalization)
24. Yamaguchi, J.; Yamaguchi, A. D.; Itami, K. *Angew. Chem., Int. Ed.* **2012**, *51*, 8960–9009.
25. Bergman, R. G. *Nature* **2007**, *446*, 391–393.
26. Janowicz, A. H.; Bergman, R. G. *J. Am. Chem. Soc.* **1982**, *104*, 352–354.
27. Hoyano, J. K.; Graham, W. A. G. *J. Am. Chem. Soc.* **1982**, *104*, 3723–3725.
28. Hartwig, J. F. *J. Am. Chem. Soc.* **2016**, *138*, 2–24.
29. Baillie, R. A.; Legzdins, P. *Acc. Chem. Res.* **2014**, *47*, 330–340.

30. Tsang, J. Y. K.; Buschhaus, M. S. A.; Graham, P. M.; Semiao, C. J.; Semproni, S. P.; Kim, S. J.; Legzdins, P. *J. Am. Chem. Soc.* **2008**, *130*, 3652–3663.
31. Baillie, R. A.; Man, R. W. Y.; Shree, M. V.; Chow, C.; Thibault, M. E.; McNeil, W. S.; Legzdins, P. *Organometallics* **2011**, *30*, 6201–6217.
32. Dryden, N. H.; Legzdins, P.; Batchelor, R. J.; Einstein, F. W. B. *Organometallics* **1991**, *10*, 2077–2081.
33. Cho, C. S. *J. Mol. Catal. A* **2005**, *240*, 55–60.
34. Fujita, K.; Asai, C.; Yamaguchi, T.; Hanasaka, F.; Yamaguchi, R. *Org. Lett.* **2005**, *7*, 4017–4019.
35. Cho, C. S. *Catal. Commun.* **2006**, *7*, 1012–1014.
36. Brunet, J. J.; Chauvin, R. *Chem. Soc. Rev.* **1995**, *24*, 89–95.
37. Tamaru, Y.; Kimura, M. Reactions of Acylpalladium Derivatives with Organometals and Related Carbon Nucleophiles. In *Handbook for Organopalladium Chemistry for Organic Synthesis*; Negishi, E.-I., Ed.; Wiley-Interscience: New York, 2002; 2425–2454.
38. Hartwig, J. F. Transition Metal-Catalyzed Coupling Reactions. *Organotransition Metal Chemistry: From Bonding to Catalysis*; University Science Books: Sausalito, CA, 2010; 877–966.
39. Dieter, R. K. *Tetrahedron* **1999**, *55*, 4177–4236.
40. Arisawa, M.; Kuwajima, M.; Toriyama, F.; Li, G. Z.; Yamaguchi, M. *Org. Lett.* **2012**, *14*, 3804–3807.
41. Baillie, R. A.; Holmes, A. S.; Lefèvre, G. P.; Patrick, B. O.; Shree, M. V.; Wakeham, R. J.; Legzdins, P.; Rosenfeld, D. C. *Inorg. Chem.* **2015**, *54*, 5915–5929.

42. Baillie, R. A. The Functionalization of Methane and Other Hydrocarbons Mediated by Organometallic Nitrosyl Complexes of Tungsten. Ph.D. Thesis, The University of British Columbia (Vancouver), February 2016.
43. Bau, R.; Mason, S. A.; Patrick, B. O.; Adams, C. S.; Sharp, W. B.; Legzdins, P. *Organometallics* **2001**, *20*, 4492–4501.
44. Tsang, J. Y. K.; Buschhaus, M. S. A.; Legzdins, P.; Patrick, B. O. *Organometallics* **2006**, *25*, 4215–4225.
45. Baillie, R. A.; Tran, T.; Thibault, M. E.; Legzdins, P. *J. Am. Chem. Soc.* **2010**, *132*, 15160–15161.
46. Baillie, R. A.; Lefèvre, G. P.; Wakeham, R. J.; Holmes, A. S.; Legzdins, P. *Organometallics* **2015**, *34*, 4085–4092.
47. Wakeham, R. J.; Baillie, R. A.; Patrick, B. O.; Legzdins, P.; Rosenfeld, D. C. *Organometallics* **2017**, *36*, 39–52.
48. Baillie, R. A.; Patrick, B. O.; Legzdins, P.; Rosenfeld, D. C. *Organometallics* **2017**, *36*, 26–38.
49. Pamplin, C. B.; Legzdins, P. *Acc. Chem. Res.* **2003**, *36*, 223–233.
50. Miyoshi, T.; Miyakawa, T.; Ueda, M.; Miyata, O. *Angew. Chem., Int. Ed.* **2011**, *50*, 928–931.
51. Li, L. Z.; Cai, P. J.; Guo, Q. X.; Xue, S. *J. Org. Chem.* **2008**, *73*, 3516–3522.
52. Hartwig, J. F. Dative Phosphorus Ligands and Heavier Congeners. *Organotransition Metal Chemistry: From Bonding to Catalysis*; University Science Books: Sausalito, CA, 2010; 33–41.

53. van Leeuwen, P.; Kamer, P. C. J.; Claver, C.; Pamies, O.; Dieguez, M. *Chem. Rev.* **2011**, *111*, 2077–2118.
54. Fernandez-Perez, H.; Etayo, P.; Panossian, A.; Vidal-Ferran, A. *Chem. Rev.* **2011**, *111*, 2119–2176.
55. Legzdins, P.; Martin, J. T.; Einstein, F. W. B.; Jones, R. H. *Organometallics* **1987**, *6*, 1826–1827.
56. Lee, K.; Legzdins, P.; Pamplin, C. B.; Patrick, B. O.; Wada, K. *Organometallics* **2005**, *24*, 638–649.
57. Debad, J. D.; Legzdins, P.; Lumb, S. A.; Batchelor, R. J.; Einstein, F. W. B. *Organometallics* **1995**, *14*, 2543–2555.
58. Burkey, D. J.; Debad, J. D.; Legzdins, P. *J. Am. Chem. Soc.* **1997**, *119*, 1139–1140.
59. Blackmore, I. J.; Semiao, C. J.; Buschhaus, M. S. A.; Patrick, B. O.; Legzdins, P. *Organometallics* **2007**, *26*, 4881–4889.
60. Fabulyak, D.; Handford, R. C.; Holmes, A. S.; Levesque, T. M.; Wakeham, R. J.; Patrick, B. O.; Legzdins, P.; Rosenfeld, D. C. *Inorg. Chem.* **2017**, *56*, 573–582.
61. Tran, E.; Legzdins, P. *J. Am. Chem. Soc.* **1997**, *119*, 5071–5072.
62. Rahman, M. M.; Liu, H. Y.; Eriks, K.; Prock, A.; Giering, W. P. *Organometallics* **1989**, *8*, 1–7.
63. Gloaguen, Y.; Jongens, L. M.; Reek, J. N. H.; Lutz, M.; de Bruin, B.; van der Vlugt, J. I. *Organometallics* **2013**, *32*, 4284–4291.
64. Penno, D.; Estevan, F.; Fernandez, E.; Hirva, P.; Lahuerta, P.; Sanau, M.; Ubeda, M. A. *Organometallics* **2011**, *30*, 2083–2094.
65. Johnson, K. R. D.; Hayes, P. G. *Organometallics* **2011**, *30*, 58–67.

66. Bottcher, H. C.; Junk, M.; Mayer, P.; Beck, W. *Eur. J. Inorg. Chem.* **2015**, No. 20, 3323–3327.
67. Debad, J. D.; Legzdins, P.; Rettig, S. J.; Veltheer, J. E. *Organometallics* **1993**, *12*, 2714–2725.
68. Tolman, C. A. *Chem. Rev.* **1977**, *77*, 313–348.
69. Darensbourg, D. J.; Andreatta, J. R.; Stranahan, S. M.; Reibenspies, J. H. *Organometallics* **2007**, *26*, 6832–6838.
70. Fabulyak, D.; Baillie, R. A.; Patrick, B. O.; Legzdins, P.; Rosenfeld, D. C. *Inorg. Chem.* **2016**, *55*, 1883–1893.
71. SHELXT: Sheldrick, G. M. *Acta Cryst.* **2015**, *71*, 3–8.
72. Cromer, D. T.; Waber, J. T. *International Tables for X-ray Crystallography*; The Kynoch Press: Birmingham, England, 1974; Vol. IV, Table 2.2A.
73. Ibers, J. A.; Hamilton, W. C. *Acta Crystallogr.* **1964**, *17*, 781–782.
74. Creagh, D. C.; McAuley, W. J. *International Tables for Crystallography*; Wilson, A. J. C., Ed.; Kluwer Academic Publishers: Boston, 1992; Vol. C, Table 4.2.6.8.
75. Creagh, D. C.; Hubbell, J. H. *International Tables for Crystallography*; Wilson, A. J. C., Ed.; Kluwer Academic Publishers: Boston, 1992; Vol C, Table 4.2.4.3.
76. SHELXL–2014: Sheldrick, G. M. *Acta Cryst.* **2015**, *71*, 3–8.
77. OLEX2–V1.2.7: Dolomanov, O. V.; Bourhis, L. J.; Gildea, R. J.; Howard, J. A. K.; Puschmann, H. *J. Appl. Cryst.* **2009**, *42*, 339–341.
78. Cho, J. Y.; Tse, M. K.; Holmes, D.; Maleczka, R. E.; Smith, M. R. *Science* **2002**, *295*, 305–308.

79. Molander, G. A.; Cavalcanti, L. N.; García-García, C. *J. Org. Chem.* **2013**, *78*, 6427–6439.
80. Percec, V.; Golding, G. M.; Smidrkal, J.; Weichold, O. *J. Org. Chem.* **2004**, *69*, 3447–3452.
81. Lu, Y.; Plocher, E.; Hu, Q. S. *Adv. Synth. Catal.* **2006**, *348*, 841–845.
82. Shang, R.; Ilies, L.; Asako, S.; Nakamura, E. *J. Am. Chem. Soc.* **2014**, *136*, 14349–14352.
83. Hamann, B. C.; Hartwig, J. F. *J. Am. Chem. Soc.* **1998**, *120*, 3694–3703.
84. Hamann, B. C.; Hartwig, J. F. *J. Am. Chem. Soc.* **1998**, *120*, 12706–12706.
85. Ogasawara, M.; Yoshida, K.; Hayashi, T. *Organometallics* **2000**, *19*, 1567–1571.
86. Klingensmith, L. M.; Strieter, E. R.; Barder, T. E.; Buchwald, S. L. *Organometallics* **2006**, *25*, 82–91.
87. Cabri, W.; Candiani, I.; Bedeschi, A.; Santi, R. *J. Org. Chem.* **1992**, *57*, 3558–3563.
88. Oyamada, J.; Kitamura, T. *Chem. Commun.* **2008**, No. 40, 4992–4994.
89. McConville, M.; Saidi, O.; Blacker, J.; Xiao, J. L. *J. Org. Chem.* **2009**, *74*, 2692–2698.
90. Feng, Z.; Min, Q. Q.; Zhao, H. Y.; Gu, J. W.; Zhang, X. G. *Angew. Chem., Int. Ed.* **2015**, *54*, 1270–1274.
91. Handford, R. C.; Wakeham, R. J.; Patrick, B. O.; Legzdins, P. *Inorg. Chem.* **2017**, *56*, 3612–3622.
92. Handford, R. C.; Legzdins, P. Unpublished observations.
93. Stiefel, E. I., Transition metal sulfur chemistry: Biological and industrial significance and key trends. In *Transition Metal Sulfur Chemistry*; ACS Symposium Series, Vol. 653; American Chemical Society: Washington, DC, 1996, 2–38.

94. Ji, Y. N.; Plata, R. E.; Regens, C. S.; Hay, M.; Schmidt, M.; Razler, T.; Qiu, Y. P.; Geng, P.; Hsiao, Y.; Rosner, T.; Eastgate, M. D.; Blackmond, D. G. *J. Am. Chem. Soc.* **2015**, *137*, 13272–13281.
95. Holmes, A. S.; Legzdins, P. Unpublished observations.
96. Drew, M. G. B.; Mitchell, P. C. H.; Pygall, C. F. *Angew. Chem., Int. Ed. Engl.* **1976**, *15*, 784–785.
97. Mealli, C.; Midollini, S.; Sacconi, L. *Inorg. Chem.* **1978**, *17*, 632–637.
98. Greenhough, T. J.; Kolthammer, B. W. S.; Legzdins, P.; Trotter, J. *Inorg. Chem.* **1979**, *18*, 3543–3548.
99. Vahrenkamp, H. *Angew. Chem., Int. Ed. Engl.* **1975**, *14*, 322–329.
100. Wachter, J. *Angew. Chem., Int. Ed. Engl.* **1989**, *28*, 1613–1626.
101. Huneke, J. T.; Enemark, J. H. *Inorg. Chem.* **1978**, *17*, 3698–3699.
102. Kawaguchi, H.; Yamada, K.; Lang, J. P.; Tatsumi, K. *J. Am. Chem. Soc.* **1997**, *119*, 10346–10358.
103. Ito, J. I.; Ohki, Y.; Iwata, M.; Tatsumi, K. *Inorg. Chem.* **2008**, *47*, 3763–3771.
104. Adams, H.; Bancroft, M. N.; Morris, M. J.; Riddiough, A. E. *Inorg. Chem.* **2009**, *48*, 9557–9566.
105. Lewis, J. *Pure Appl. Chem.* **1965**, *10*, 11–36.
106. Allen, F. H.; Kennard, O.; Watson, D. G.; Brammer, L.; Orpen, A. G.; Taylor, R. *J. Chem. Soc., Perkin Trans. 2*, **1987**, S1–S19.
107. Boezio, A. A.; Pytkowicz, J.; Cote, A.; Charette, A. B. *J. Am. Chem. Soc.* **2003**, *125*, 14260–14261.
108. Cote, A.; Lindsay, V. N. G.; Charette, A. B. *Org. Lett.* **2007**, *9*, 85–87.

109. Desrosiers, J. N.; Charette, A. B. *Angew. Chem., Int. Ed.* **2007**, *46*, 5955–5957.
110. Carrow, B. P.; Nozaki, K. *J. Am. Chem. Soc.* **2012**, *134*, 8802–8805.
111. Wu, C. L.; Zhou, J. R. *J. Am. Chem. Soc.* **2014**, *136*, 650–652.
112. Muller, A.; Jaegermann, W.; Enemark, J. H. *Coord. Chem. Rev.* **1982**, *46*, 245–280.
113. Steudel, R. *Angew. Chem., Int. Ed. Engl.* **1975**, *14*, 655–664.
114. Kutney, G. W.; Turnbull, K. *Chem. Rev.* **1982**, *82*, 333–357.
115. Kochi, J. K.; Powers, J. W. *J. Am. Chem. Soc.* **1970**, *92*, 137–146.
116. Dykerman, B. A.; Smith, J. J.; McCarvill, E. M.; Gallant, A. J.; Doiron, N. D.; Wagner, B. D.; Jenkins, H. A.; Patrick, B. O.; Smith, K. M. *J. Organomet. Chem.* **2007**, *692*, 3183–3190.
117. Poli, R. *Angew. Chem., Int. Ed.* **2006**, *45*, 5058–5070.
118. Wessjohann, L. A.; Schmidt, G.; Schrekker, H. S. *Tetrahedron* **2008**, *64*, 2134–2142.
119. Zhou, W.; MacLeod, K. C.; Patrick, B. O.; Smith, K. M. *Organometallics* **2012**, *31*, 7324–7327.
120. Kraatz, H. B.; van der Boom, M. E.; Ben-David, Y.; Milstein, D. *Isr. J. Chem* **2001**, *41*, 163–171.
121. Schwartsburd, L.; Cohen, R.; Konstantinovski, L.; Milstein, D. *Angew. Chem., Int. Ed.* **2008**, *47*, 3603–3606.
122. Ji, X. X.; Yang, D. W.; Tong, P.; Li, J. Z.; Wang, B. M.; Qu, J. P. *Organometallics* **2017**, *36*, 1515–1521.
123. Pitman, C. L.; Finster, O. N. L.; Miller, A. J. M. *Chem. Commun.* **2016**, *52*, 9105–9108.

124. Quintana, L. M. A.; Johnson, S. I.; Corona, S. L.; Villatoro, W.; Goddard, W. A.; Takase, M. K.; VanderVelde, D. G.; Winkler, J. R.; Gray, H. B.; Blakemore, J. D. *Proc. Natl. Acad. Sci. U.S.A.* **2016**, *113*, 6409–6414.
125. Pedersen, A.; Tilset, M. *Organometallics* **1993**, *12*, 3064–3068.
126. Jones, W. D.; Kuykendall, V. L.; Selmecky, A. D. *Organometallics* **1991**, *10*, 1577–1586.
127. Lewis, J.; Nyholm, R. S. *Sci. Prog. (London)* **1964**, *52*, 557–580
128. Cotton, F. A. *Q. Rev. Chem. Soc.* **1966**, *20*, 389–401
129. Armarego, W. L. F.; Chai, C. C. L., *Purification of Laboratory Chemicals*, 5 ed.; Elsevier: Amsterdam, 2003.
130. SDBSWeb: <http://sdfs.db.aist.go.jp> (National Institute of Advanced Industrial Science and Technology, June 08 2017).
131. He, X. D.; Maisonnat, A.; Dahan, F.; Poilblanc, R. *Organometallics* **1989**, *8*, 2618–2626.
132. Doppiu, A.; Englert, U.; Salzer, A. *Inorg. Chim. Acta* **2003**, *350*, 435–441.
133. Krut'ko, D. P.; Borzov, M. V.; Veksler, E. N.; Churakov, A. V.; Kuz'mina, L. G. *J. Organomet. Chem.* **2005**, *690*, 4036–4048.
134. Becker, E.; Mereiter, K.; Puchberger, M.; Schmid, R.; Kirchner, K. *Organometallics* **2003**, *22*, 3164–3170.

Appendices

Appendix A Supplementary Materials for Chapter 2

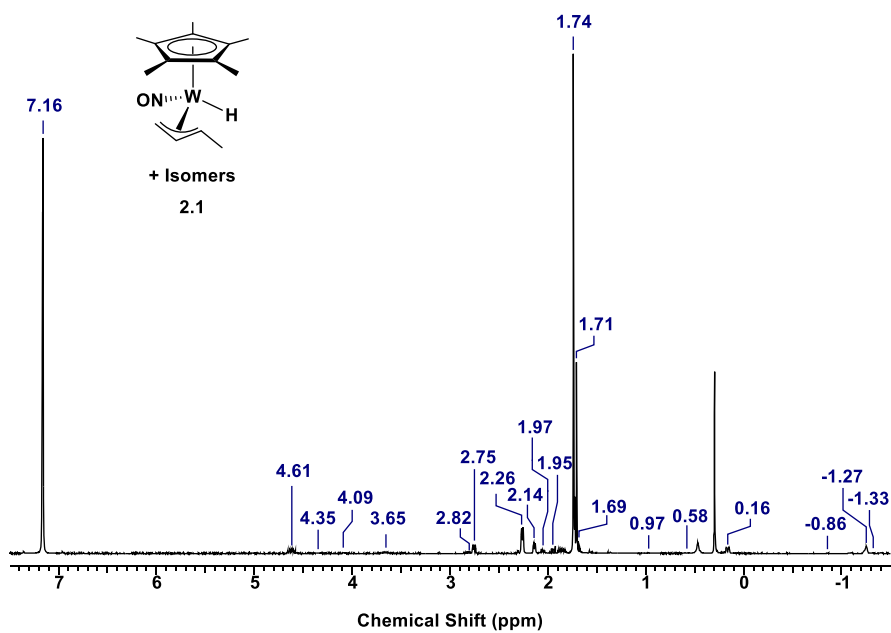


Figure A.1. The ^1H NMR spectrum (400 MHz, C_6D_6) of the isomers of **2.1**.

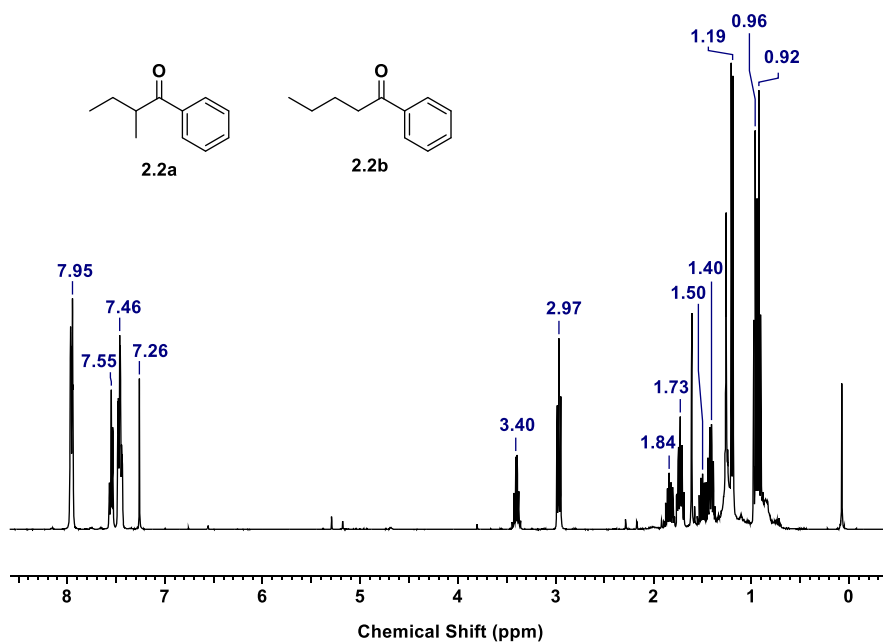


Figure A.2. The ^1H NMR spectrum (400 MHz, CDCl_3) of complexes **2.2a** and **2.2b**.

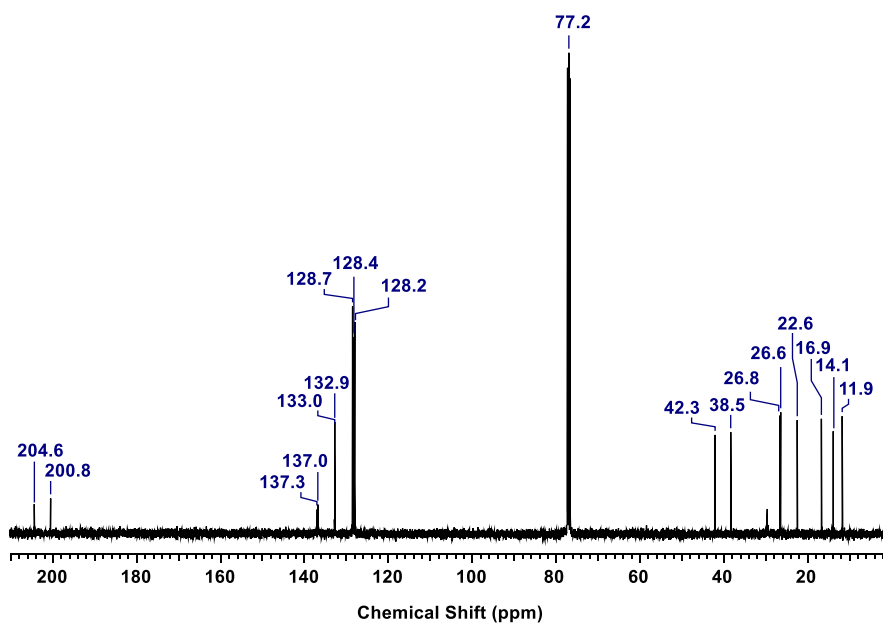


Figure A.3. The $^{13}\text{C}\{^1\text{H}\}$ NMR spectrum (100 MHz, CDCl_3) of complexes **2.2a** and **2.2b**.

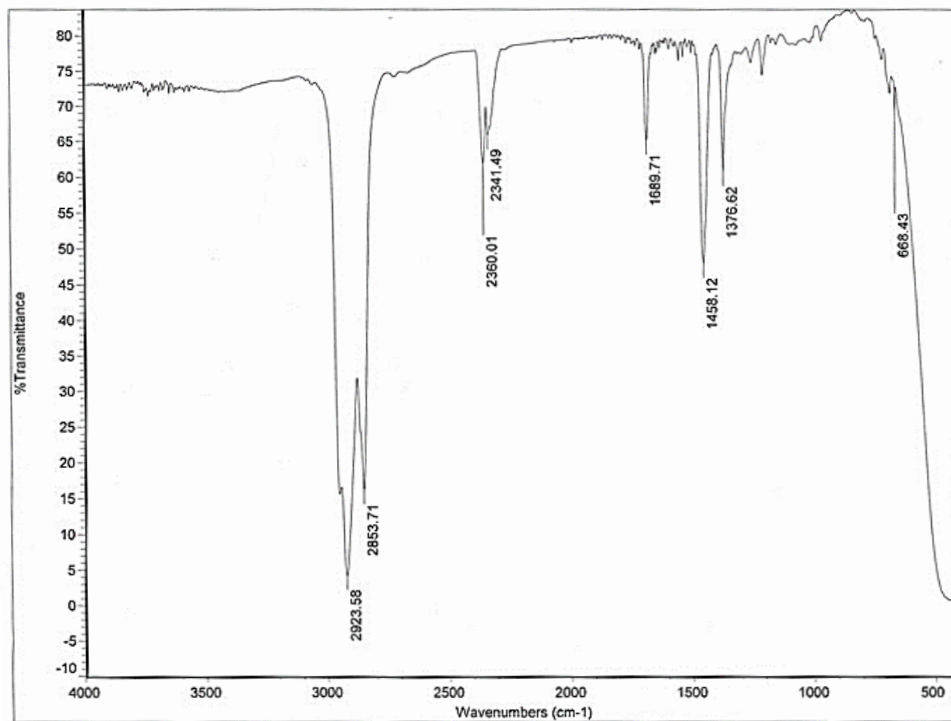


Figure A.4. Nujol mull IR spectrum of complexes **2.2a** and **2.2b**.

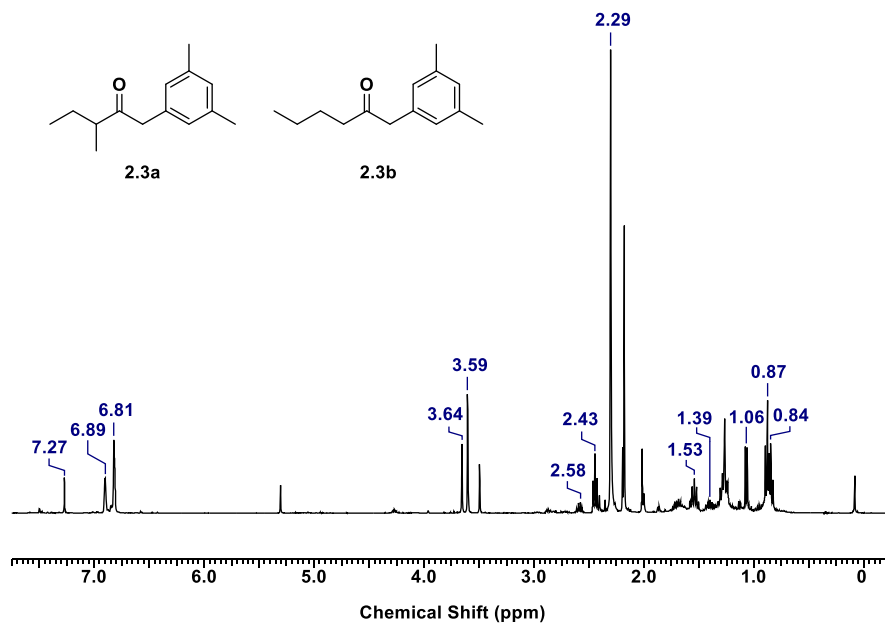


Figure A.5. The ^1H NMR spectrum (400 MHz, CDCl_3) of complexes **2.2a** and **2.3b**.

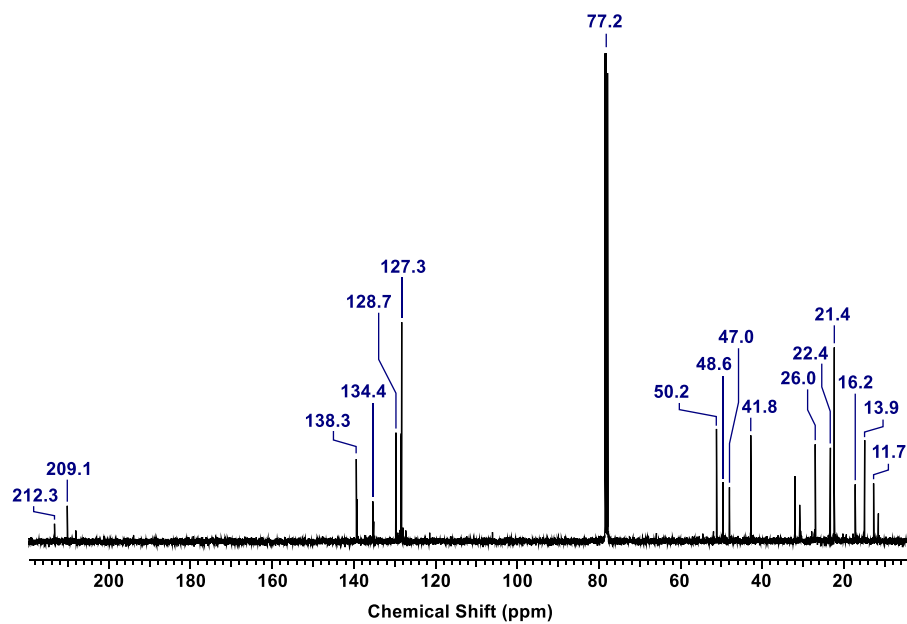


Figure A.6. The $^{13}\text{C}\{^1\text{H}\}$ NMR spectrum (100 MHz, CDCl_3) of complexes **2.3a** and **2.3b**.

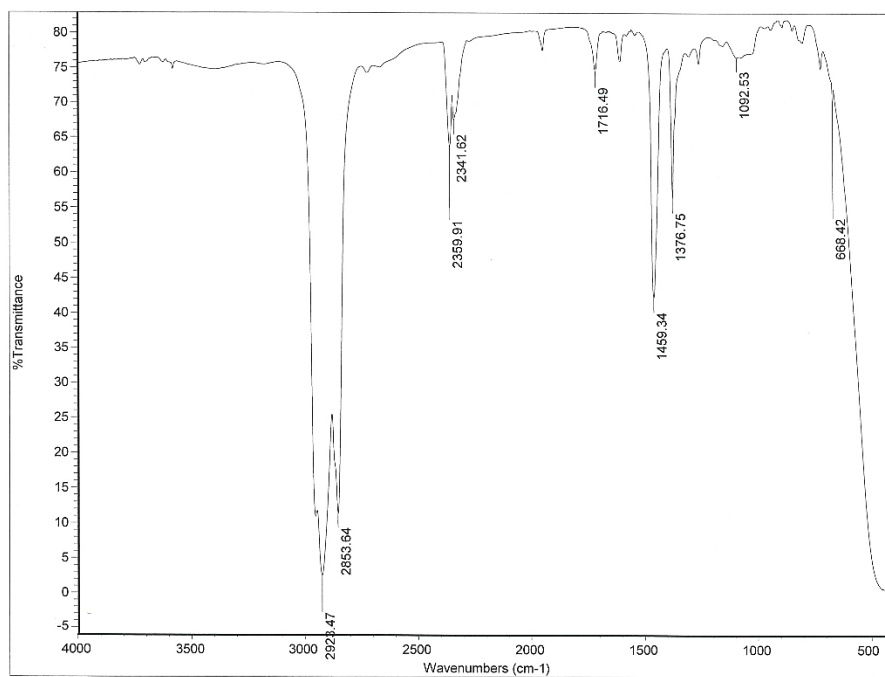


Figure A.7. The Nujol Mull IR spectrum of complexes **2.3a** and **2.3b**.

Appendix B Supplementary Materials for Chapter 3

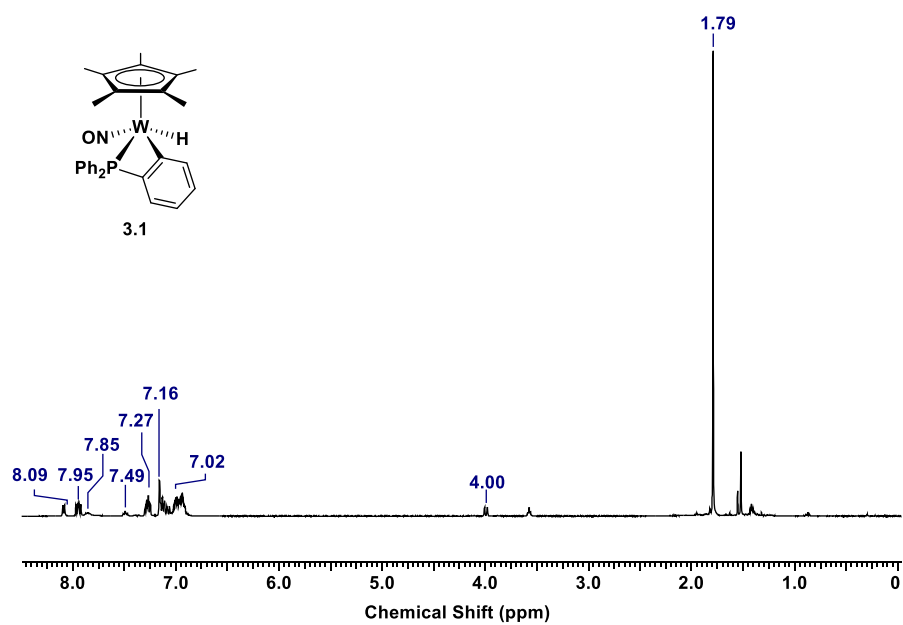


Figure B.1. The ^1H NMR spectrum (400 MHz, C₆D₆) of complex **3.1**.

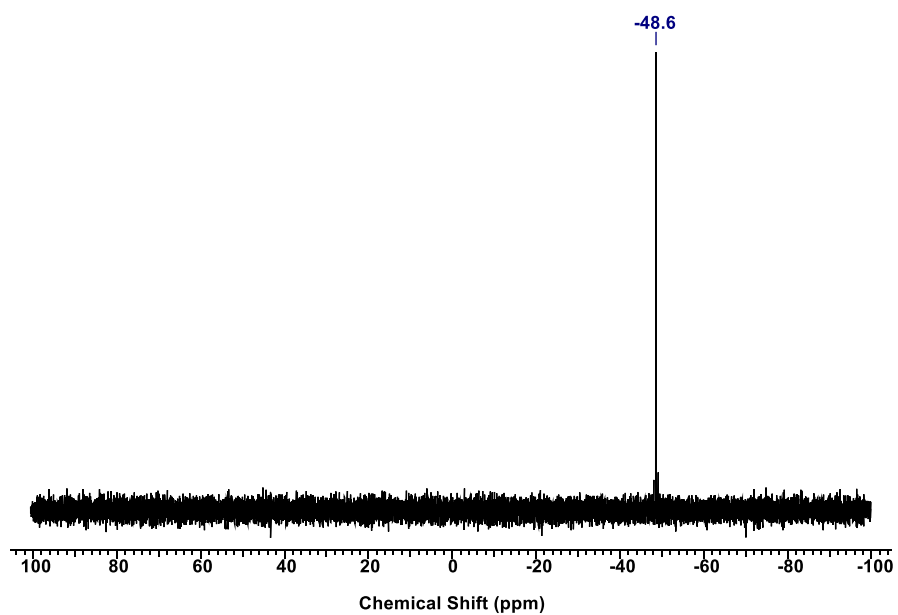


Figure B.2. The $^{31}\text{P}\{^1\text{H}\}$ NMR spectrum (162 MHz, C₆D₆) of complex **3.1**.

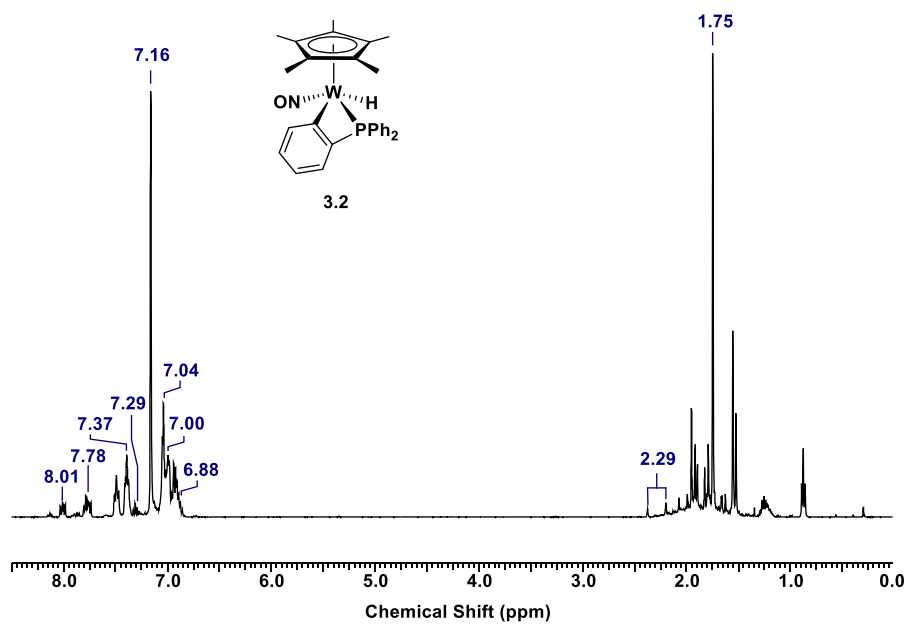


Figure B.3. The ¹H NMR spectrum (400 MHz, C₆D₆) of a crude reaction mixture containing complex 3.2.

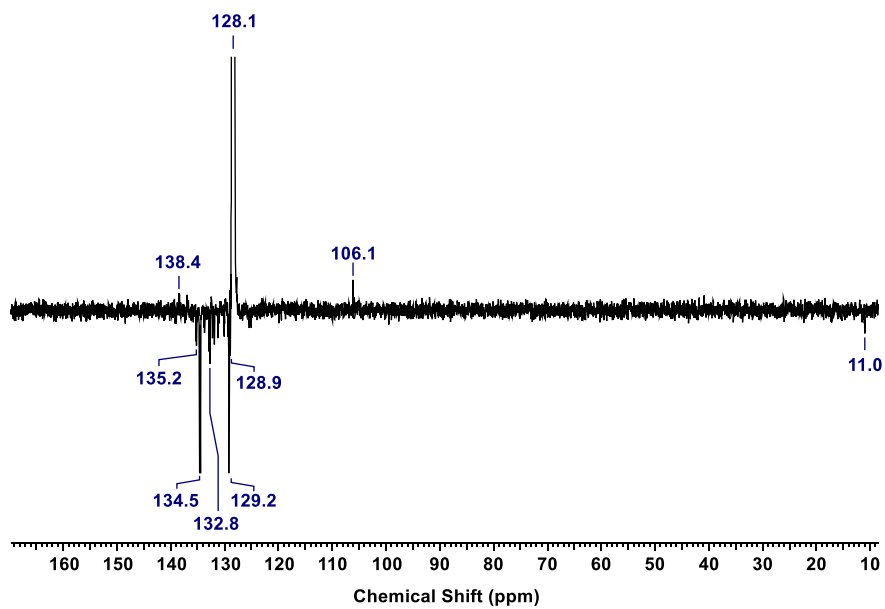


Figure B.4. The ¹³C APT NMR spectrum (100 MHz, C₆D₆) of complex 3.2.

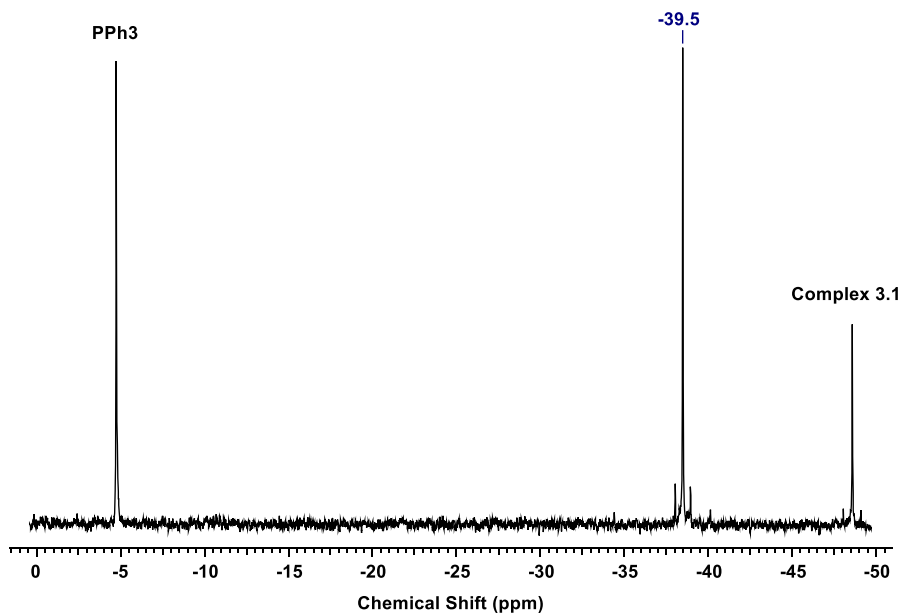


Figure B.5. The $^{31}\text{P}\{^1\text{H}\}$ NMR spectrum (162 MHz, C_6D_6) of complex **3.2**.

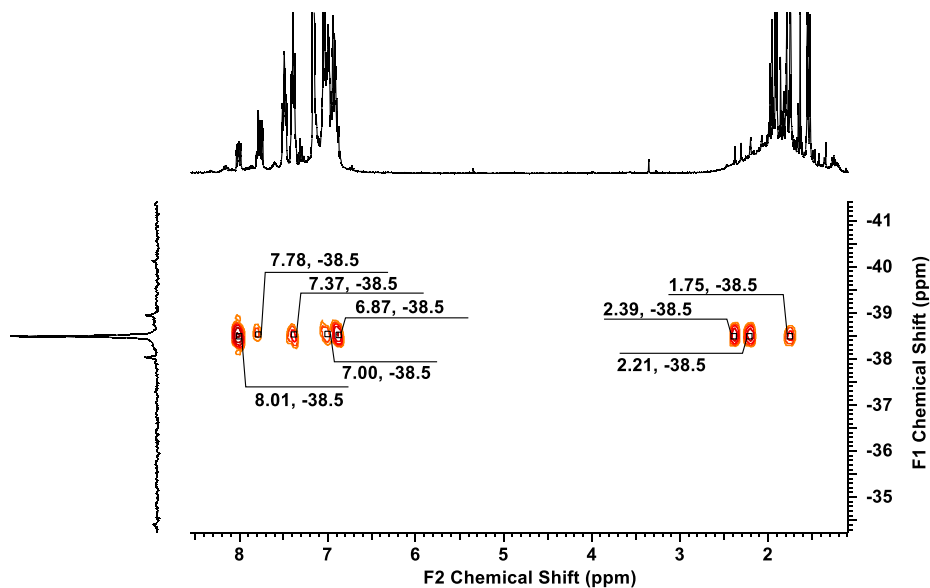


Figure B.6. Expansion of the $\{^1\text{H}-^{31}\text{P}\}$ HMBC NMR spectrum (400 MHz, 162 MHz, C_6D_6) for complex **3.2** from δ 0.00 to 8.57 ppm on the F2 axis and δ -34.2 to -41.5 ppm on the F1 axis.

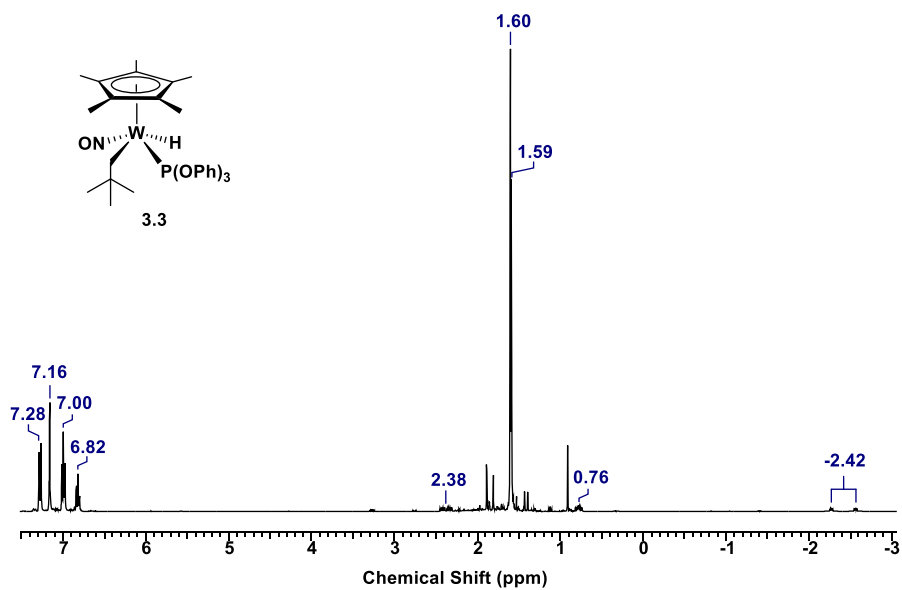


Figure B.7. The ^1H NMR spectrum (400 MHz, C_6D_6) for complex **3.3**.

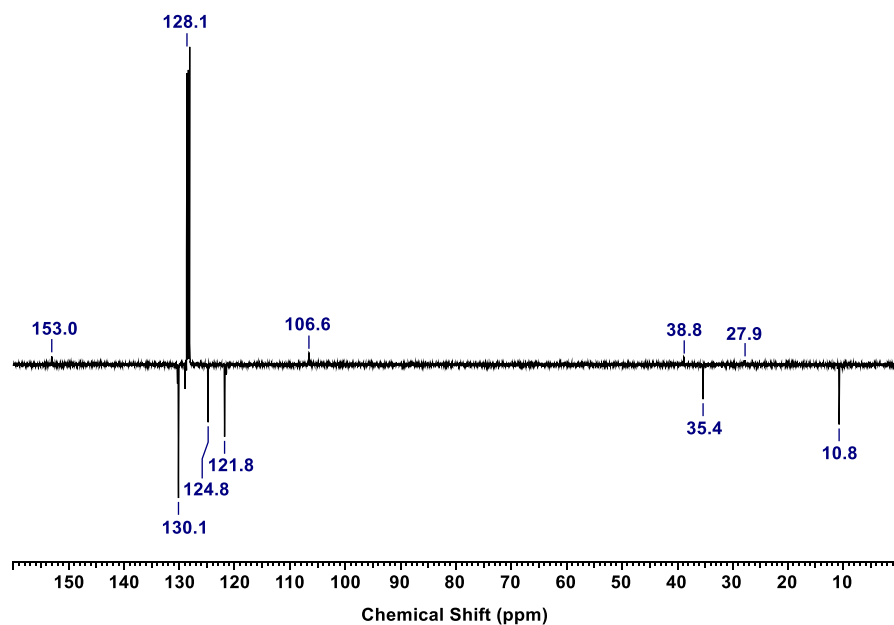


Figure B.8. The ^{13}C APT NMR spectrum (100 MHz, C_6D_6) of complex **3.3**.

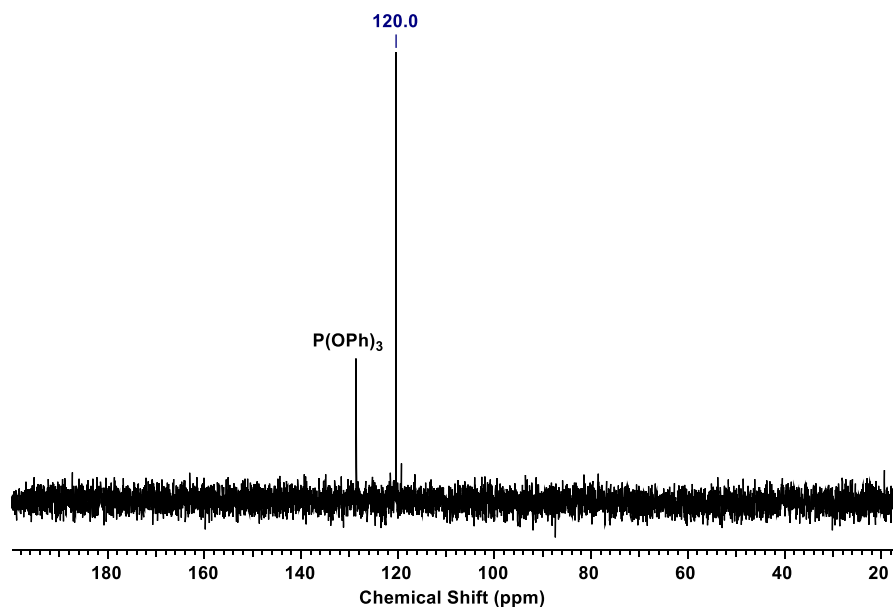


Figure B.9. The $^{31}\text{P}\{^1\text{H}\}$ NMR spectrum (162 MHz, C_6D_6) of complex **3.3**.

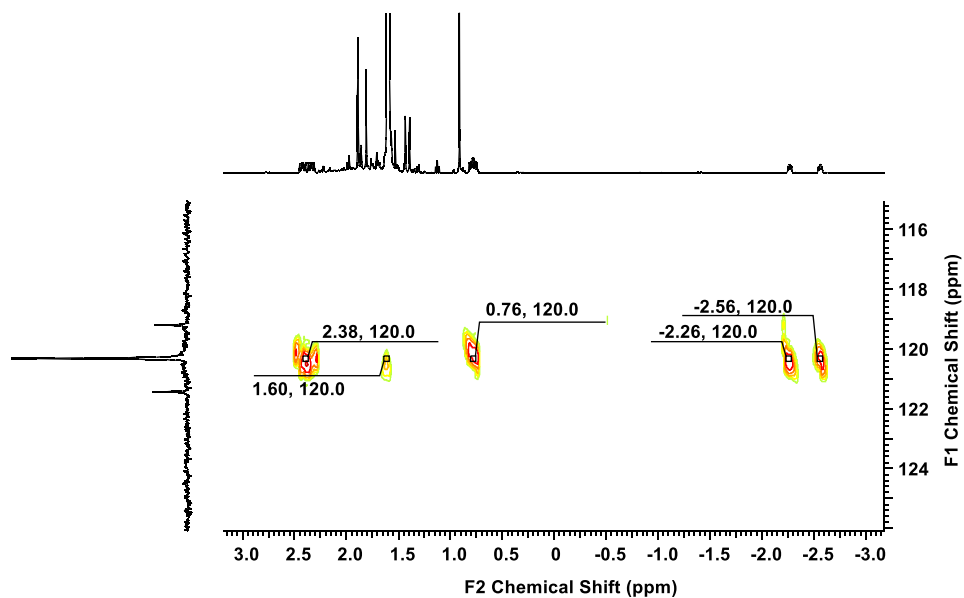


Figure B.10. Expansion of the $\{^1\text{H}-^{31}\text{P}\}$ HMBC NMR spectrum (400 MHz, 162 MHz, C_6D_6) for complex **3.3** from $\delta -3.16$ to 3.17 ppm on the F2 axis and $\delta 115.2$ to 126.0 ppm on the F1 axis.

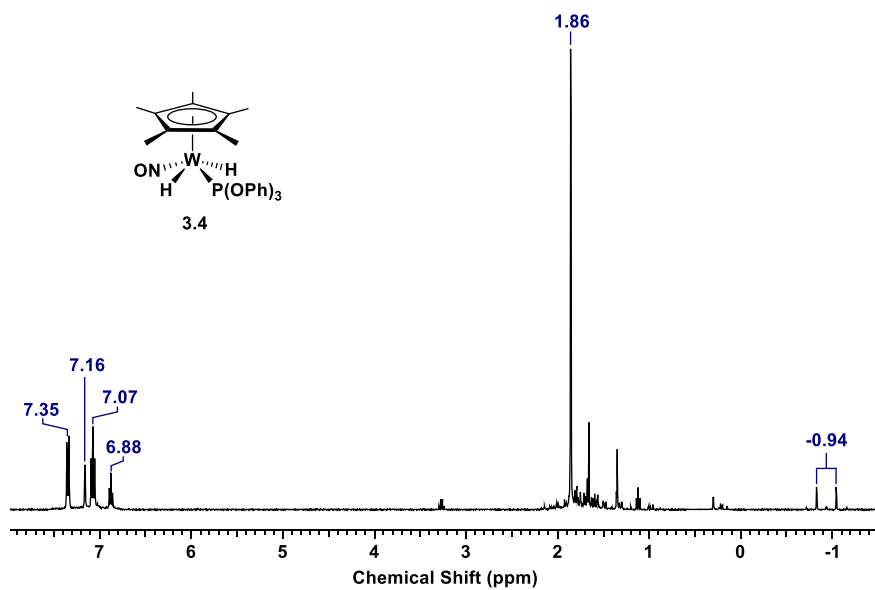


Figure B.11. The ¹H NMR spectrum (400 MHz, C₆D₆) of complex **3.4**.

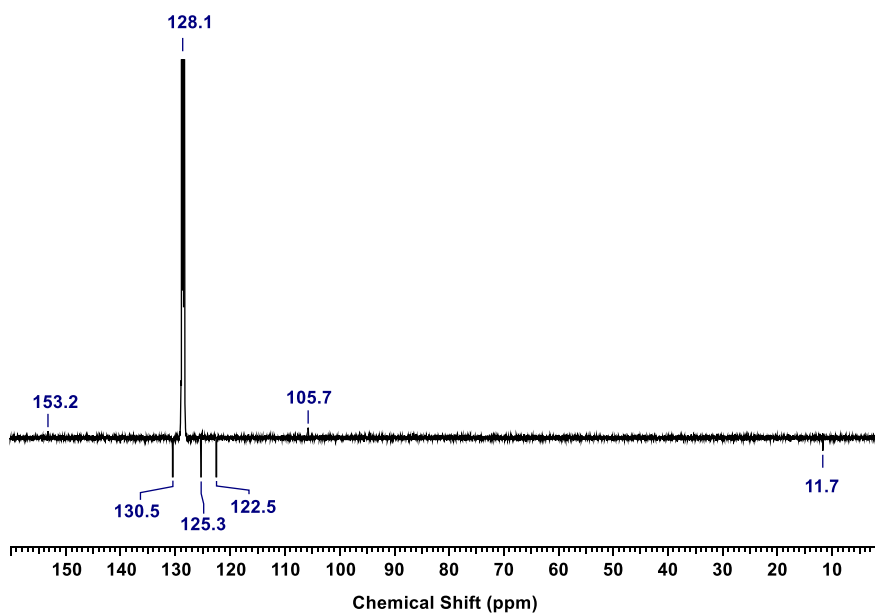


Figure B.12. The ¹³C APT NMR spectrum (100 MHz, C₆D₆) of complex **3.4**.

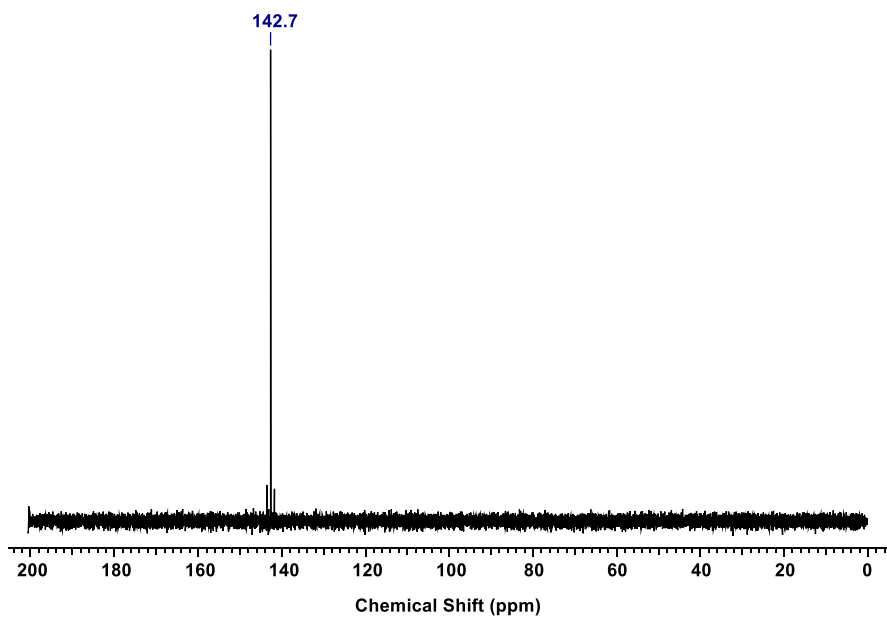


Figure B.13. The $^{31}\text{P}\{^1\text{H}\}$ NMR spectrum (162 MHz, C_6D_6) of complex **3.4**.

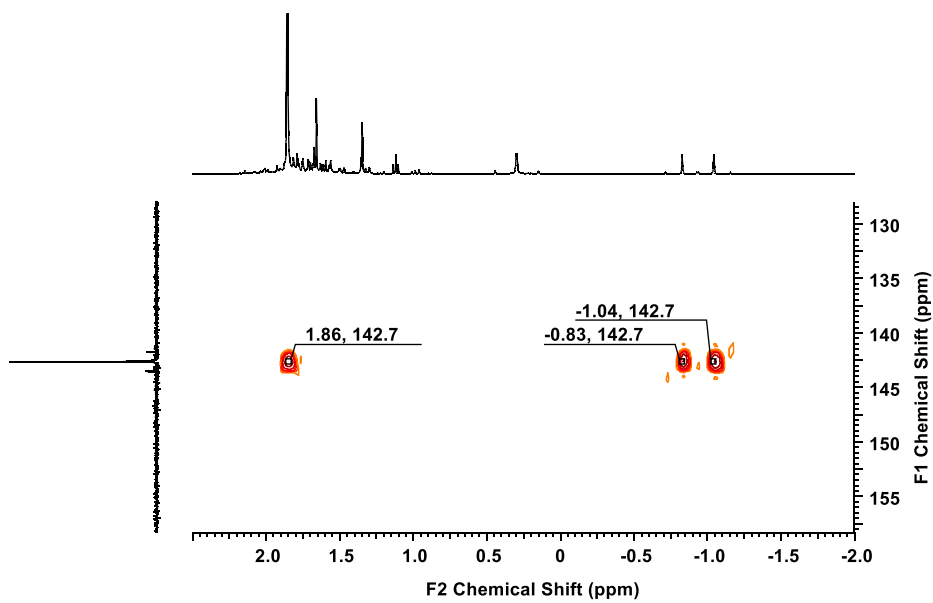


Figure B.14. Expansion of the $\{^1\text{H}-^{31}\text{P}\}$ HMBC NMR spectrum (400 MHz, 162 MHz, C_6D_6) for complex **3.4** from δ -2.00 to 3.00 ppm on the F2 axis and δ 128.0 to 158.3 ppm on the F1 axis.

Appendix C Supplementary Materials for Chapter 4

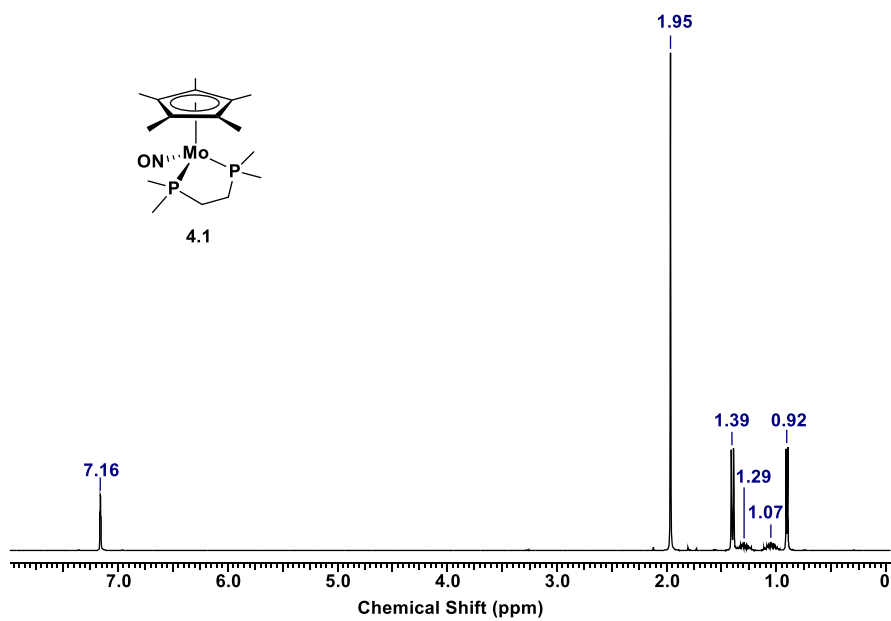


Figure C.1. The ¹H NMR spectrum (400 MHz, C₆D₆) of complex **4.1**.

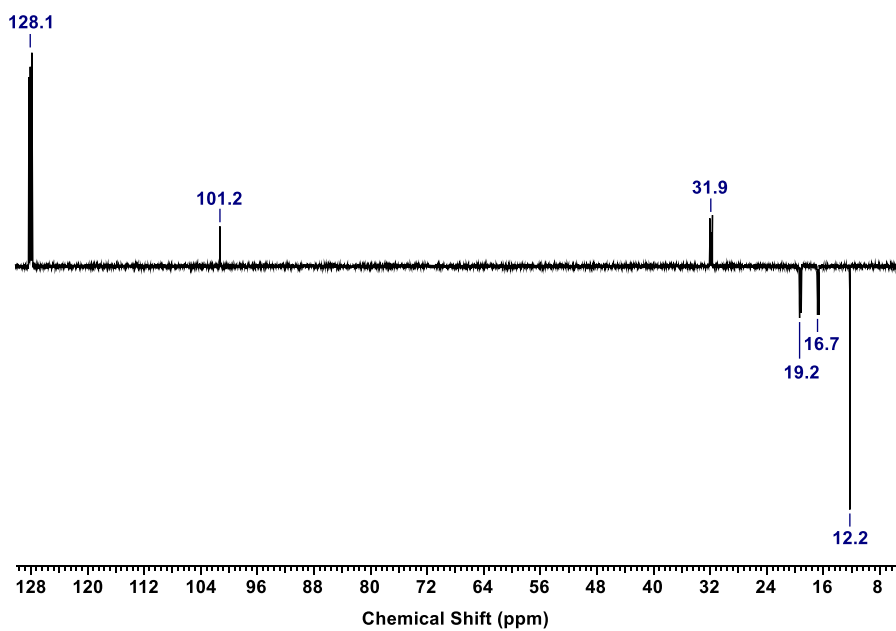


Figure C.2. The ¹³C APT NMR spectrum (100 MHz, C₆D₆) of complex **4.1**.

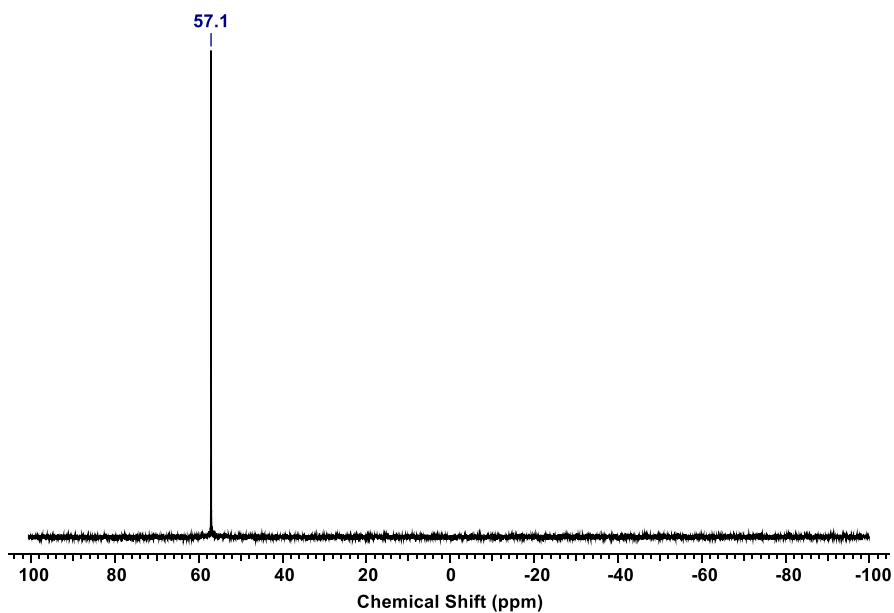


Figure C.3. The $^{31}\text{P}\{^1\text{H}\}$ NMR spectrum (162 MHz, C_6D_6) of complex **4.1**.

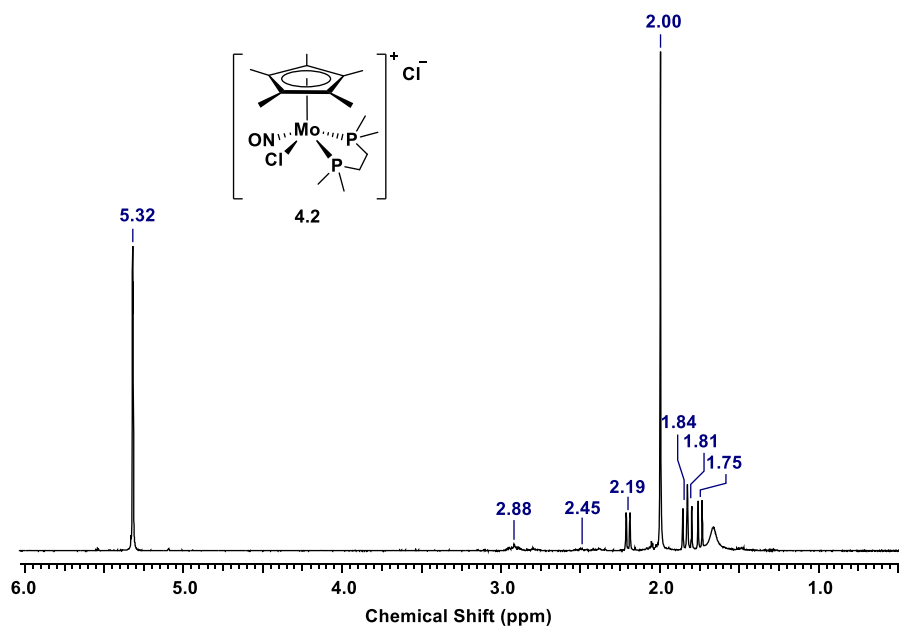


Figure C.4. The ^1H NMR spectrum (400 MHz, CD_2Cl_2) of complex **4.2**.

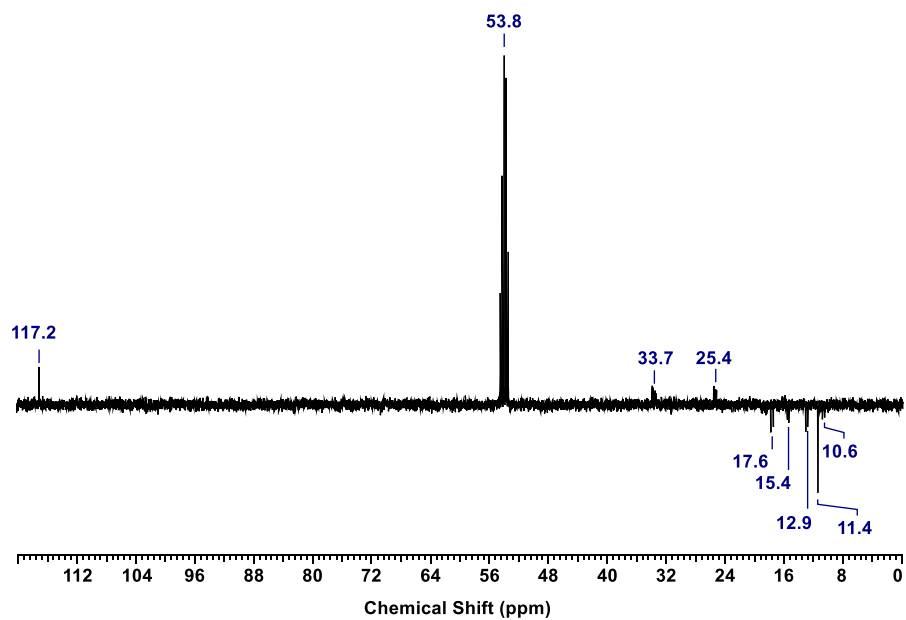


Figure C.5. The ^{13}C APT NMR spectrum (100 MHz, CD_2Cl_2) of complex **4.2**.

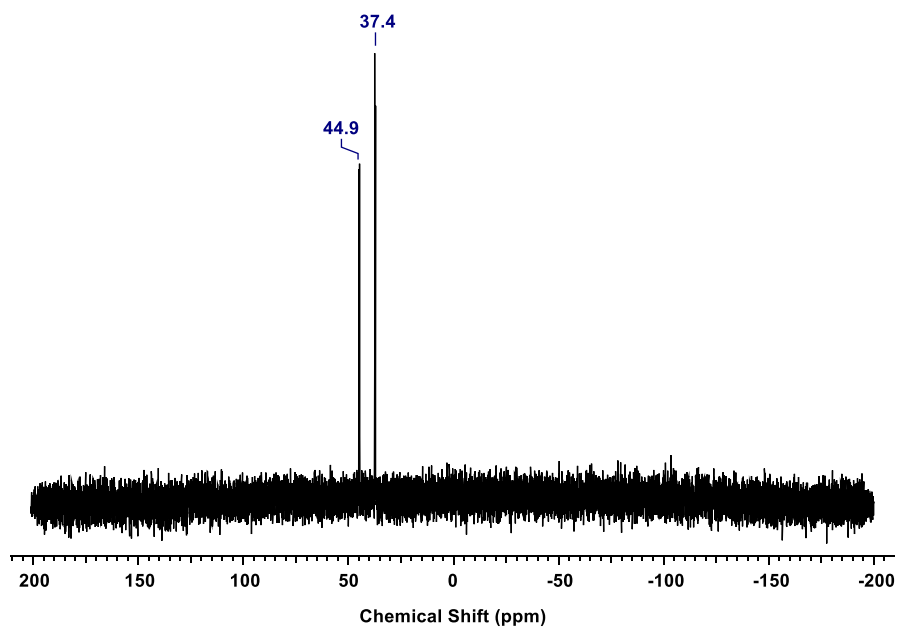


Figure C.6. The $^{31}\text{P}\{^1\text{H}\}$ NMR spectrum (162 MHz, CD_2Cl_2) of complex **4.2**.

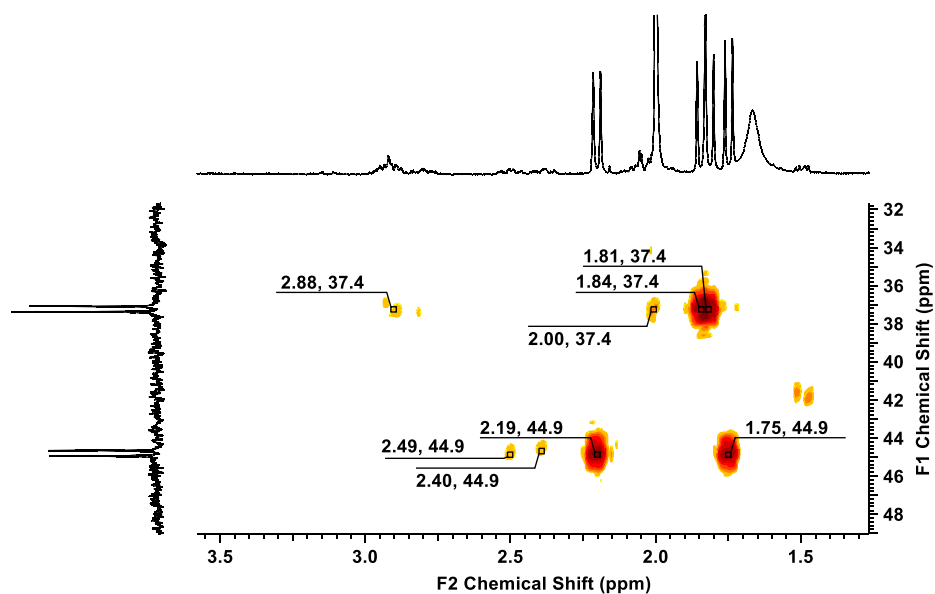


Figure C.7. Expansion of the $\{^1\text{H}-^{31}\text{P}\}$ HMBC NMR spectrum (400 MHz, 162 MHz, C_6D_6) for complex **4.2** from δ 1.27 to 3.58 ppm on the F2 axis and δ 31.8 to 49.0 ppm on the F1 axis.

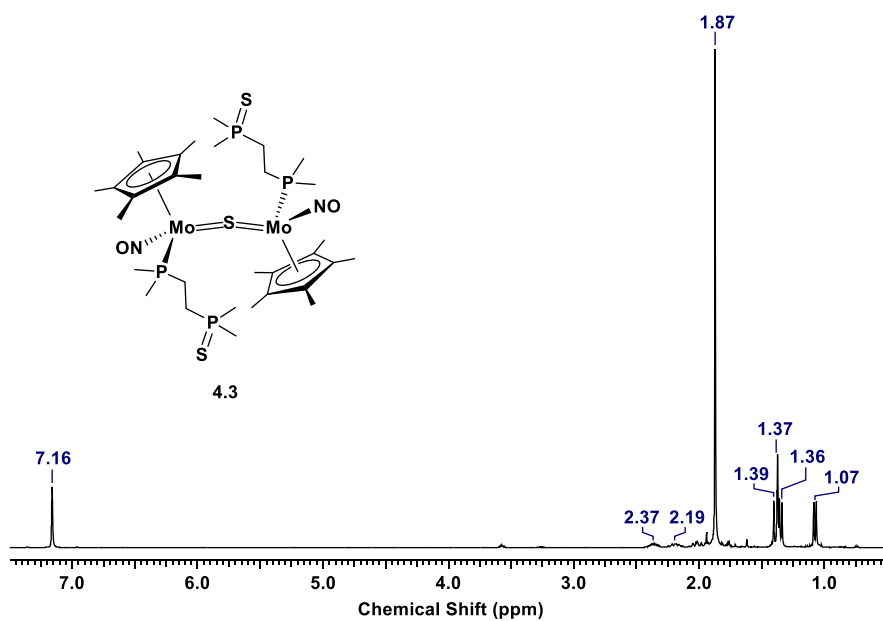


Figure C.8. The ^1H NMR spectrum (400 MHz, C_6D_6) of complex **4.3**.

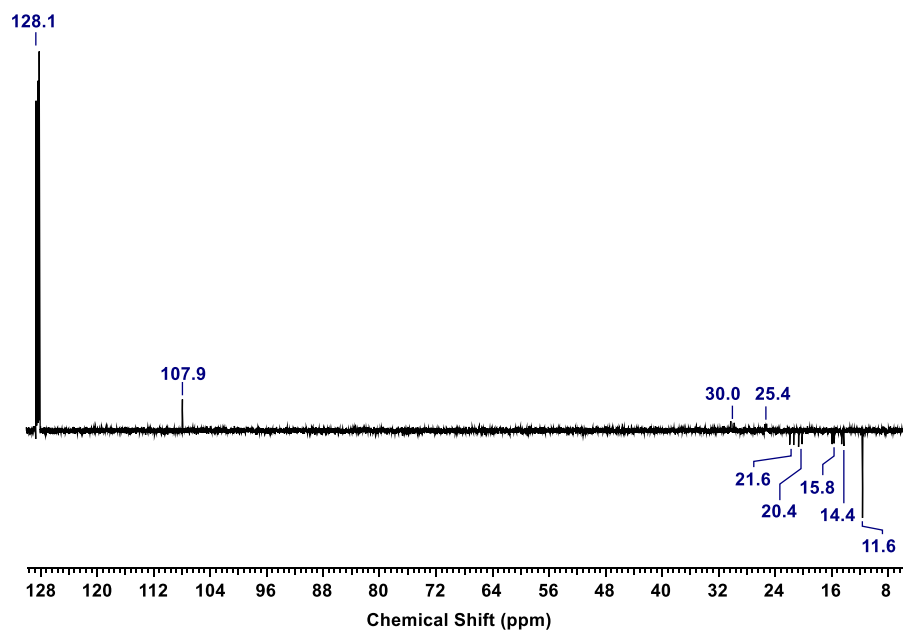


Figure C.9. The ^{13}C APT NMR spectrum (100 MHz, C_6D_6) of complex **4.3**.

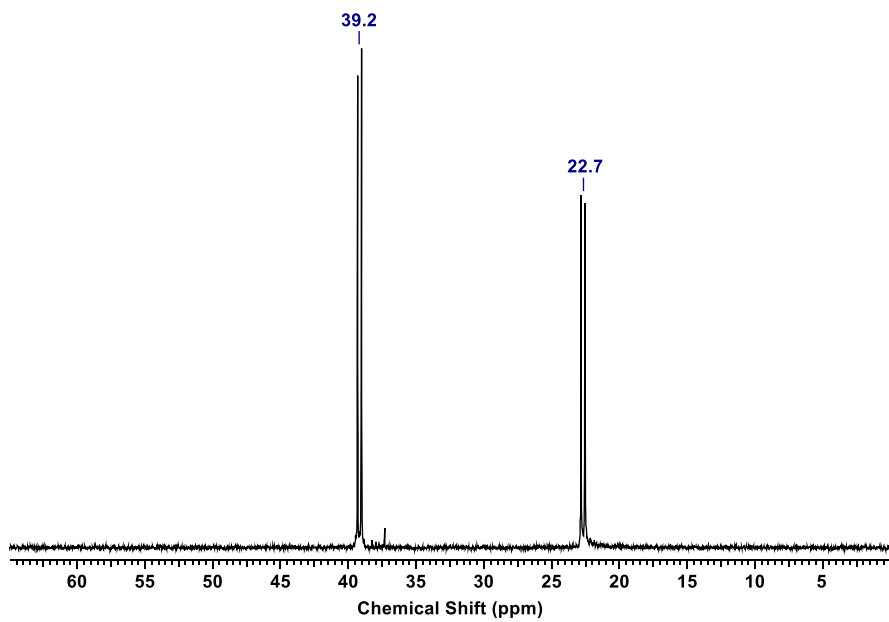


Figure C.10. The $^{31}\text{P}\{^1\text{H}\}$ NMR spectra (162 MHz, C_6D_6) of complex **4.3**.

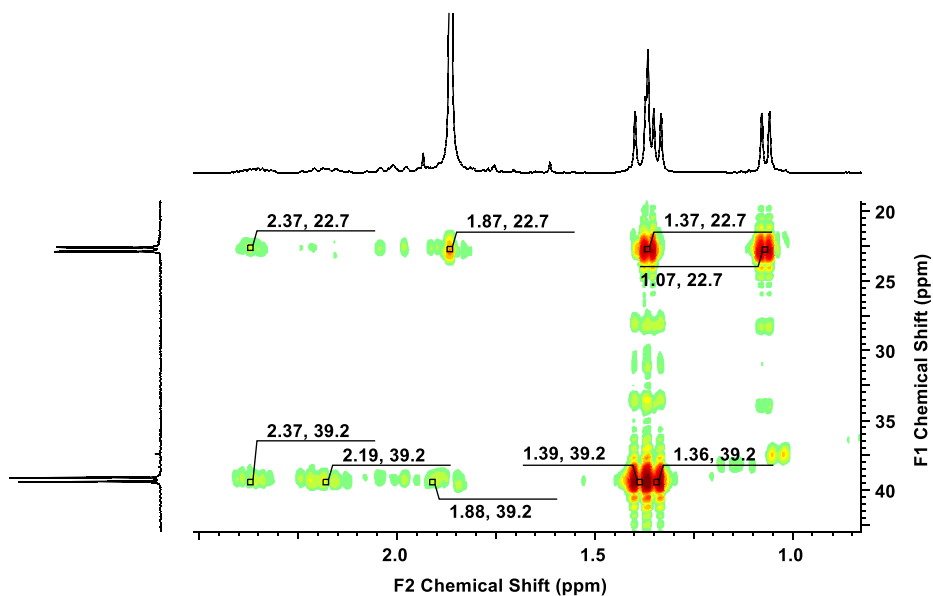


Figure C.11. Expansion of the $\{^1\text{H}-^{31}\text{P}\}$ HMBC NMR spectrum (400 MHz, 162 MHz, C_6D_6) for complex **4.3** from δ 0.83 to 2.51 ppm on the F2 axis and δ 19.5 to 42.5 ppm on the F1 axis.

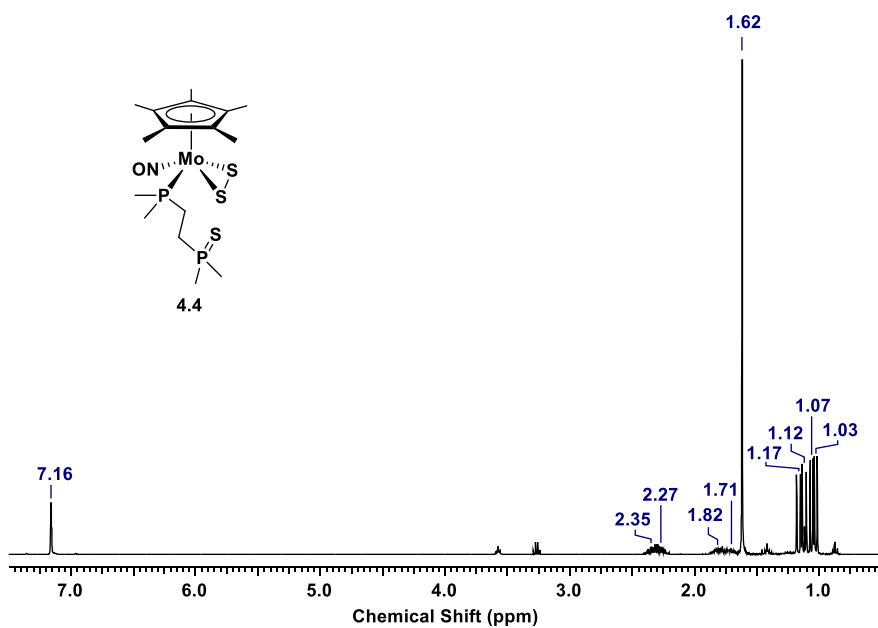


Figure C.12. The ^1H NMR spectrum (400 MHz, C_6D_6) of complex **4.4**.

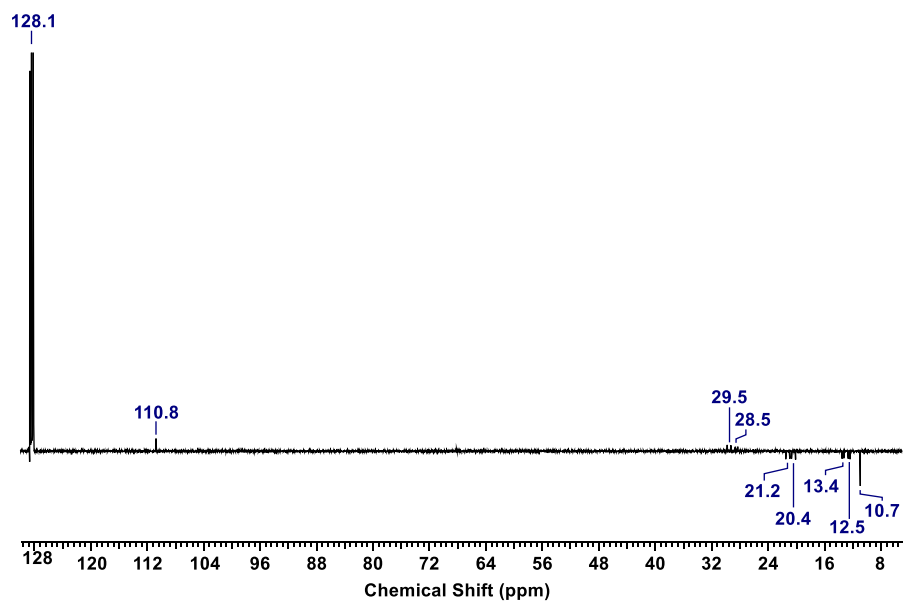


Figure C.13. The ^{13}C APT NMR spectrum (100 MHz, C_6D_6) of complex **4.4**.

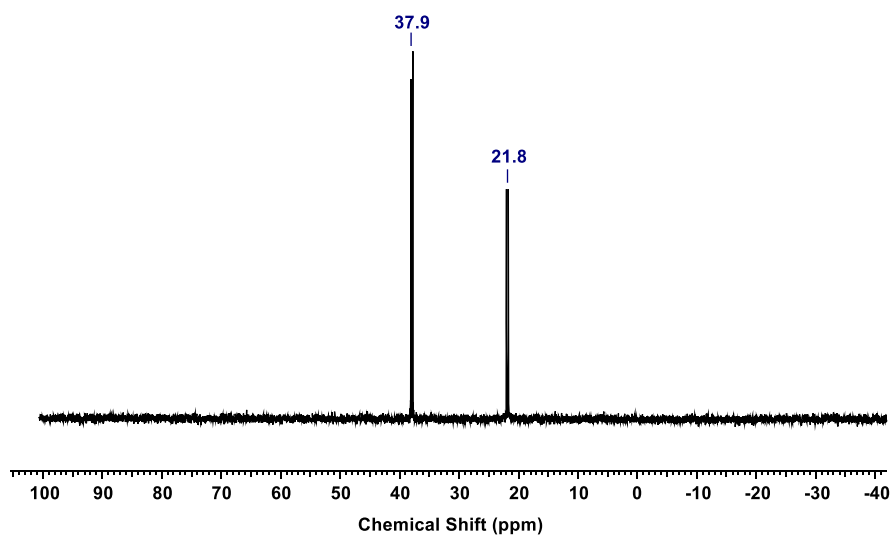


Figure C.14. The $^{31}\text{P}\{^1\text{H}\}$ NMR spectrum (162 MHz, C_6D_6) of complex **4.4**.

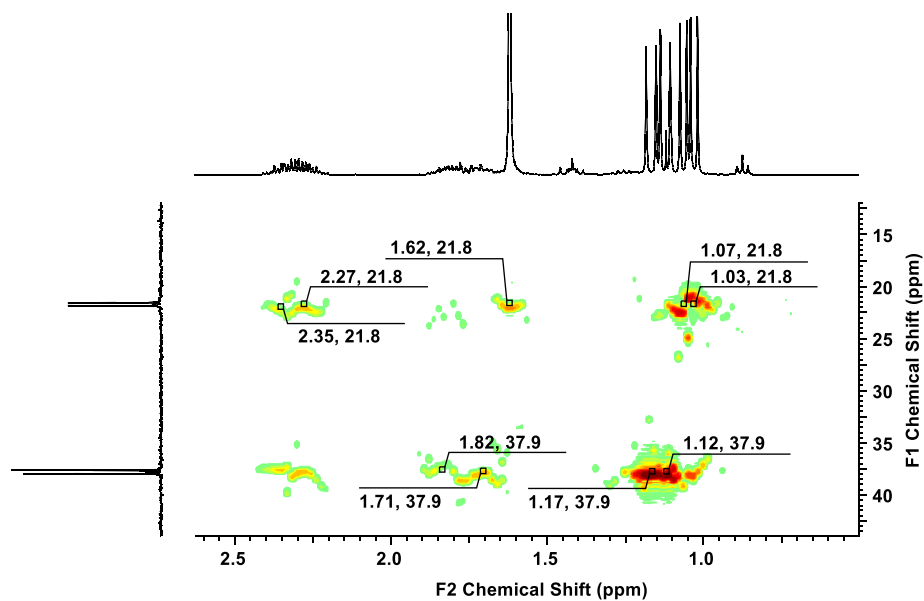


Figure C.15. Expansion of the $\{^1\text{H}-^{31}\text{P}\}$ HMBC NMR spectrum (400 MHz, 162 MHz, C_6D_6) for complex **4.4** from δ 0.50 to 2.63 ppm on the F2 axis and δ 12.0 to 43.6 ppm on the F1 axis.

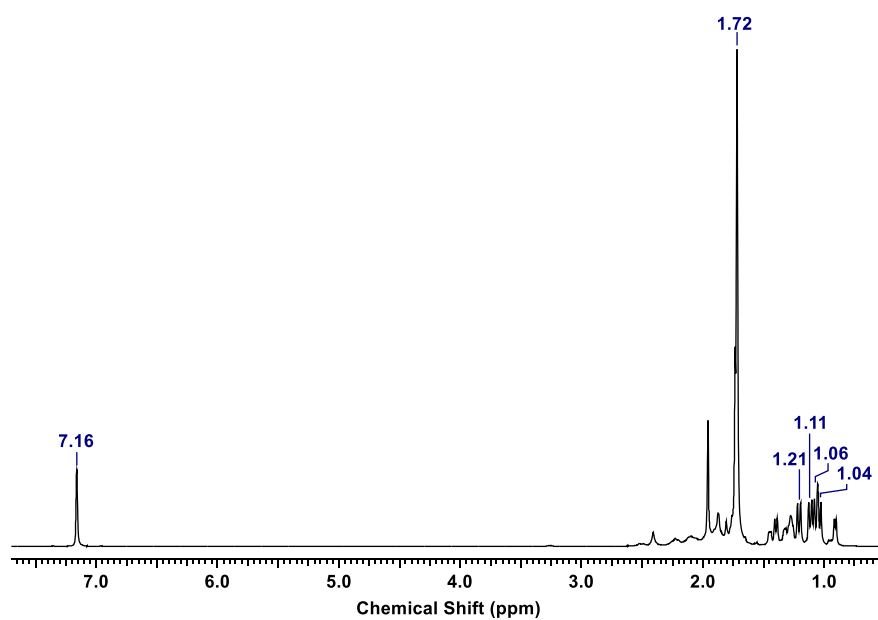


Figure C.16. The ^1H NMR spectrum (400 MHz, C_6D_6) of the reaction mixture of complex **4.1** exposed to oxygen.

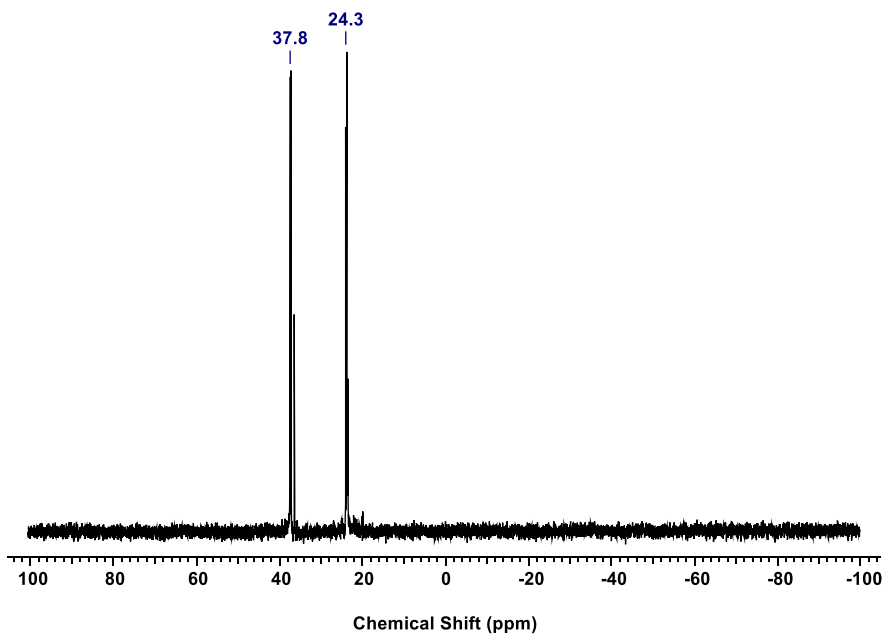


Figure C.17. The $^{31}\text{P}\{^1\text{H}\}$ NMR spectrum (400 MHz, C_6D_6) of the reaction mixture of complex **4.1** after exposure to oxygen.

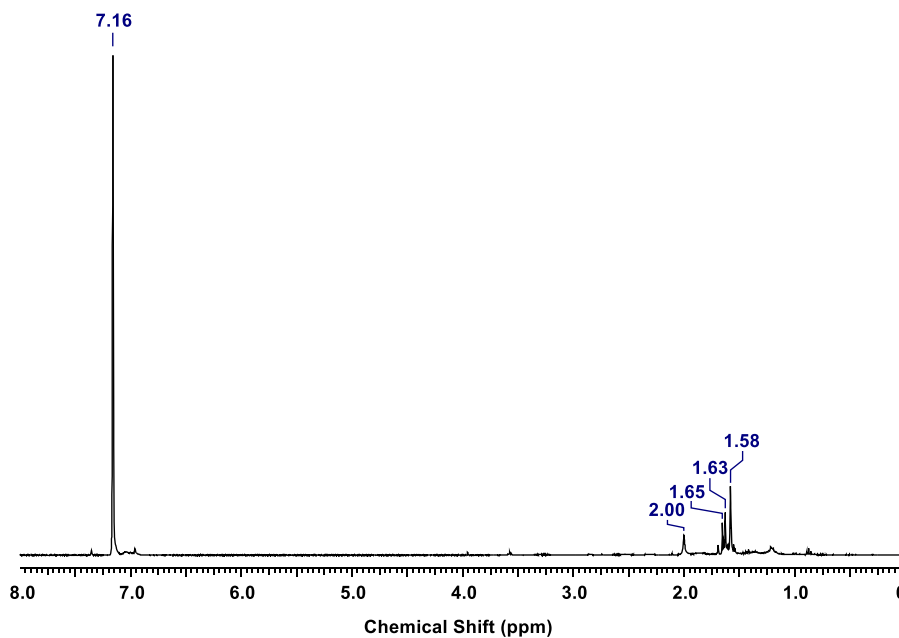


Figure C.18. The ^1H NMR spectrum (400 MHz, C_6D_6) of the unknown precipitate from the reaction of complex **4.1** with benzyl bromide.

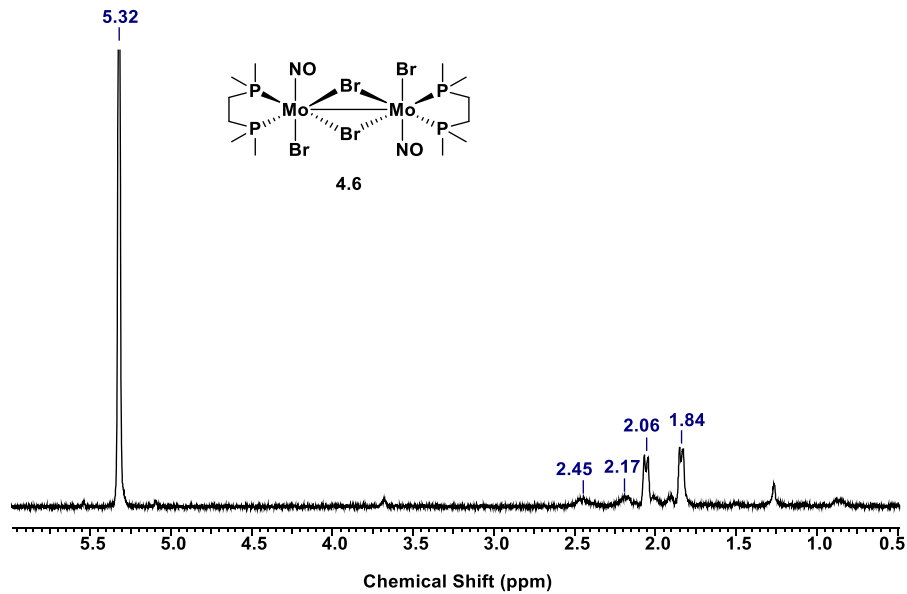


Figure C.19. The ^1H NMR spectrum (400 MHz, CD_2Cl_2) of complex **4.6**.

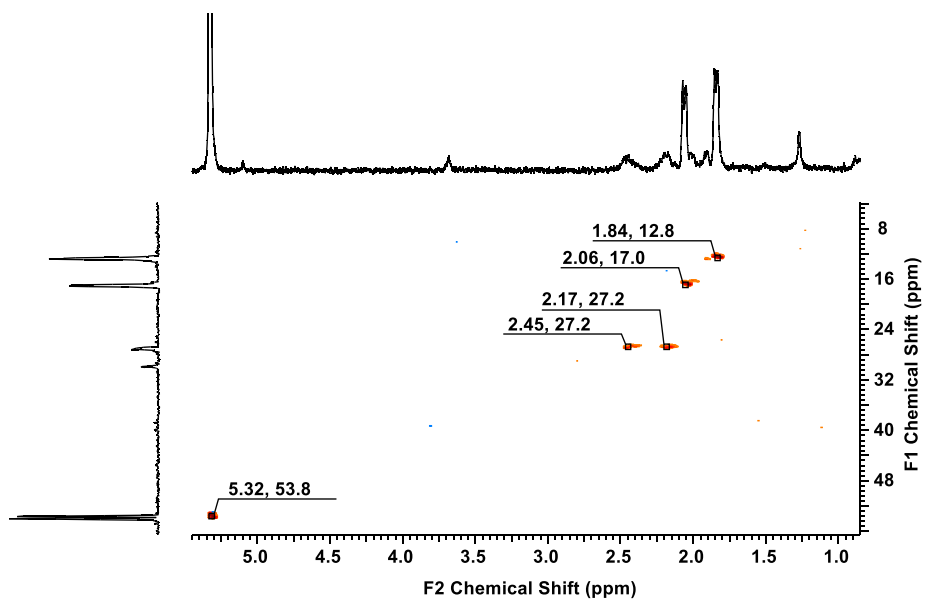


Figure C.20. Expansion of the $\{^1\text{H}-^{13}\text{C}\}$ HMBC NMR spectrum (400 MHz, 100 MHz, CD_2Cl_2) for complex **4.6** from δ 0.07 to 6.00 ppm on the F2 axis and δ 4.0 to 50.0 ppm on the F1 axis.

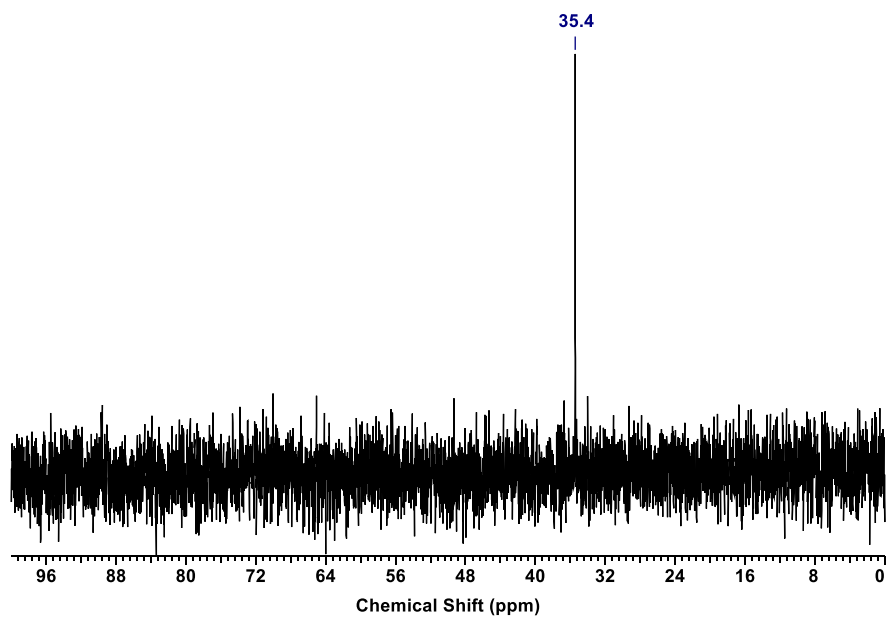


Figure C.21. The $^{31}\text{P}\{^1\text{H}\}$ NMR spectrum (162 MHz, CD_2Cl_2) for complex **4.6**.